ARL-PROP-TM-472 AR-006-601

DEPARTMENT OF DEFENCE

DEFENCE SCIENCE AND TECHNOLOGY ORGANISATION

AERONAUTICAL RESEARCH LABORATORY

MELBOURNE, VICTORIA

Propulsion Technical Memorandum 472

WIND TUNNEL TESTS ON JINDIVIK AIR INTAKE DUCT WITH AND WITHOUT AN AUXILIARY INTAKE

by

A.M. ABDEL-FATTAH
Y.Y. LINK

Approved for public release.

MARCH 1992

AR-006-601

DEPARTMENT OF DEFENCE
DEFENCE SCIENCE AND TECHNOLOGY ORGANISATION
AERONAUTICAL RESEARCH LABORATORY

Propulsion Technical Memorandum 472

WIND TUNNEL TESTS ON JINDIVIK AIR INTAKE DUCT WITH AND WITHOUT AN AUXILIARY INTAKE

by

A.M. ABDEL-FATTAH
Y.Y. LINK

SUMMARY

Results are presented for a wind tunnel program to investigate the effect of forward speed, incidence and yaw angle on the aerodynamic performance of an auxiliary air intake system fitted to the Jindivik target aircraft. Tests were carried out on a 1/4 scale model of an unmodified air intake duct, and one modified with several designs of auxiliary intake developed during static tests. The wind tunnel tests showed that worthwhile improvements in pressure recovery can be achieved at take-off speeds with simple intake modifications without excessive flow distortion at the engine face. In terms of pressure recovery at the engine face, performance improved with forward speed for all intake geometries tested. In the range of test parameters, the effects of both aircraft incidence and yaw were found to be negligible. Coefficients for distortion in total pressure distribution at the engine face were found to be within the acceptable range specified by the engine manufacturer.

DSTO AUSTRALIA

POSTAL ADDRESS: Director, Aeronautical Research Laboratory
506 Lorimer Street, Fishermens Bend 3207
Victoria Australia

CONTENTS

NOTATION

A	Auxiliary intake cross-sectional area [cm^2].
DC(60)	Distortion factor across all of the engine face.
DC(cir)	Distortion factor around a circumferential probe ring in the engine face.
DC(rad)	Distortion factor along a radial probe rake in the engine face.
FCSD	Fully Closed Sliding Door.
FOSD	Fully Open Sliding Door.
HOSD	Half Open Sliding Door.
m	Engine air mass flow [kg/sec].
$m\sqrt{T_o}/P_o$	Engine face air mass flow parameter.
N	Engine rotational speed [RPM].
P_o	Ambient or tunnel free stream total pressure [kPa].
P_s	Air intake duct local static pressure [kPa]
P_t	Total pressure at the engine face [kPa].
$(P_t/P_o)_{av}$	Pressure recovery (average of 30 separate P_t/P_o values at the engine face).
$P_{t,max}$	Maximum total pressure along a radial probe rake, or a circumferential probe ring in the engine face.
$P_{t,min}$	Minimum total pressure along a radial probe rake, or a circumferential probe ring in the engine face.
T_o	Ambient or tunnel free stream total temperature [K].
U	Forward speed or tunnel air velocity [m/sec].
V	Air velocity at the engine face [m/sec].
x	Axial length of the auxiliary intake [mm].
y	Lateral width of the auxiliary intake [mm].
ρ	Density of air at the engine face.
α	Incident angle [deg] - nose up positive.
β	Yaw angle [deg] - nose to port positive.

1. INTRODUCTION

At the request of RAN, an R & D program was undertaken by the Propulsion Branch at ARL to investigate means of improving the take-off performance of Jindivik target aircraft. On the grounds of cost-effectiveness, the adopted approach was to modify the air intake duct with the incorporation of an auxiliary intake which is deployed only during the take-off phase, increasing engine face pressure recovery and mass flow.

This concept was initially explored through theoretical appraisal, where the availability of improvements in the aerodynamic performance of the air intake duct was assessed and evaluated, Reference 1. The theoretical results were verified experimentally at static conditions with 1/4 scale model tests of the air intake duct. In the static phase of the experimental program, Reference 2, the auxiliary intake geometry was optimised in terms of aperture size, lip profile and location along the air intake duct, to give maximum pressure recovery and minimum flow distortion at the engine face. It was clearly indicated from these tests that worthwhile improvements in the aerodynamic performance could be achieved with a simple auxiliary intake modification to the air intake duct. In terms of pressure recovery at the engine face, these improvements were found to be at least similar to those achieved with the 'horse collar' attachment to the main intake lip, a bell-mouth arrangement currently used on Jindivik during ground runs on hot summer days, to prevent the engine from encountering any of its operational limits, Reference 3.

This report presents the results of the second phase of the experimental program, performed in the low speed wind tunnel at ARL. The tunnel tests were carried out over a range of forward speeds, incidence and yaw angles simulating a wide envelope of take-off conditions. The tests were used to confirm the results of the static phase of the program, and to assess some practical designs of the auxiliary intake configuration in terms of pressure recovery and flow uniformity at the engine face. The range of test conditions, and the practical auxiliary intake configurations tested, were planned in consultation with Aerospace Technologies of Australia Pty. Ltd. (ASTA), the authority responsible for developing the full scale auxiliary intake configuration of the Jindivik aircraft.

2. TEST MODEL, RIG AND INSTRUMENTATION

The 1/4 scale model of Jindivik air intake system is shown mounted in the wind tunnel in figure 1. A Schematic diagram of air intake duct is shown in figure 2; details of the duct are presented and fully described in Reference 1. The model static test rig is shown schematically integrated with the low speed wind tunnel rig in figure 3.

Total pressure measurements at the engine face were made with a 30 probe rake, details of which are shown in figure 4. The rake was comprised of six strakes equally spaced about the engine face annulus and each having five total pressure probes. The probes were radially disposed in five circumferential rings located at the centres of equal areas in the engine face annulus. Internal static pressure was measured with flush tapping points at 15 axial locations along the air intake duct, and 6 tapping points equally spaced around the

engine face location in the duct. The pressure tubes were connected to two SCANCO 48 D scani valves located under the working section of the tunnel, and pressures were measured with strain gauge transducers. Signals from the transducers were directly connected to a computerised data acquisition system with output in both tabular (digital) and graphic forms. The data acquisition system and software programs are described fully in Reference 3.

The engine air flow was simulated with a remote duplex blower. Air mass flow was measured with a Venturi meter with the appropriate lengths of upstream and downstream ducting to ensure as uniform flow as possible at the meter tappings. The Venturi pressures were recorded with inclined water manometers. Air temperatures upstream of the Venturi and in the tunnel were measured with mercury in glass thermometers while measurement of static pressure in the tunnel was made with a digital manometer accurate to 0.01 mbar.

The model structure was strengthened without altering any of its aerodynamic features for the low speed wind tunnel test program. To facilitate its mounting in the tunnel a steel fitting consisting of a pivot and cranked sting was bolted to the main tube carrying the model duct. The model was then mounted in the working section of the tunnel on a one piece centre pylon which was bolted to the top frame of the mechanical balance, located under the working section, figure 3

The model was pitched using a strut connecting the cranked rear sting from the model to the pitching arm of the mechanical balance. Model incidence (a) was measured by an accelerometer mounted on the balance pitch arm and calibrated against the model incidence using an inclinometer. Yaw (β) attitudes were obtained by rotating the mechanical balance.

Flexible steel coil reinforced tubing connected the model duct to a tilted steel down pipe leading to the Venturi meter and duplex blower, figure 3. The down pipe was supported to the floor of the tunnel and to 'earth' using collar and stand arrangements; in the wind tunnel test section wire stays connected the down pipe to the tunnel walls.

2.1 Test Configurations.

Six model geometries were each tested at similar combinations of forward speed, incidence and yaw angles in the tunnel. These were:

2.1.1 The Unmodified (Unmod) Air Intake Duct.
Full details are presented in Reference 1.

2.1.2. Duct Modified with an Auxiliary Intake.
a. Fully Open Sliding Door (FOSD).
b. Half Open Sliding Door (HOSD).
c. Fully Closed Sliding Door (FCSD).

Details of the sliding door configuration in the fully closed, fully open and half open positions are shown in figures 5-a, 5-b, and 5-c respectively. When fully open, the aperture

size of this geometry was A = 48 cm^2 with an aspect ratio (y/x) of 1.33, the lip curvature at the downstream lateral edge of the aperture being comparable to that used in the static tests with profiled lipped apertures, Reference 1.

d. Louvered (Louv) Aperture.

Details of this design of are shown in figure 6. The streamwise dimension of the aperture was chosen so as with the two louvers in the fully open position and tilted at a fixed maximum angle of 45^o, they would protrude to only one third of the duct height immediately under the aperture location. This restriction limited the effective length of the aperture to 40 mm, as is shown in figure 6. With a lateral width of 110 mm, which was limited by the curvature of the duct and canopy surfaces, the effective aperture area was therefore A = 44 cm^2, with an aspect ratio y/x = 2.75.

e. Profiled (Prof) Lipped Aperture.

The profiled lip geometry was developed and optimized in the static phase of the test program, where it produced the best aerodynamic performance in terms of pressure recovery at the engine face. This geometry, with details shown in figure 7, had the aperture size of A = 48 cm^2, with an aspect ratio of y/x = 3.52.

Geometries a. and d. were designed and suggested by ASTA. Their aperture sizes were chosen using the static test results presented in Reference 1, with compromises being made for practical engineering considerations. The HOSD, geometry b, was included in the test program at the suggestion of ASTA to simulate a condition during the sliding door closing process after take-off or during aircraft climb. Tests with the FCSD, geometry c, were also requested by ASTA to examine the effect on performance of the cavity created between the sliding door surface and the edges of the aperture at the condition after take-off and completion of climb, or during aircraft cruise.

2.2 Range Of Test Parameters.

Tests in the wind tunnel were carried out over a range of forward speeds U = 0 - 80 m/sec, and incidence (a) and yaw (b) angles in the range between -2 and 10 degrees. These ranges were selected in consultation with ASTA as being representative of the aircraft take-off conditions. Within these ranges, up to fourteen different combinations of the above three parameters were tested, and these are shown in table 1. Geometries 2.1.2, a and d were tested with all the 14 different U, a and b combinations shown in table 1. The other three geometries were tested at all four forward speeds, but with fewer incidence and yaw combinations. Actual test configurations are indicated by (*) in table 1.

3. RESULTS AND DISCUSSION

3.1. Pressure Recovery:

3.1.1 Tests with $\alpha = \beta = 0^o$.

With the model axis aligned with the tunnel axial direction ($\alpha = \beta = 0^o$), the results in terms of pressure recovery $(P_t/P_o)_{av}$ versus engine air mass flow parameter $(m\sqrt{T_o}/P_o)$ obtained with the unmodified air intake duct at various forward speeds are shown in figure 8. Corresponding results, obtained for each of the auxiliary intake geometries a,b,c,d and e, are presented in figures 9, 10, 11, 12 and 13 respectively. All of these figures exhibit a similar trend, with both pressure recovery and engine air mass flow increasing with forward speed of the aircraft. This trend was most apparent at the relatively high engine air mass flows corresponding to the take-off range of engine rotational speeds. Superimposed on these figures are the engine characteristics corresponding to the fixed engine rotational speeds of N = 13800 RPM and N = 12000 RPM. The first of these represents the engine maximum design speed, while the second, N = 12000 RPM, is the maximum speed achievable on hot days ($T > 25^o$ C) with the unmodified intake before the maximum limit on jet pipe temperature (JPT) is exceeded.

Most of the losses occurring in this intake at take-off conditions result from flow separation at the main intake lip. The magnitude of the lip loss is known to be a function of the ratio of the inlet plane velocity to free stream velocity, (Reference 5), which affects the streamline curvature at the lips and the levels of the corresponding local pressure gradients. Hence the general improvement in pressure recovery with forward speed and decline of pressure recovery with engine mass flow exhibited in figures 9 - 13. The auxiliary inlet acted to both decrease the main intake velocity ratio, and reduce the proportion of engine mass flow ingested via the main intake; the extent to which overall pressure recovery was improved depended on how successfully the losses experienced by the flow ingested by the auxiliary intake - again, mainly due to local flow separations - could be minimised. Hence the variation in pressure recovery with auxiliary intake configuration.

The characteristics obtained at static conditions or U = 0 m/sec for each auxiliary intake modification are compared with that corresponding to the unmodified configuration in figure 14. The characteristics for the unmodified and the profiled lip configurations coincide with those obtained during tests with the static test rig and reported in Reference 2. It is obvious that the best pressure recoveries were achieved with the profiled lipped auxiliary intake. This was followed in descending order by: FOSD, Louv., HOSD and the unmodified configuration.

Similar comparisons at U = 80 m/sec are presented for all intake geometries in figure 15. The best aerodynamic performance was, once more, achieved with the profiled lipped auxiliary intake. The performance was followed with similar descending order to that obtained at static conditions, but with the difference that the pressure recoveries produced by the HOSD auxiliary intake geometry at this high forward speed, exceeded those of the louvered auxiliary intake design.

The characteristics defining the pressure recovery variations with aircraft forward speed obtained for each of the above auxiliary intake geometries are compared in figure 16 with that corresponding to the unmodified configuration at the maximum engine design speed; N = 13800 RPM. This figure clearly indicates that the auxiliary intake with profiled lip, which was optimized in the previous static phase of the experimental program, appeared also to produce the best aerodynamic performance across the entire tested range of forward speeds. In general, in the range of forward speed U > 50 m/sec, this was followed in descending order by: FOSD, Louv., Unmod. and the FCSD configuration. The above mentioned reversal in the performance of the louvered aperture auxiliary intake as compared to that of the HOSD geometry appeared in this figure to occur at about U = 48 m/sec. In the range beyond U = 48 m/sec the HOSD geometry appeared to be more effective in improving engine face pressure recovery than the louvered door auxiliary intake.

Although the profiled lipped and the FOSD auxiliary intake geometries had the same aperture area A = 48 cm^2, figures 14, 15 and 16 clearly show that the profiled lip geometry was more effective than the sliding door design in improving engine face pressure recovery at all forward speeds tested. This was mainly due to the fact of that the aspect ratio y/x = 3.52 of the profiled lipped aperture was much larger than y/x = 1.33 for the FOSD configuration, Reference 2.

The performance of the louvered auxiliary intake geometry as shown in figures 14, 15 and 16 was always inferior to that of the FOSD geometry, despite the fact that it's aperture aspect ratio was almost twice that of the FOSD aperture: This could be due to a combination of two reasons:

* Firstly, the slightly smaller area of the louvered aperture, A = 44 cm^2 compared with A = 48 cm^2 for the FOSD.

* Secondly and more importantly, particularly at higher forward speeds, the losses resulting from the obstruction caused by the presence of the two rigid louvers fixed at the arbitrary angle of 45° with the vertical in the air intake duct. The obstruction, and the resultant separation losses at the louvers' edges, might have been reduced had the louvers, instead of being fixed, been allowed to take a floating position aligned with the local streamlines as dictated by both the main and auxiliary intake flows.

The sliding door in the fully closed position created a cavity in the upper surface of the intake duct, figure 5-a, with a depth equal to the thickness of the aircraft skin structure. The effect of this cavity was to reduce the performance of the intake slightly as the forward speed increased, figure 16. However, in general, this effect was small in comparison to the gains to be achieved with the door in the fully open position.

3.1.2 Effect of Aircraft Attitude.

The measured pressure recovery for the unmodified configuration at several combinations of U, α, and β is shown as functions of air mass flow parameter and forward speed, at an equivalent engine speed of 13800 RPM, in figures 17 and 18 respectively. To reduce crowding in figure 17 results have not been presented for U = 0 or 65 m/sec or for α = 5 degrees. In the relatively high range of engine air mass flow corresponding to the take-off range of engine speeds, the effect of increased yaw and incidence appeared in figure 18 to be favourable, where it produced slight improvements in pressure recoveries at the engine face. At the take-off condition of $\beta = 0^o$, N = 13800 RPM and U = 65 m/sec, the maximum effect observed was an increase in pressure recovery of the unmodified intake by some 0.4% when the aircraft incidence was varied from -2 to 10 degrees. The measured changes in pressure recovery can be explained in relation to the intake geometry, figure 2, in that the upper lip flow separation is alleviated by the increase in incidence of the free stream on the upper lip, there being no lower lip to experience a compensating increase in separation.

Similar plots showing the effects of α and β on performance are presented in figures 19, 21, 23, 25 and 27 for auxiliary intake geometries a,b,c,d and e respectively. To reduce overcrowding, the data are again only presented for U = 30 and 80 m/sec, at the three fixed attitudes of $\alpha = \beta = 0^o$, $\alpha = 10^o$, $\beta = 0^o$ and $\alpha = \beta = 10^o$. The corresponding $(P_t/P_o)_{av.}$ variation with forward speed at an engine speed of N =13800 RPM for all of the tested α, β combinations, are presented in figures 20, 22, 24, 26 and 28 respectively. The effect of α and β on performance appeared in all of the above figures to be slightly favourable in the low range of forward speed, and detrimental at higher speeds. These effects in general, as was the case with the unmodified configuration, were found to be very small.

3.2 Total Pressure Distribution at the Engine Face.

A further aspect of this investigation was to examine the time-mean distribution of total pressure at the engine face. The uniformity of this distribution is important in relation to both compressor blade stressing and flow stability. Quantitative measures for total pressure irregularities at the engine face are here expressed in terms of DC(60), DC(rad) and DC(cir) distortion coefficients. Definitions for these terms are presented in Appendix 1.

3.2.1 The Unmodified (Unmod) Air Intake Duct.

The characteristics for flow irregularities at the engine face in terms of DC(60) versus engine air mass flow parameter obtained for the unmodified air intake duct at various U, α, and β combinations, are presented in figure 29. For the region of interest, that is the characteristics corresponding to an engine speed of N = 13800 RPM, the DC(60) variation with forward speeds at various α & β combinations are included in figure 18. It is obvious from both figures 29 and 18 that there is no consistent trend in the variation of DC(60) with forward speed. The plots for the total pressure distribution at the engine face, in terms of $(P_t/P_o)_{av}$ contours, which are shown in figure 30 for the zero incidence condition ($\alpha = \beta = 0^o$) and N = 12000 RPM for various forward speeds, all appeared to be

qualitatively similar, and the corresponding variation in DC(60) shown in figure 18 results mainly from variation in the mean dynamic head of the flow at the engine face which appears in the denominator of the expression for DC(60). No data at this condition is available for N = 13800 RPM. The 60° sector with minimum average total pressure used in the definition of DC(60) was located in the top region of the engine face for all forward speeds tested with this configuration. The DC(60) and the DC(cir) for all of the distribution plots in figure 30 were found to be below the corresponding upper limits nominated by the engine manufacturer, Rolls Royce. The DC(rad), on the other hand, appeared to be relatively high, and increased with forward speed to the extent of exceeding the specified upper limit in the bottom region of the engine face, as is shown in figure 30 - c for U = 80 m/sec.

For $\beta = 0^o$ and N = 13800 RPM, figure 18 indicates a progressive decrease in DC(60) as a is increased from 0° to 10°, at all of the forward speeds tested. This decrease appeared to be consistent with the slight improvements in pressure recovery at the engine face, and probably occurred for the same reasons. The effect of aircraft incidence on the total pressure distribution, at a fixed forward speed of U = 65 m/sec with zero yaw ($\beta = 0^o$), is shown in figure 31 at an equivalent engine speed of N = 12000 RPM. The progressive improvement in the qualitative uniformity of the total pressure contours with the progressive increase in α is evident from figure 31. As was the case with N = 13800 RPM shown in figure 18, the progressive increase in α was also associated with a progressive reduction in both DC(60) and DC(cir) with slight improvements in pressure recoveries at the engine face. By contrast, the DC(rad) increased with α and exceeded the manufacturer's limit of 0.90 at both $\alpha = 5^o$ and $\alpha = 10^o$ as shown in figures 31 - c and 31 -d respectively.

For the extreme attitude of $\alpha = \beta = 10^o$, the DC(60) appeared in figure 18 as a rapidly increasing function of forward speed. The total pressure distribution at the engine face, plotted for this attitude, is compared with the corresponding $\alpha = \beta = 0^o$ plot in figure 32 for the fixed condition of U = 80 m/sec and N = 13800 RPM. The contours defining the relatively high levels of total pressure appeared in figure 32 - a for $\alpha = \beta = 0^o$ to be located in the lower region of the engine face, whereas the opposite applied for $\alpha = \beta = 10^o$, figure 32-b. The DC(60) for the $\alpha = \beta = 10^o$ attitude (figure 18) was relatively high, and the specified upper limit of 0.30 (Appendix 1) would probably be exceeded with further increase in forward speed. All the DC(cir) on the other hand, appeared smaller than those of the $\alpha = \beta = 0^o$ condition. The DC(rad) for both cases was generally high, and exceeded the 0.90 upper limit for $\alpha = \beta = 0^o$ and $\alpha = \beta = 10^o$ respectively.

3.2.2 Duct Modified with an Auxiliary Intake.

a. Fully Open Sliding Door (FOSD).

The DC(60) versus $m\sqrt{T_0}/P_0$ characteristics, calculated for the air intake duct modified with the FOSD auxiliary intake geometry, at various U, α, and β combinations, are presented in figure 33. The variation of DC(60) at an equivalent engine speed of N = 13800 RPM is plotted against forward speed in figure 20, for the same combinations of α & β.

Figure 33 shows that the trends in variation of DC(60) with engine mass flow parameter are highly dependent on the range of engine mass flow, aircraft attitude and forward speed. For example, for the condition $\alpha = \beta = 0^o$, and in the region of interest of relatively high mass flow or high engine speeds, the U = 0 and U = 30 m/sec characteristics appear as increasing functions of mass flow, while the opposite is true for the U = 65 and 80 m/sec characteristics. Much the same applies for the attitude $\alpha = 10^o$ and $\beta = 0^o$. The total pressure distributions at the engine face, obtained at the condition of U = 80 m/sec and engine speed slightly lower than N = 13800 RPM, for $\alpha = \beta = 10^o$ and $\alpha = \beta = 0^o$, are shown in figure 34 - a and figure 34 - b respectively. Figure 34 - b features significantly larger variations of total pressure over the engine face annulus than does figure 34 - a, and the DC(60) factor is correspondingly higher.

From figure 20 it can be seen that the DC(60) for all combinations decreased with forward speed in the low speed range reaching a minimum before, in general, increasing with forward speed. As was the case with the unmodified configuration, the effect of both incidence and yaw appeared to be to reduce flow irregularities at the engine face, possibly for the same reasons discussed earlier in relation with the unmodified geometry.

Plots of the total pressure distribution at the engine face, and distortion coefficients DC(cir) and DC(rad) calculated for each plot, obtained for various forward speeds at $\alpha = \beta = 0^o$ and N = 12000 RPM, are shown in figure 35. The values of these coefficients, as well as those shown in figure 34 for different attitude and engine speed, were below the corresponding manufacturer's upper limit. In general, these values were much lower than those of the unmodified configuration at the same test conditions shown in figure 30.

b. Half Open Sliding Door (HOSD).

The variation of DC(60) with $(m\sqrt{T_0}/P_0)$ for the half open sliding door geometry is shown in figure 36, and with U at N = 13800 RPM in figure 22. As this represents a transient rather than a steady state condition, the DC(60) factor limit which applies to this geometry should more appropriately be the transient value specified by Rolls Royce; namely 0.5, rather than 0.3. Within the range of forward speeds tested in this investigation, all the DC(60) values shown in figure 22 were below the specified upper limit. However, for speeds above U = 30 m/sec, figure 22 shows DC(60) as a rapidly increasing function with forward speed, with a value of 0.351 at the condition U = 80 m/sec and $\alpha = \beta = 0^o$. The total pressure distribution at the engine face obtained for this condition is presented in figure 37. This result caused some concern, as the range of forward speeds which is relevant to this half open door position is that occurring after take-off. Extrapolating the recorded DC(60) values into a higher forward speed range, arguably the manufacturer's transient upper limit of DC(60) = 0.50 could be encountered at a forward speed of about U = 130 m/sec. This would probably be acceptable, as it is expected that the door would be fully closed at forward speeds less than U = 130 m/sec.

Tests at attitudes other than $\alpha = \beta = 0^o$ were only performed for U = 80 m/sec. In terms of pressure recovery, the effect of attitude appeared very small, as is shown in figure 22. The effect on DC(60), while also small, was favourable especially with aircraft yaw $\beta = 10^o$.

c. Fully Closed Sliding Door (FCSD).

The variation of DC(60) with $(m\sqrt{T_o}/P_o)$, obtained for this geometry for a range of forward speeds, are shown in figure 38. The variation of DC(60), at N = 13800 RPM, is given with respect to forward speed in figure 24. The DC(60) measured for this geometry was generally lower than the corresponding values shown in figure 18 for the unmodified configuration in all the tested range of wind tunnel speeds. This result is surprising, as it is not consistent with the detrimental effects of the cavity, figure 5-a, on engine face pressure recovery. The range of forward speeds relevant to this closed door geometry is that in the proximity of cruise condition , U = 270 m/sec; which is far beyond the maximum U = 80 m/sec achieved in the current wind tunnel tests. The results in Figure 24 can not be extrapolated that far, but there is no evidence to suggest that the specified upper limit of DC(60) = 0.30 would be exceeded. The total pressure distribution at the engine face is compared at U = 80 m/sec, $\alpha = \beta = 0^o$ and N = 13800 RPM with that of the unmodified configuration in figure 39. As was the case with DC(60), the DC(cir) and DC(rad) calculated for the duct modified with the cavity (which are presented in figure 39), were always found to be lower than those for the corresponding values obtained at the same conditions for the unmodified configuration. The DC(60) and all values of DC(cir), for both geometries, were below the corresponding manufacturer's upper limit. In the case of DC(rad), apart from that corresponding to the bottom of the face in both cases, all DC(rad) values were also below the upper limit of DC(rad) = 0.90.

d. Louvered (Louv) Aperture.

The variations of DC(60) with engine air mass flow parameter for this auxiliary intake design at all of the U, α and β combinations are presented in figure 40, and as functions of aircraft forward speed at N = 13800 RPM in figure 26. In terms of DC(60) these two figures clearly indicate that this geometry produced the least flow distortions at the engine face, for the entire range of engine air mass flow. In the region of interest of relatively high engine air mass flows or high engine rotational speeds, all the DC(60) values were within the range 0.045 to 0.085.

Examples of total pressure distribution at the engine face for various forward speeds at the fixed condition of N = 12000 RPM and $\alpha = \beta = 0^o$, are presented in figure 41. In all of these plots, the 60^o sector with minimum average total pressure was found to be located in the top region of the engine face. For the condition N = 13800 RPM and U = 80 m/sec, the total pressure distribution at the engine face for zero incidence is compared in figure 42 with that obtained at the extreme attitude $\alpha = \beta = 10^o$. All the calculated distortion factors for both attitudes are shown in the figure to be generally low and quantitatively comparable. The only effect of attitude appears in the figure to be qualitative, where the location of the DC(60) sector has been shifted to a location which is consistent with the imposed attitude of the intake duct.

e. Profiled (Prof) Lipped Aperture.

The DC(60) values obtained for this optimised auxiliary intake configuration for all the U, α and β combinations tested, are plotted against engine air mass flow parameter in figure 43, and against forward speed for N = 13800 RPM in figure 28. For the condition $\alpha = \beta = 0^o$, the DC(60) measured for U = 0 and 30 m/sec was much higher than for U = 65 and 80 m/sec. The DC(60) values for U = 0 and 30 m/sec were 0.356 and 0.355 respectively, exceeding the 0.30 upper limit specified by the engine manufacturer. The corresponding values in the higher speed range were 0.146 and 0.094 for U = 65 and 80 m/sec respectively which are far below the 0.30 limit. The effects of forward speed on total pressure distribution at the engine face for N = 13800 RPM and $\alpha = \beta = 0^o$ are shown in figure 44. The 60^o sector with minimum average total pressure occurred at the same location in the upper region of the engine face for all speeds tested, but the total pressure deficit in this sector diminished with forward speed. This is obvious from the comparison between figures 44 - b and 44 - c obtained for U = 30 and 65 m/sec respectively. The calculated DC(cir) and DC(rad) are also shown in figure 44, and all were found to be below the engine manufacturer's specified upper limit.

The level of distortion with this configuration at the take-off condition (N = 13800 RPM, U = 65 m/sec, $\alpha = 10^o$) would be unacceptable. As the incidence increased from 0^o to 10^o a significant total pressure decrement appeared in the upper sector of the engine face, as can be seen in figure 45. In this respect the behaviour was different from that of the FOSD geometry, which essentially differed only in aspect ratio of the auxiliary intake. The contrast can arguably be attributed to difference in behaviour of the vortices emanating from the streamwise edges of the aperture, which were sensitive to aspect ratio.

f. Summary

The effect of the various intake configurations on the engine face distortion at zero incidence are summarised as follows:

* In figure 46 in terms of DC(60) against engine mass flow at static conditions.
* In figure 47 in terms of DC(60) against engine mass flow at U = 80 m/sec.
* In figure 48 in terms of DC(60) against forward speed at N = 13800 RPM.

The above figures show that the variation of DC(60) is highly dependent on both intake geometry and ranges of forward speed and engine mass flow parameter. Apart from the profiled lip and the HOSD geometries in the low and high ranges of speed respectively, all the DC(60) values measured for any intake configuration are below the DC(60) = 0.30 upper limit nominated by the engine manufacturer.

3.3 Internal Static Pressure Distribution.

The internal surface static pressure distribution along the air intake duct, in terms of P_s/P_o versus distance from the engine face, is given in figure 49, for the three auxiliary intake geometries a, d and e together with that for the unmodified configuration. These

pressures were recorded at the operating condition of N = 12000 RPM, $\alpha = \beta = 0^o$ and U = 80 m/sec. Along the entire axial length of the intake duct the wall static pressures measured for the unmodified configuration were always lower than those measured for any of the auxiliary intake modifications. This trend in static pressure differential would provide a good case for eliminating the need for the splitter used in current Jindivik installations to prevent duct collapse due to suction forces at high engine RPM and low forward speed.

Figure 49 shows that the highest static pressure upstream of the auxiliary intake was recorded with the louvered geometry, indicating that the main intake flow was lower in this case in comparison to that of the other intake configurations. This would most probably have been due to the blockage effect of the rigid louvers in the duct, discussed in section 3.2.2.d above.

4 CONCLUSIONS

1- As expected and predicted by theory, the measured pressure recovery at the engine face improved with aircraft forward speed for all intake configurations tested. The rate of improvement varied with the intake geometry, range of engine air mass flow and range of forward speeds.

2- In terms of pressure recovery at the engine face, the best aerodynamic performance was achieved with the profiled lipped auxiliary intake configuration at all forward speeds in the wind tunnel. This was followed in descending order by: fully open sliding door, louvered aperture and the unmodified geometry. At static conditions, the performance of the profiled lipped auxiliary intake was similar to that obtained with the "horse collar" currently in use for full scale static engine running..

3- In terms of DC(60) the improvements in pressure recovery, in some cases, were found to be at the expense of flow distortion at the engine face. At static conditions, this was the case only with the profiled lipped and the fully open sliding door auxiliary intake geometries. However, tests in the take-off range of forward speeds showed the opposite to be true. Apart from the case of the half open sliding door, and that of the profiled lip at a = 10^o, the DC(60) values obtained for all auxiliary intake geometries were actually lower than those corresponding to the unmodified configuration, and all were below the manufacturer's specified upper limit of 0.30.

4- The variation in trends of DC(60) with forward speed were highly dependent on both the geometry of the auxiliary intake and the range of forward speeds.

5- The louvered auxiliary intake geometry produced the lowest DC(60) in all ranges of forward speed. At static conditions, it was followed in descending order by: FCSD, HOSD, unmodified configuration, FOSD and the profiled lipped auxiliary intake geometry. At U = 80 m/sec, however, the above order appeared very different, and in descending order was as follows: Louvered geometry, profiled lipped aperture, FOSD, FCSD, unmodified configuration and HOSD.

6- In the high range of engine speed, the calculated values of both DC(rad) and DC(cir) for all auxiliary intake configurations tested were found to be below the upper limit 0.90 recommended by Rolls Royce for the Viper II engine. This limit was only exceeded in terms of DC(rad) in the bottom region of the engine face in some cases with the unmodified air intake duct, and the sliding door in the fully closed position.

7- It can be concluded from the above, that significant improvements in pressure recovery can be achieved with a practical auxiliary intake design without serious penalties in distortion levels at the engine face.

ACKNOWLEDGMENT

The authors would like to take this opportunity to express their thanks to Mr. S.A. Fisher of the Propulsion Branch - ARL for his support and useful comments. The support of Mr. M.A. Fisher of the same Branch in carrying out the model tests and maintaining the test rig are gratefully acknowledged. In addition, thanks are also due to both Mr. K. A. O'Dwyer and Mr. P.T. Malone of the Flight Mechanics Branch - ARL, for their technical support and participation in carrying out the wind tunnel model tests.

REFERENCES

1- Abdel-Fattah, A.M., and Fisher, S.A., "An Auxiliary Intake System for un Unmanned Aircraft." Proceedings of the 10th ISABE, Nottingham - England, Sept., 1991.

2- Abdel-Fattah, A.M., "Modification of Jindivik Air Intake Duct with an Auxiliary Intake - Static Aerodynamic Tests." ARL-PROP-TM-460, Aug., 1991

3- Wrigley, A.K., " A Note on the Effect of Jindivik Installation on Ground Running of Viper II Engines.", G.A.F Aerodynamic Note B3/24, April 1961.

4- Link, Y.Y., "A Fortran Program for Processing Low Speed Wind Tunnel Test Data for the Jindivik Auxiliary Intake.", ARL - Flight Mechs-TM-426, NOV., 1990.

5- Seddon, J., & Goldsmith, E. L., " Intake Aerodynamics." Collins, 1st edition, 1985.

6- Pemberton, J.O., private correspondence, Rolls Royce - England, Ref. A812JP289, June, 1990.

APPENDIX

The uniformity of total pressure distribution at the engine face is important in relation to compressor blade stressing and flow stability. Expressions for distortion coefficients for the quantitative measure of flow irregularities or total pressure distortion at the engine face are given below. The first of these DC(60) is presented and fully discussed in ref. 4. Reference 5 describes the coefficients which are usually used in UK by Rolls Royce and recommended for use with Viper installations at steady state conditions. These are:

1. Over the entire face annulus:
$$DC(60) = (P_{t.av} - P_{t.av.min60})/(\rho V^2/_2)$$

2. Along any radial total pressure rake in the face annulus:
$$DC(rad) = (P_{t.max} - P_{t.min})/(\rho V^2/_2)$$

3. Around any circumferential total pressure ring at constant radius in the face annulus:
$$DC(cir) = (P_{t.max} - P_{t.min})/(\rho V^2/_2)$$

The upper limits for these coefficients as specified by the engine manufacturer - Rolls Royce, for the Viper II, are:

DC(60)	steady state	= 0.30
	transient	= 0.50
DC(rad) & DC(cir)	steady state	= 0.90
	transient	= 1.10

TABLE 1

Test	(U)	(α)	(β)	Unmod	FOSD	HOSD	FCSD	Louv	Prof
1	0	0	0	*	*	*	*	*	*
2	30	0	0	*	*			*	
3		5	0	*	*			*	
4		10	0	*	*			*	*
5		10	10	*	*			*	
6	65	-2	0	*	*			*	
7		0	0	*	*	*	*	*	*
8		5	0	*	*			*	
9		10	0	*	*			*	*
10		10	10	*	*			*	
11	80	0	0	*	*	*	*	*	*
12		5	0	*	*	*		*	
13		10	0	*	*	*	*	*	*
14		10	10	*	*	*	*	*	

Table 1: Test combinations of forward speed and Jindivik model attitude in the low speed wind tunnel.

Figure 1: Photograph of the 1/4 model scale of the Jindivik air intake system in the wind tunnel.

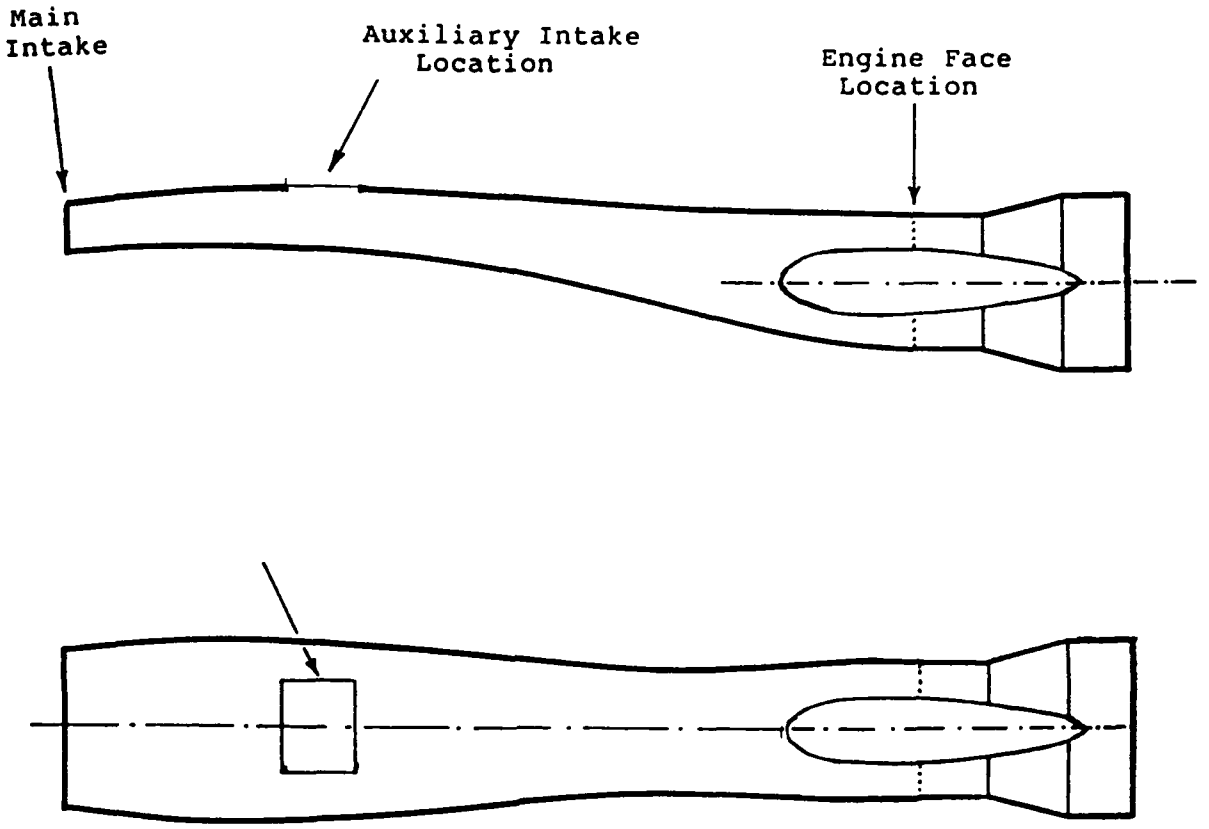

Figure 2: Schematic diagram for
the Jindivik air intake duct.

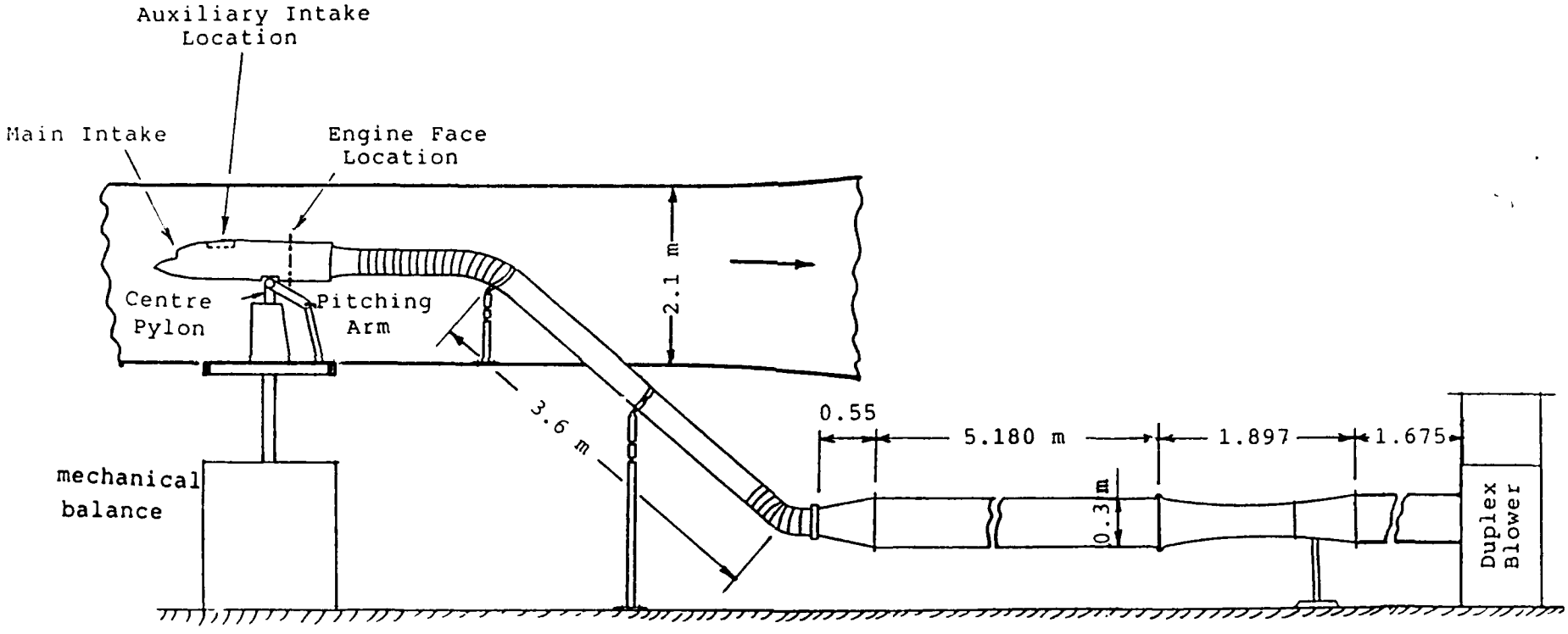

Figure 3: Experimental set-up of the Jindivik air intake model in the wind tunnel test rig.

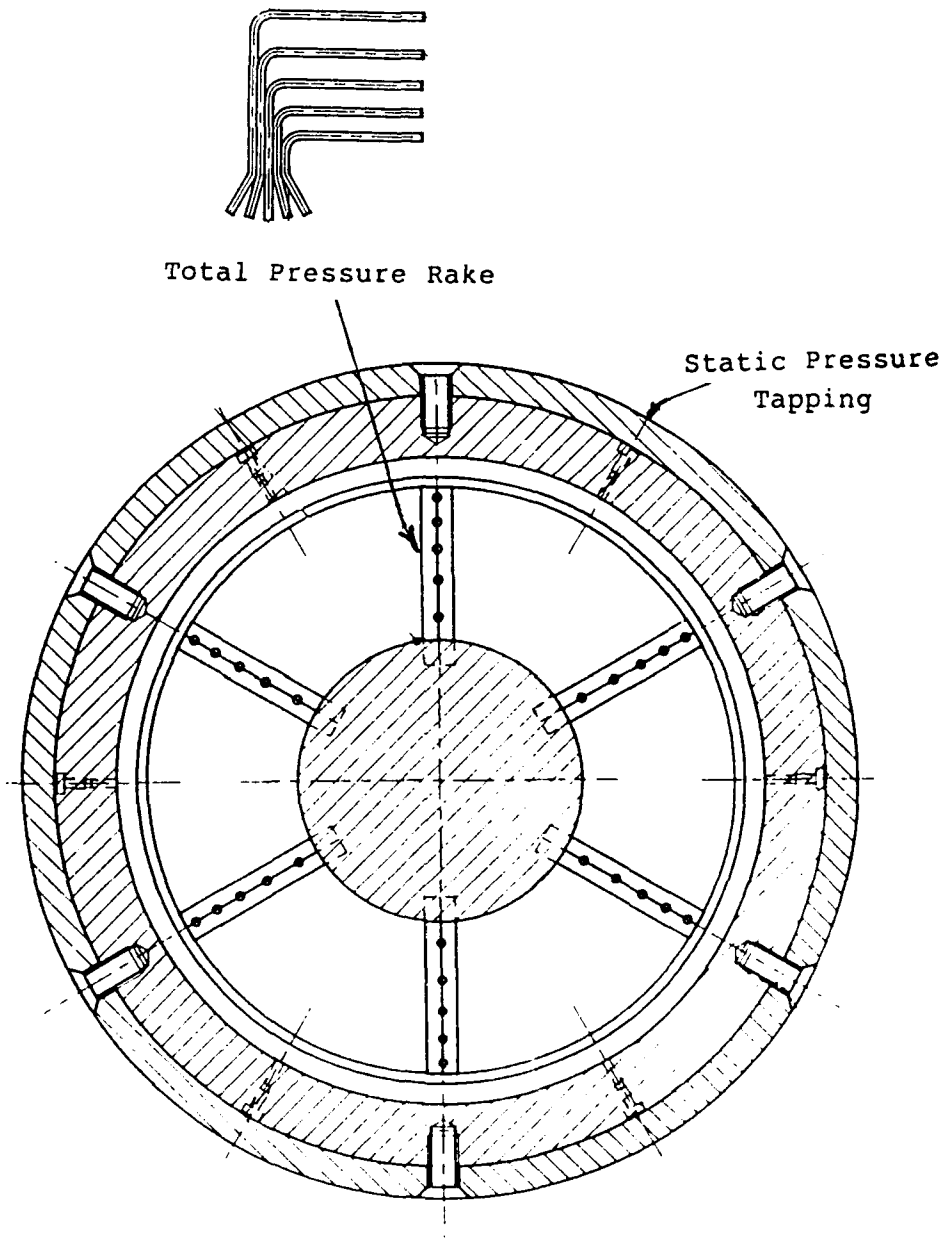

Figure 4: Details of the total pressure rake at the engine face.

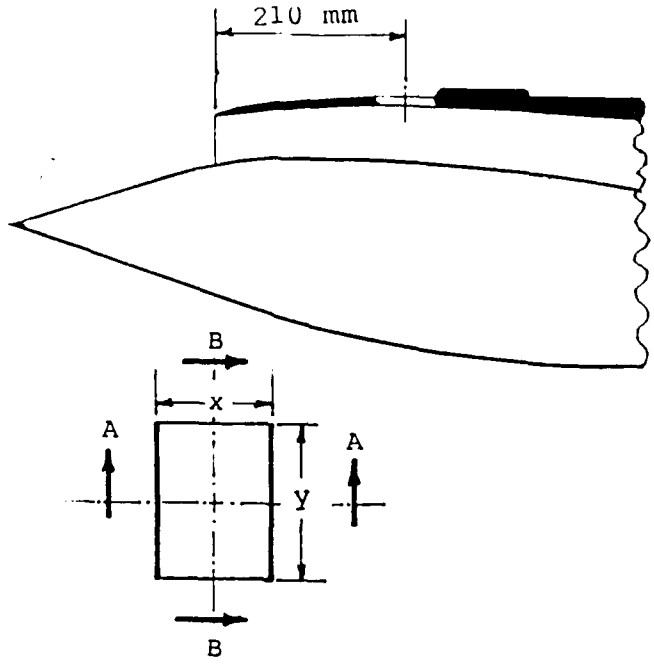

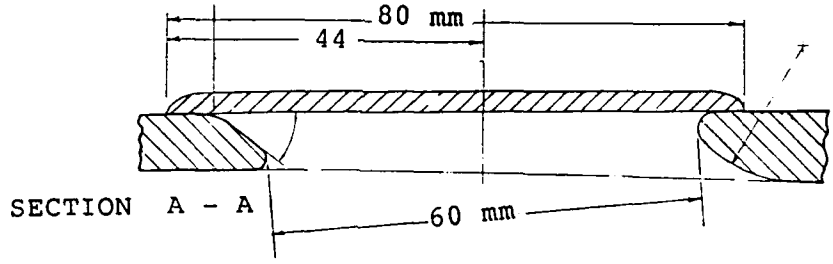

(a)- Fully Closed Sliding Door.

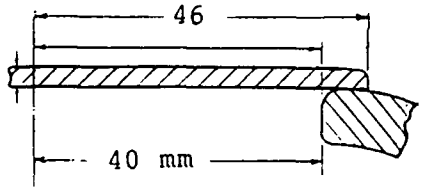

(b)- Fully Open Sliding Door.

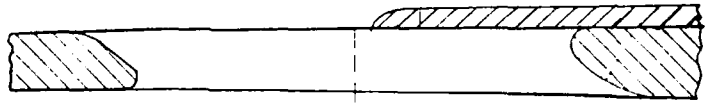

(c)- Half Open Sliding Door.

Figure 5: Details of the auxiliary intake sliding door geometry.

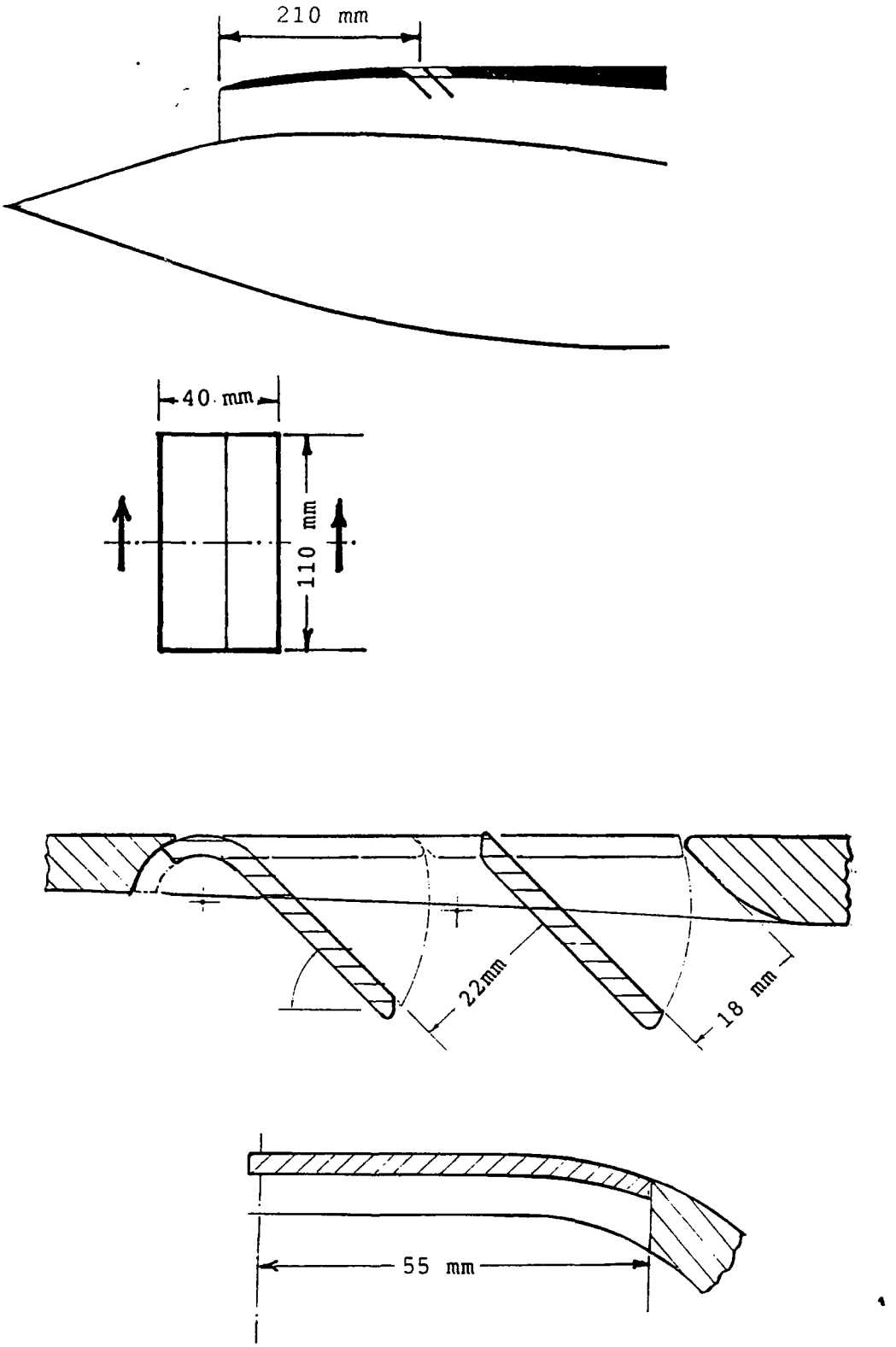

Figure 6: Details of louvered aperture auxiliary intake geometry.

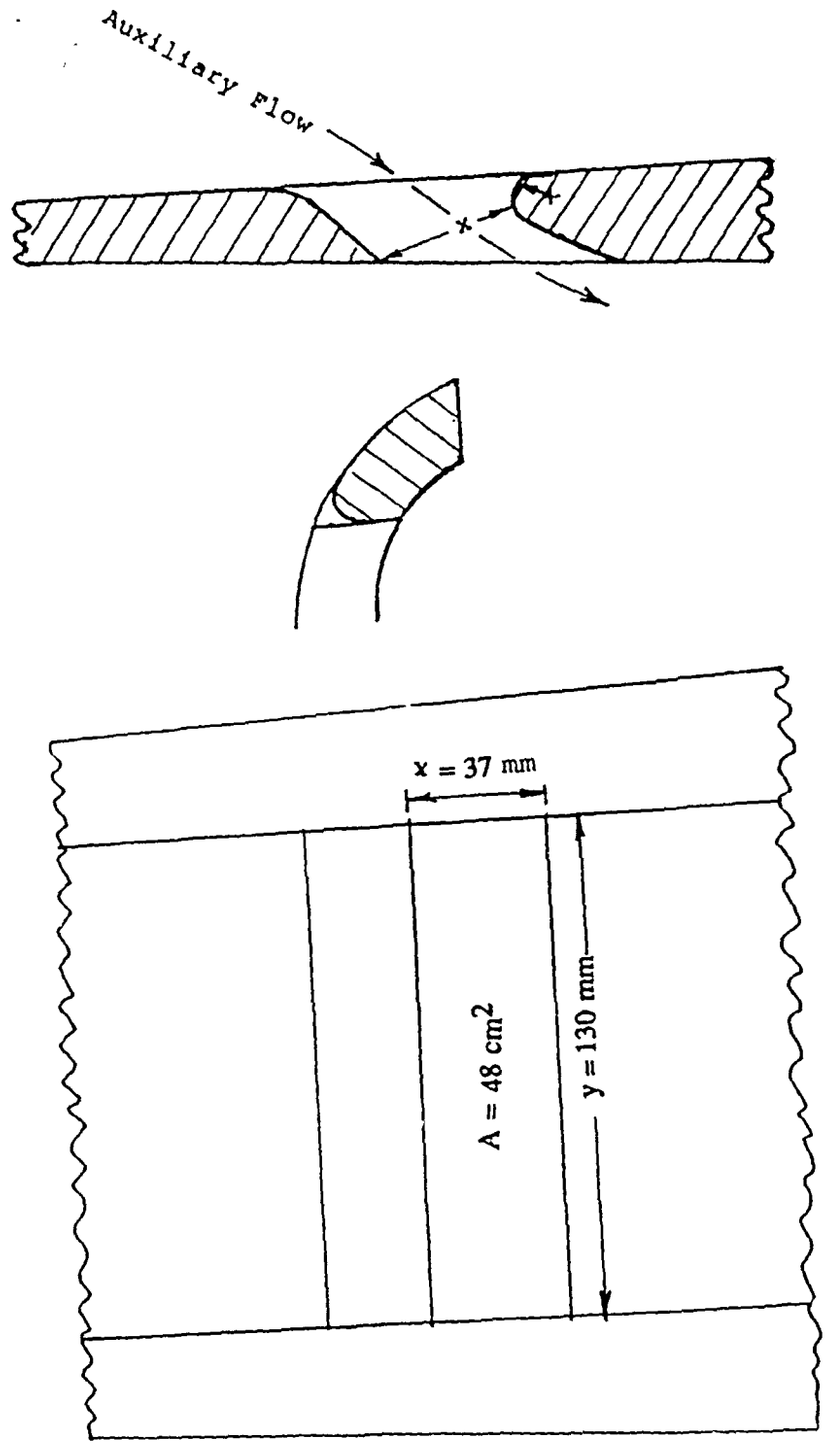

Figure 7: Details of the profiled lip auxiliary intake geometry.

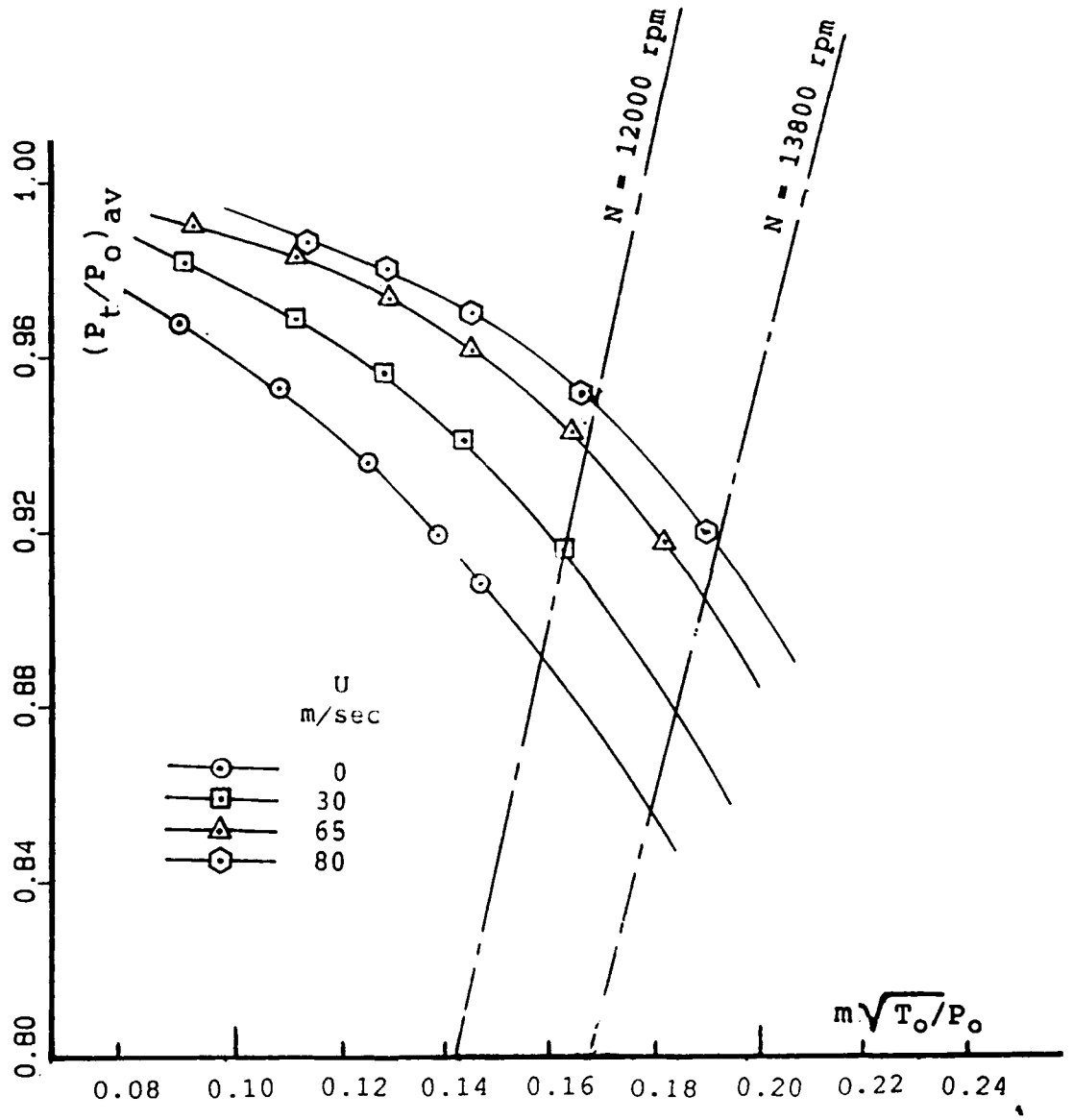

Figure 8: Engine face pressure recoveries for the unmodified configuration at various forward speeds and $\alpha = \beta = 0^{o}$.

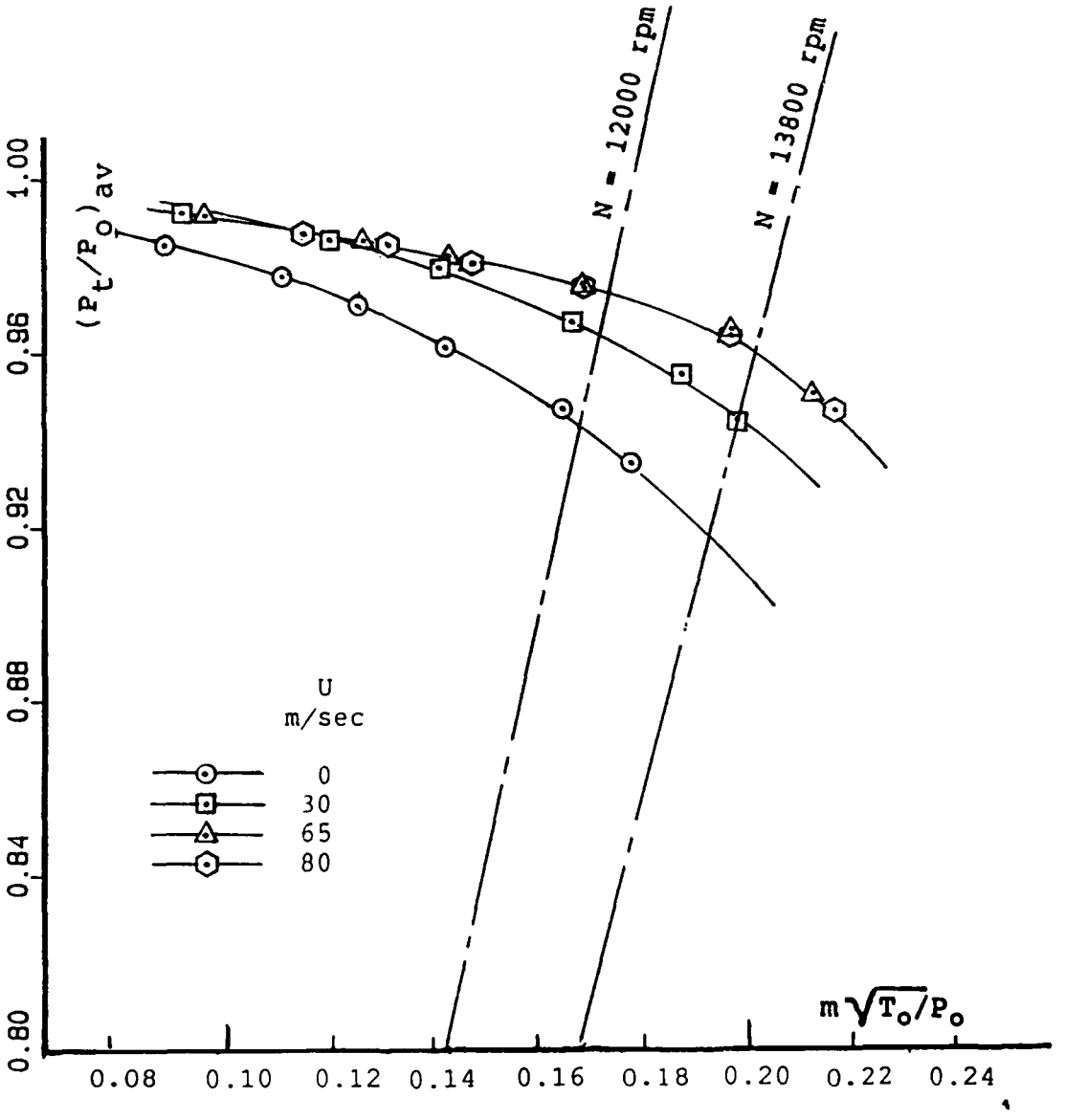

Figure 9: Engine face pressure recoveries for the FOSD configuration at various forward speeds and $\alpha = \beta = 0^{o}$.

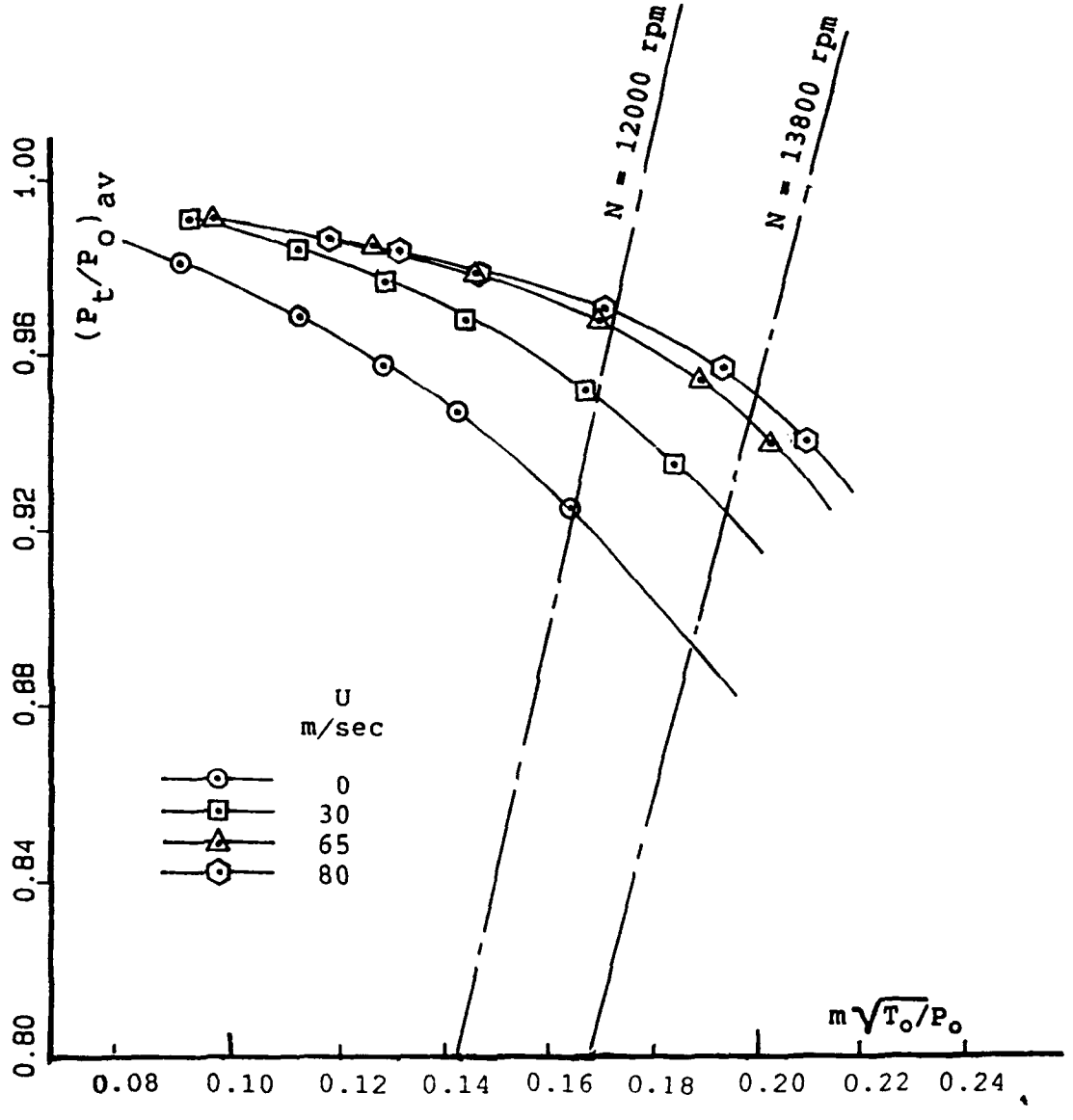

Figure 10: Engine face pressure recoveries for the HOSD configuration at various forward speeds and $\alpha = \beta = 0^{o}$.

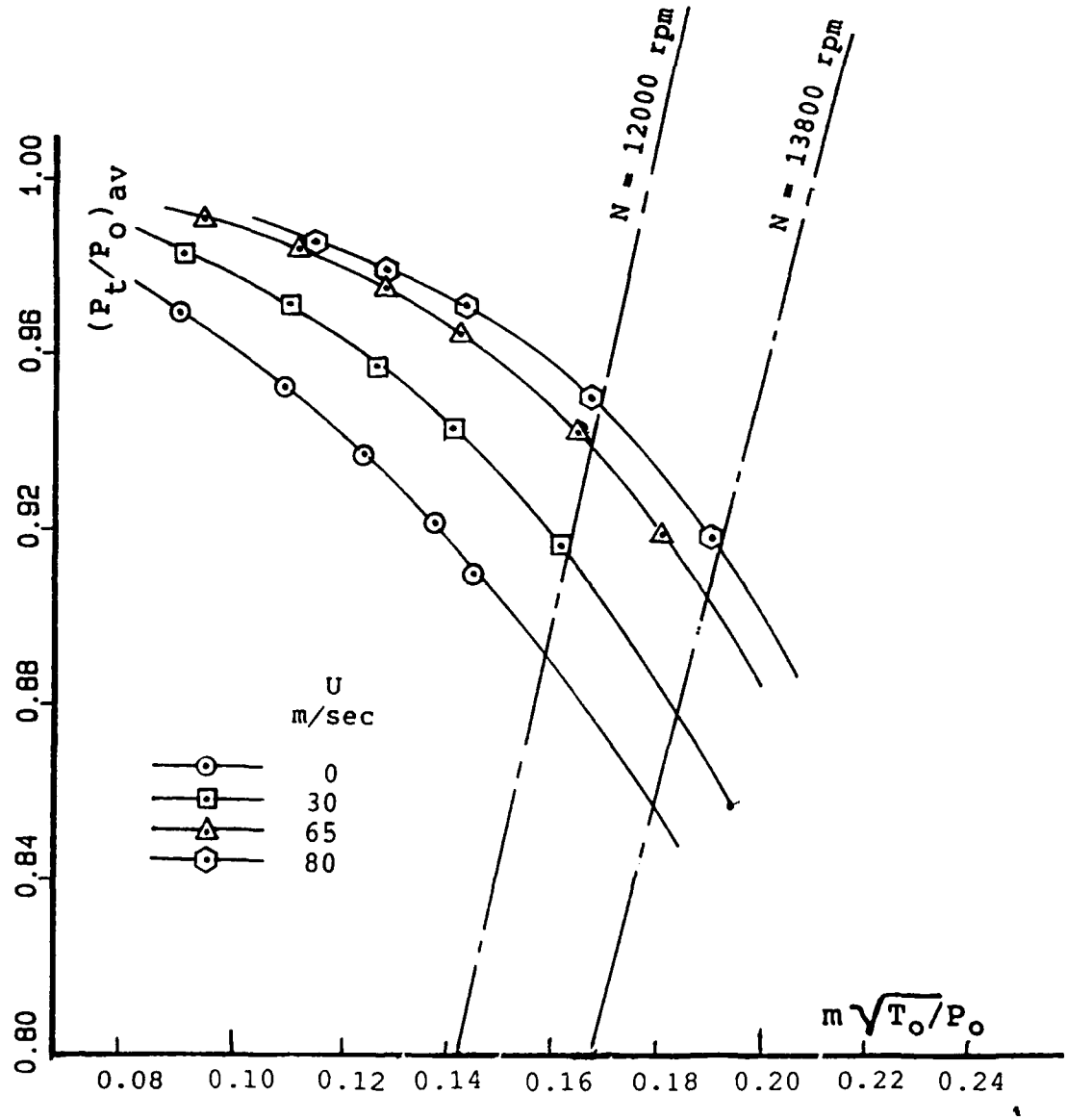

Figure 11: Engine face pressure recoveries for the FCSD configuration at various forward speeds and $\alpha = \beta = 0^o$.

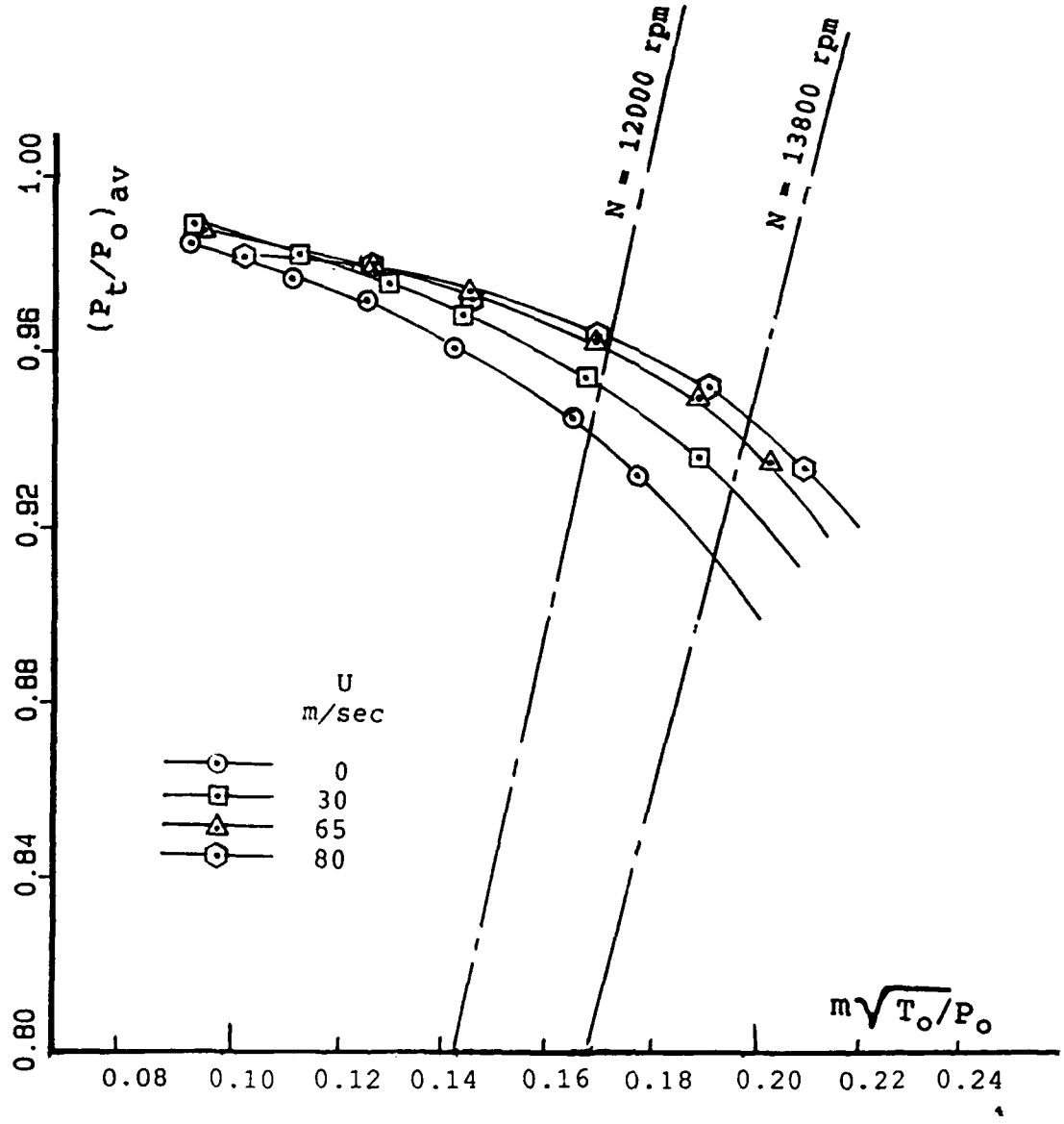

Figure 12: Engine face pressure recoveries for the Louvered aperture auxiliary intake configuration at various forward speeds and $\alpha = \beta = 0^{\circ}$.

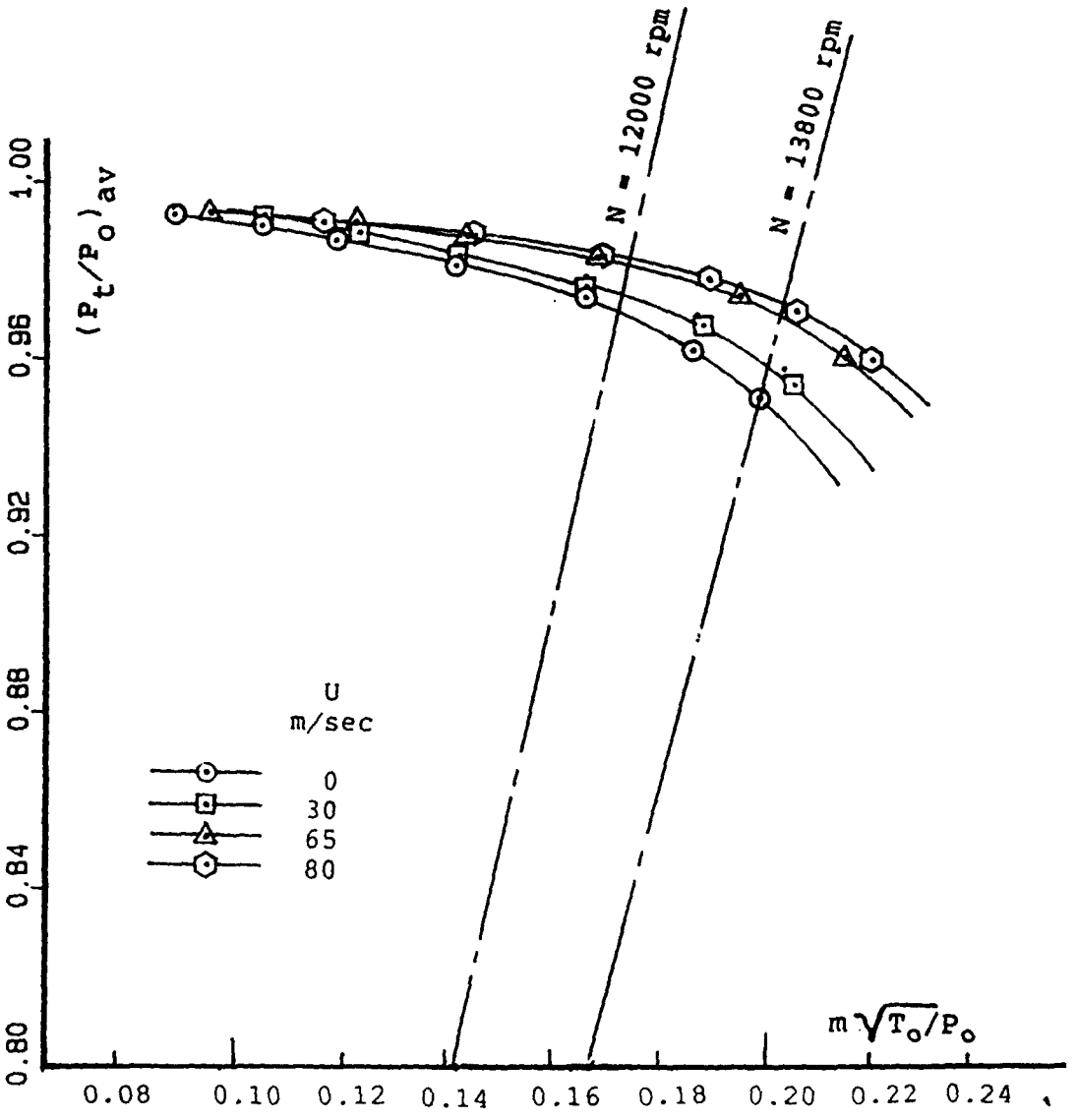

Figure 13: Engine face pressure recoveries for the profiled lipped auxiliary intake configuration at various forward speeds and $\alpha = \beta = 0^o$.

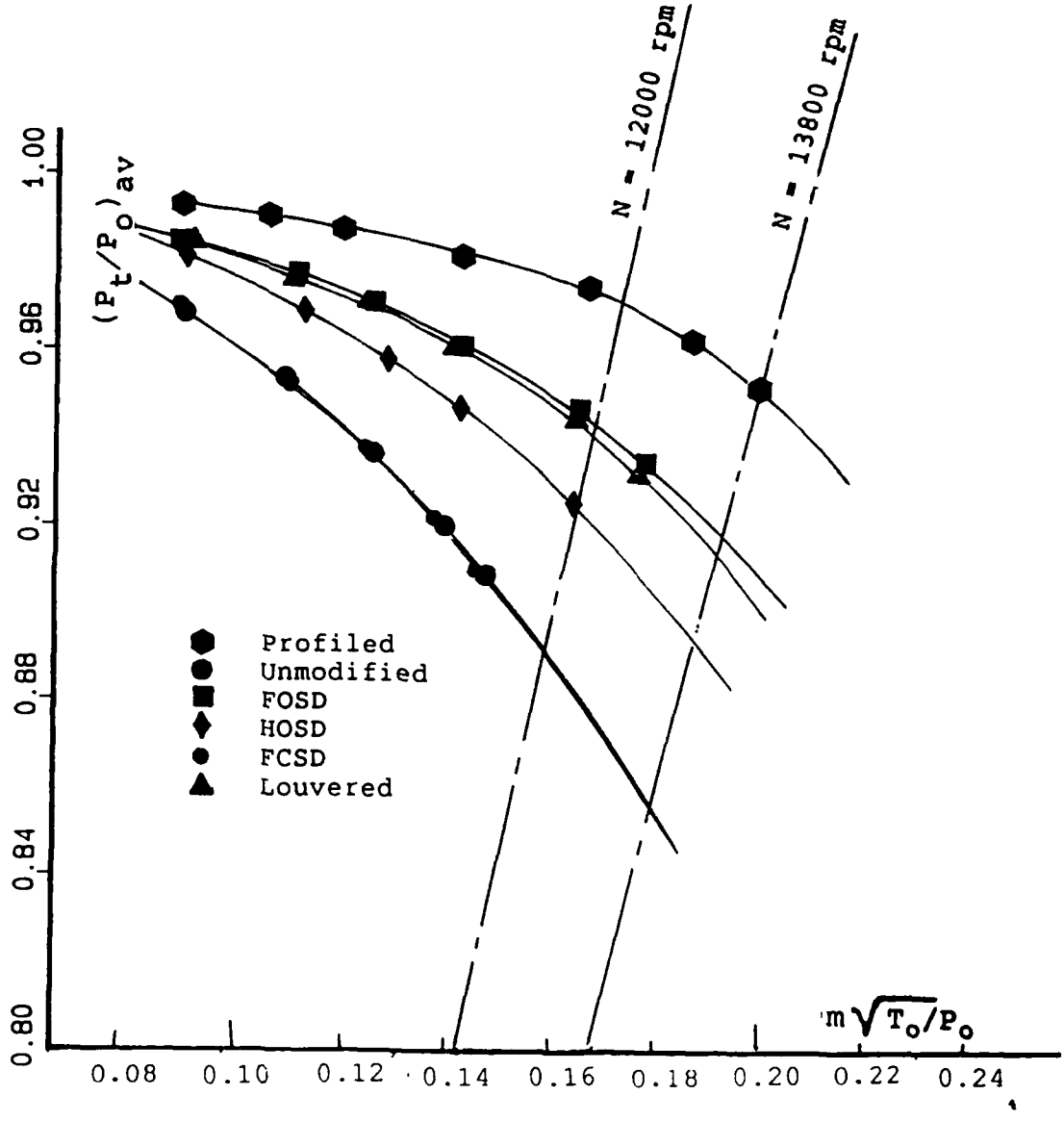

Figure 14: Comparison between all of the auxiliary intake geometries and the unmodified air intake duct in terms of pressure recoveries at the engine face at zero incidence and U = 0 m/sec.

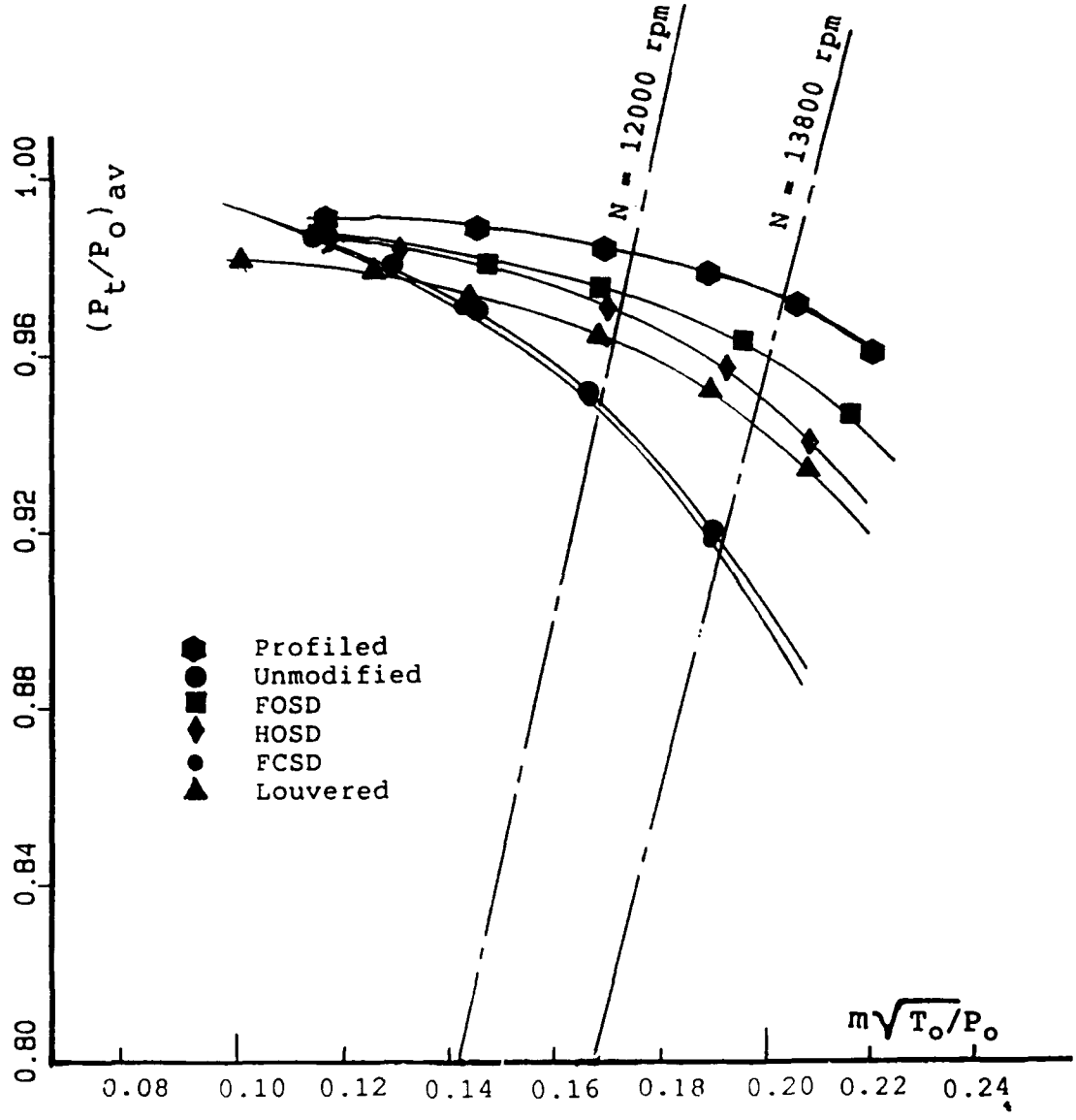

Figure 15: Comparison between all of the auxiliary intake geometries and the unmodified air intake duct in terms of pressure recoveries at the engine face at zero incidence and U = 80 m/sec.

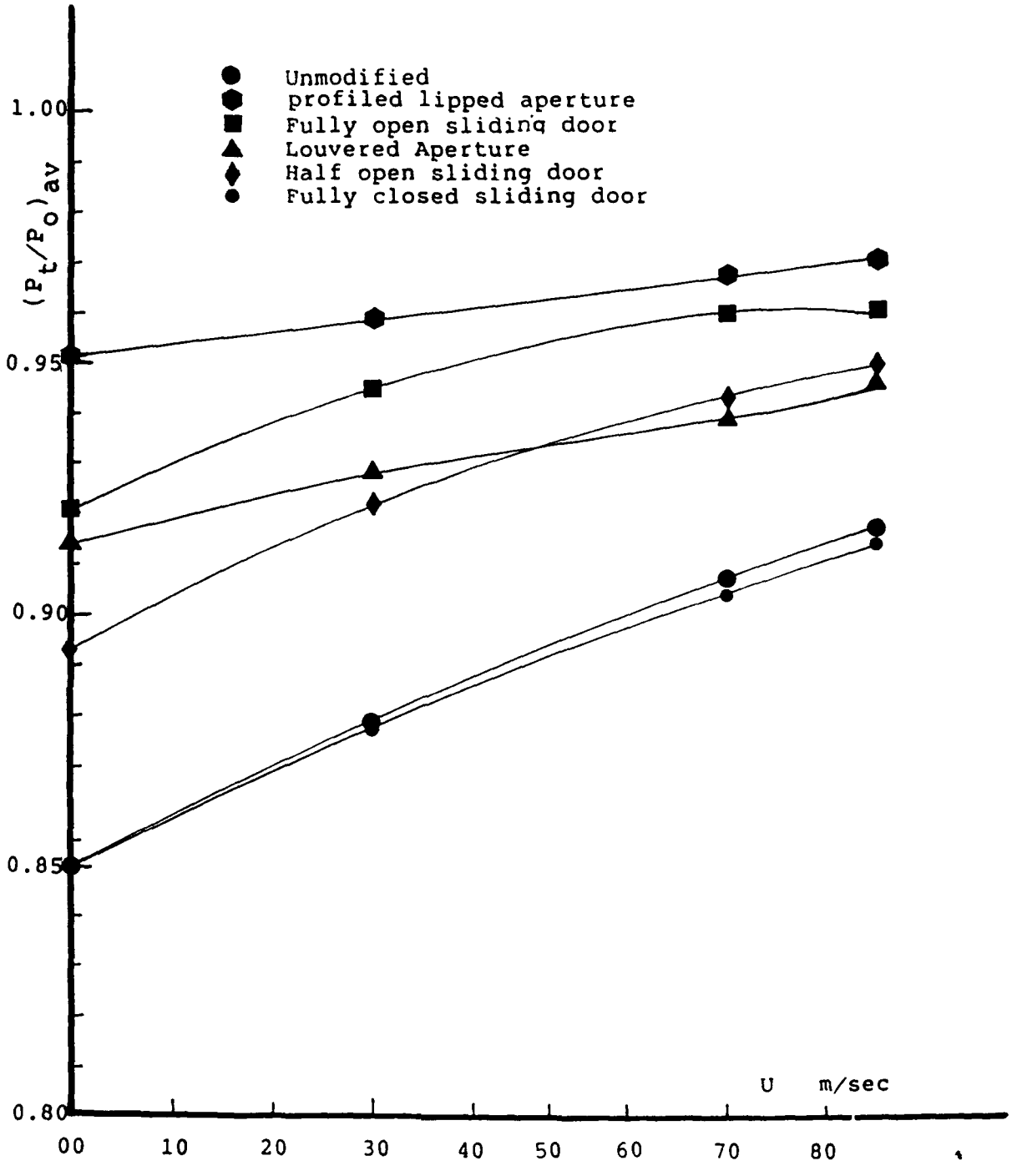

Figure 16: Comparison between all of the auxiliary intake geometries at the fixed engine speed of 13800 RPM and at zero incidence, in terms of engine face pressure recoveries versus aircraft forward speed.

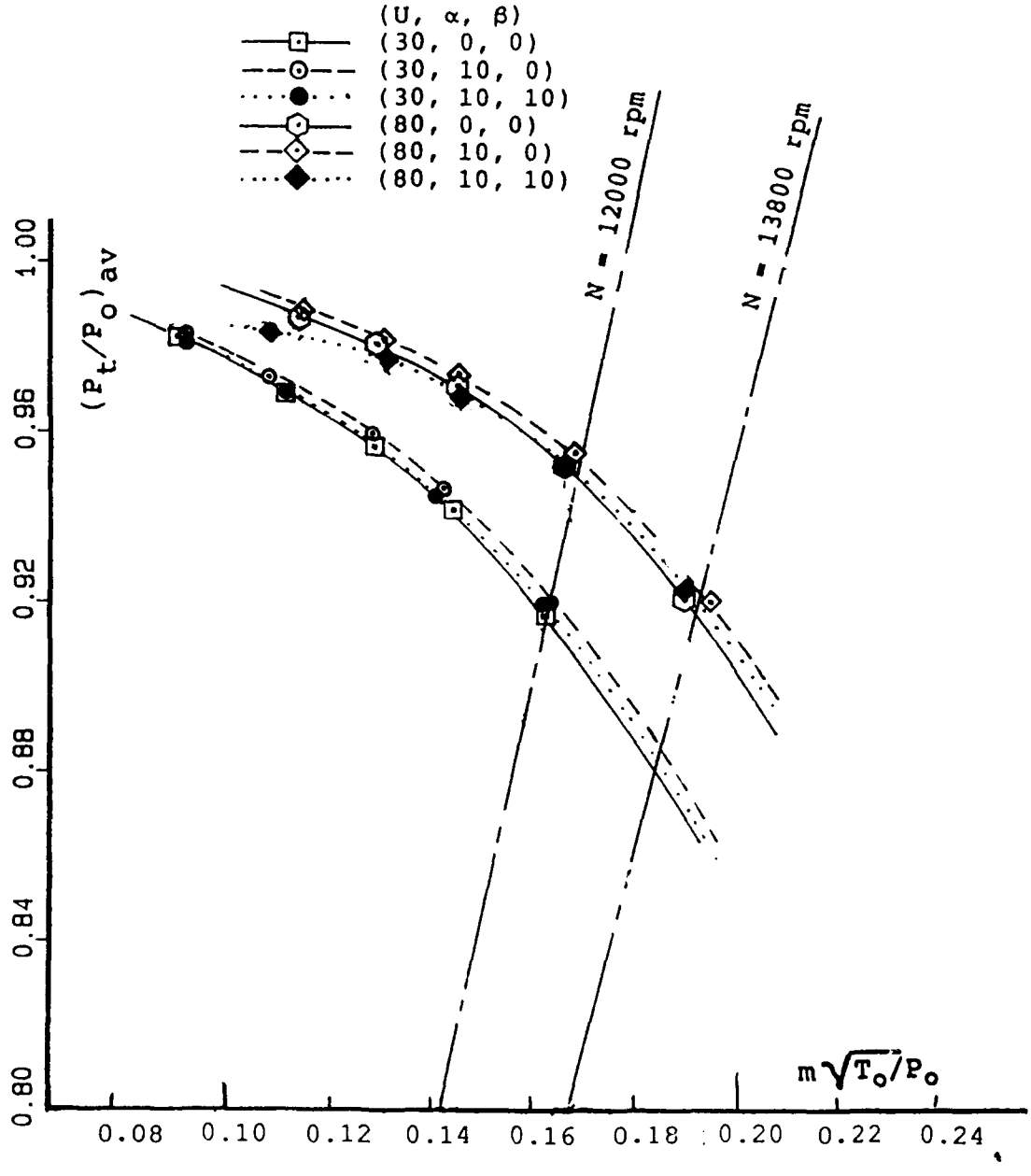

Figure 17: Engine face pressure recoveries for the unmodified configuration at various forward speeds and α & β combinations.

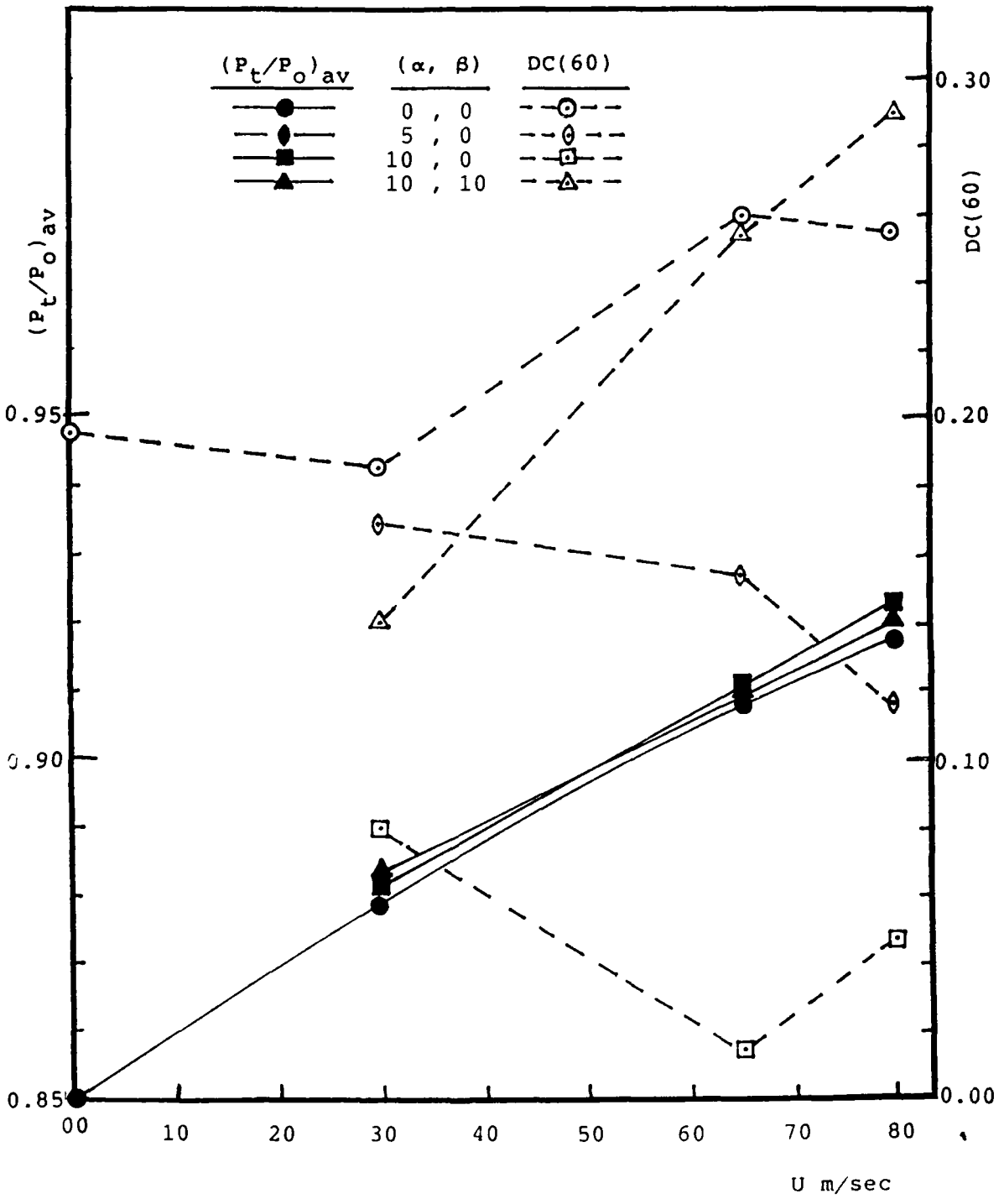

Figure 18: Effect of forward speed on the performance of the unmodified air intake duct for various α & β combinations, at N = 13800 RPM.

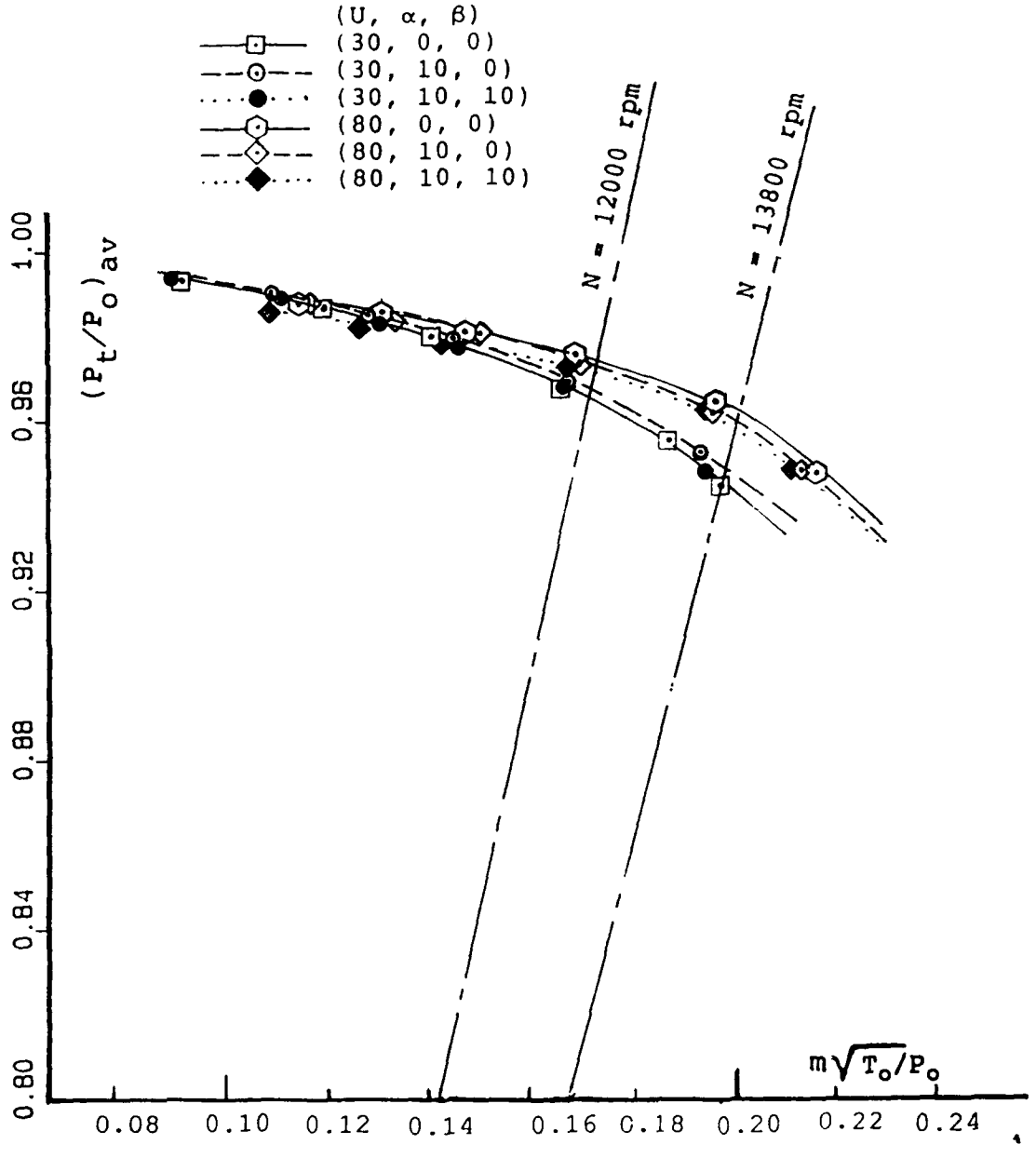

Figure 19: Engine face pressure recoveries for the FOSD auxiliary intake configuration at various forward speeds and α & β combinations.

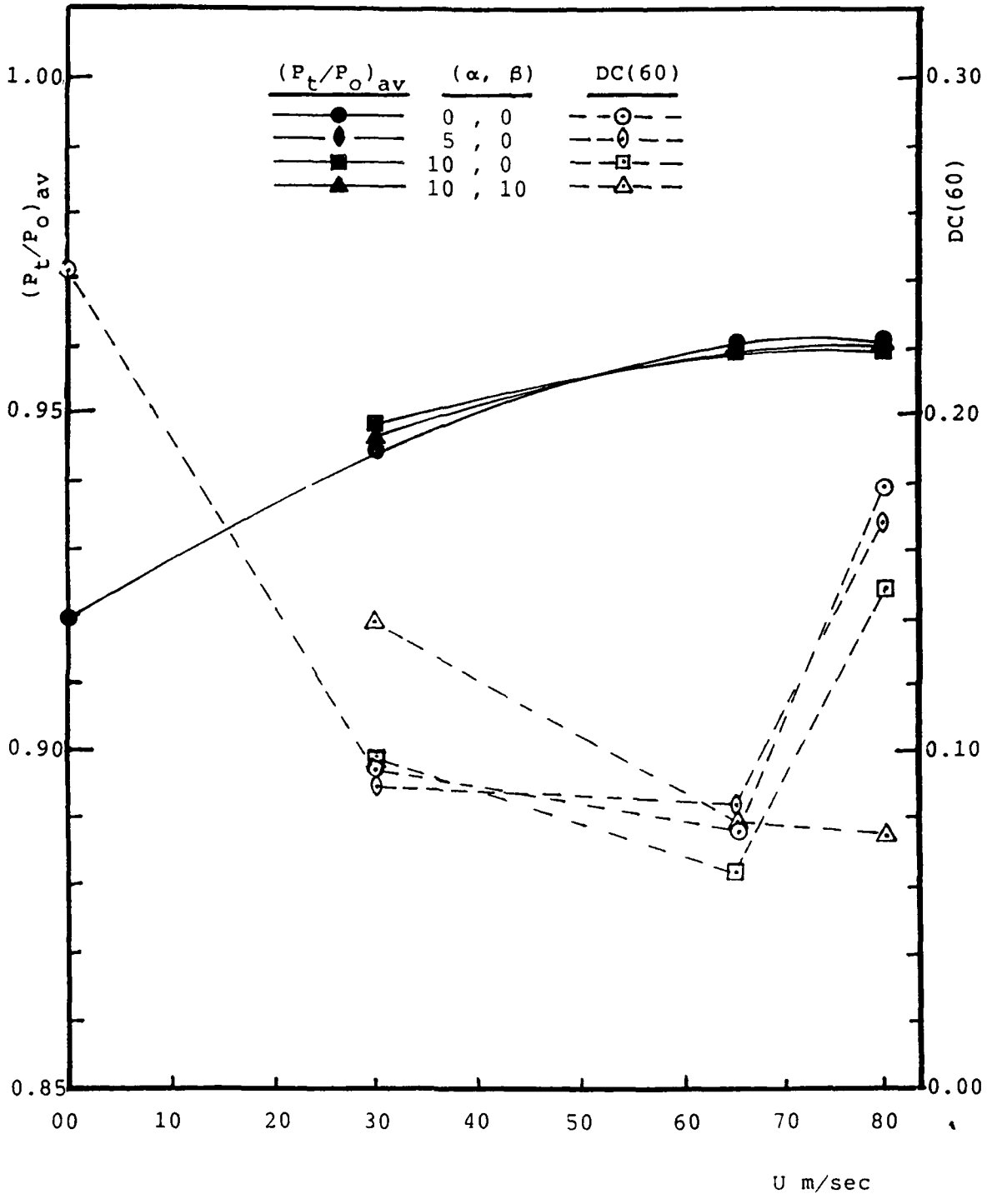

Figure 20: Effect of forward speed with the FOSD auxiliary intake for various α & β combinations, at N = 13800 RPM.

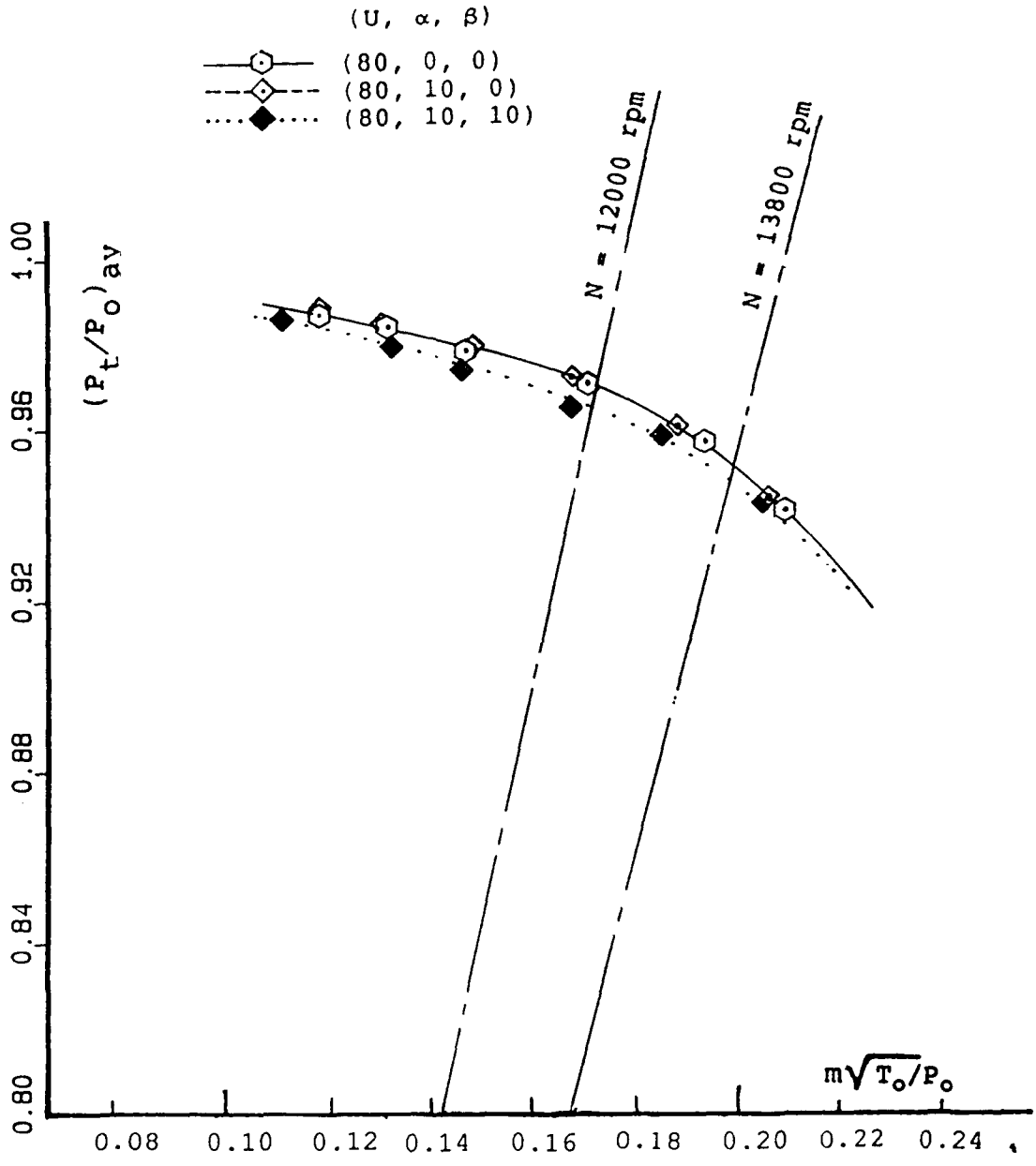

Figure 21: Engine face pressure recoveries for the HOSD auxiliary intake configuration at various forward speeds and α & β combinations.

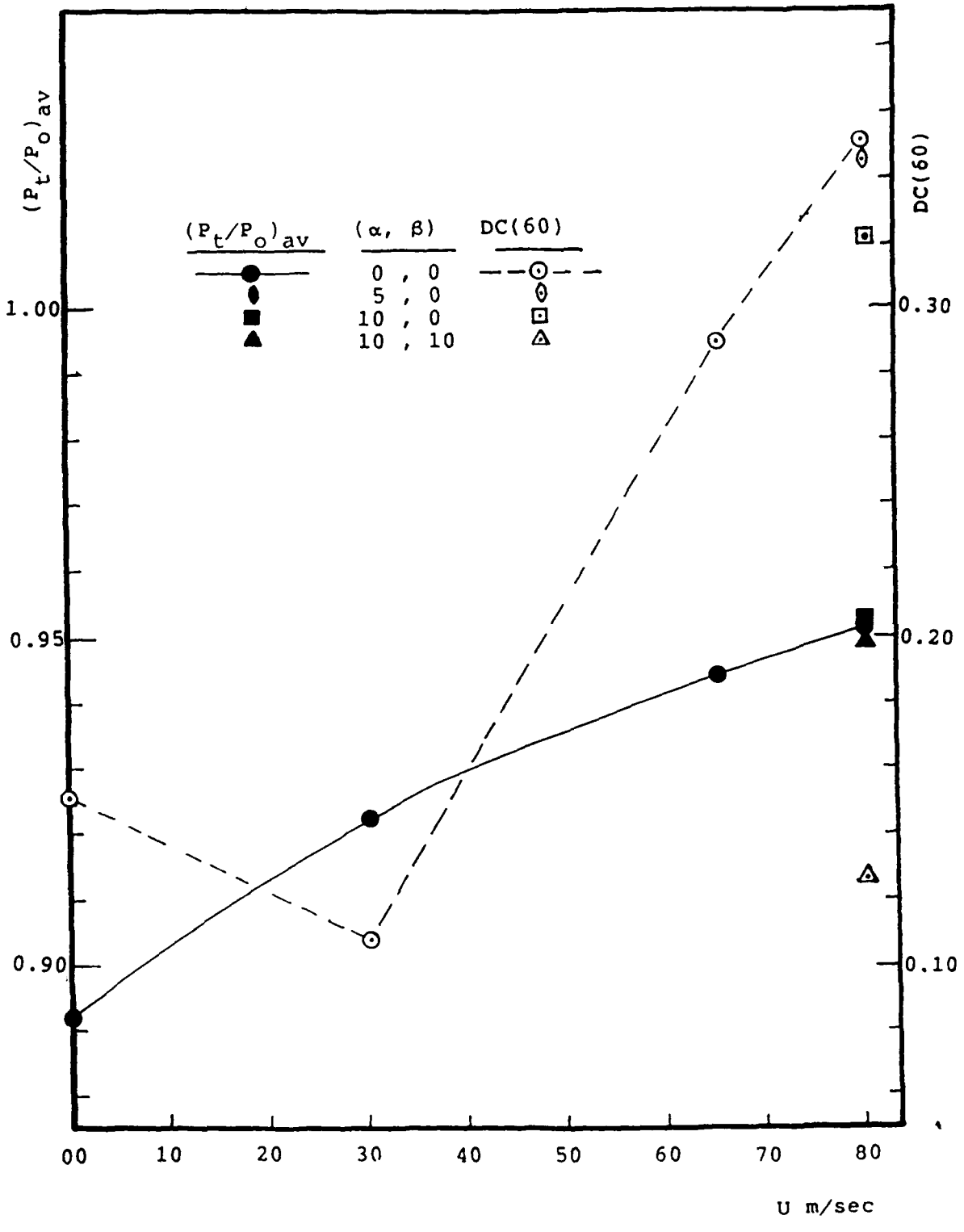

Figure 22: Effect of forward speed with the HOSD auxiliary intake for various α & β combinations, at N = 13800 RPM.

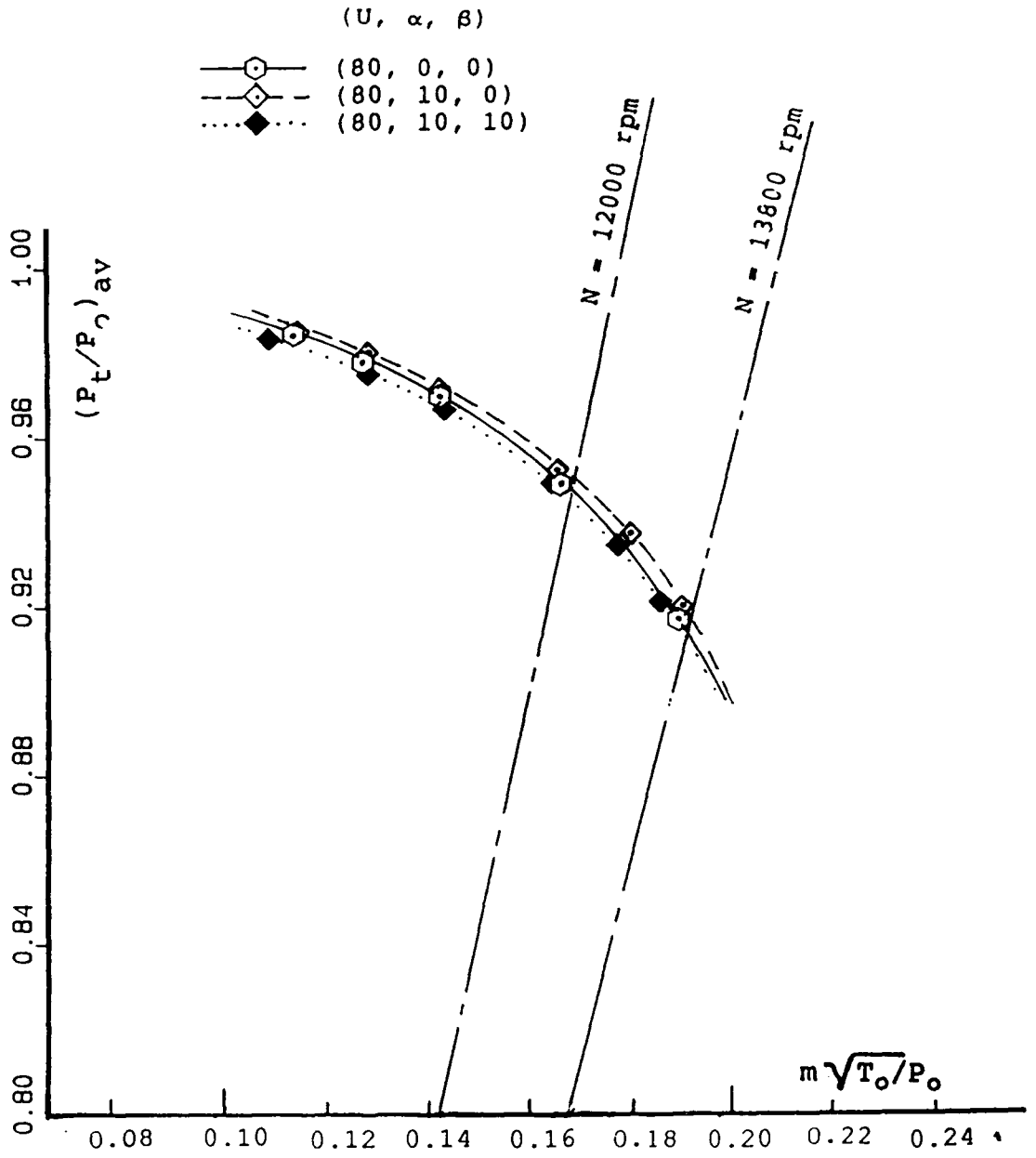

Figure 23: Engine face pressure recoveries for the FCSD auxiliary intake configuration at various forward speeds and α & β combinations.

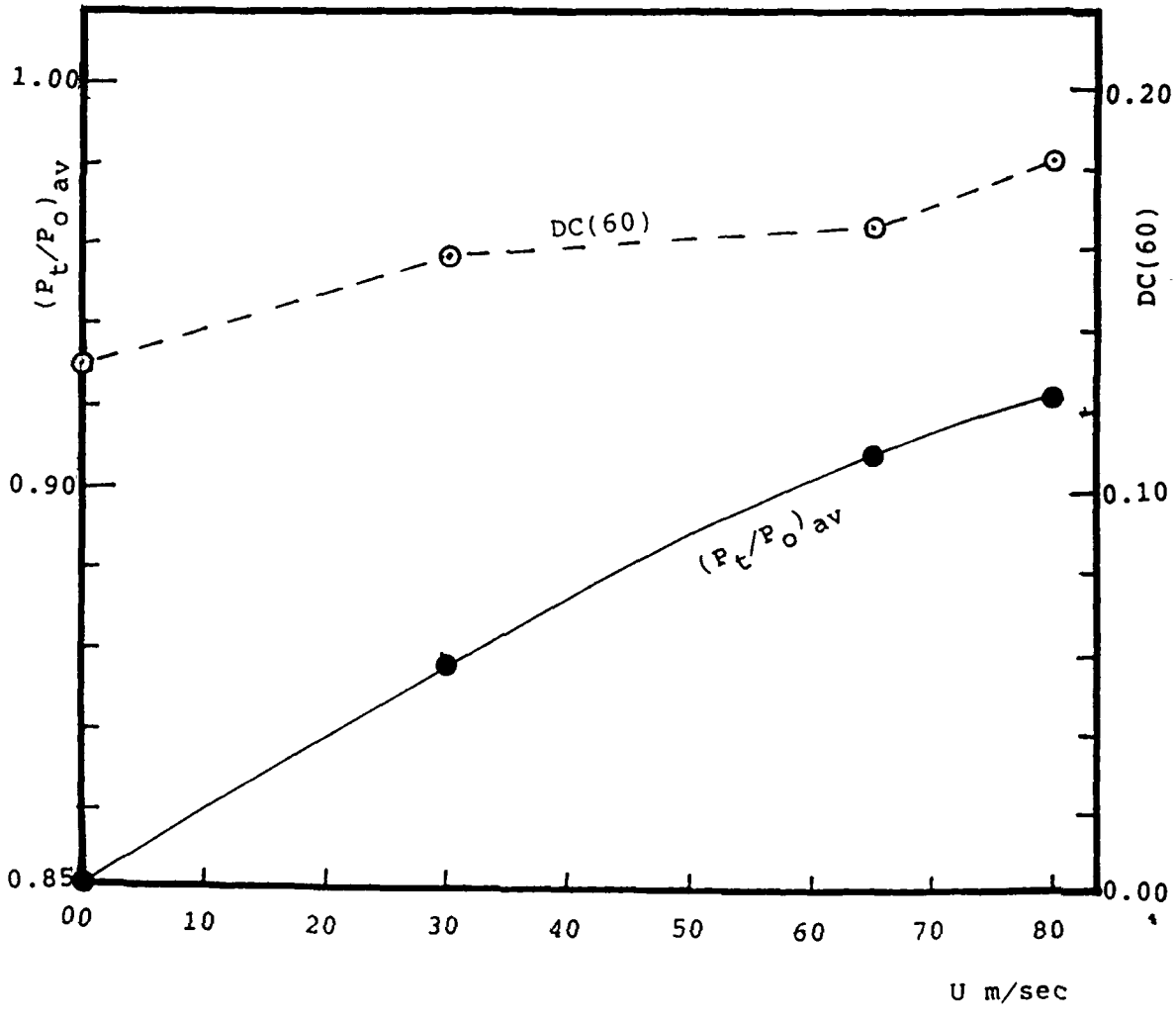

Figure 24: Effect of forward speed with the FCSD auxiliary intake for various α & β combinations, at N = 13800 RPM.

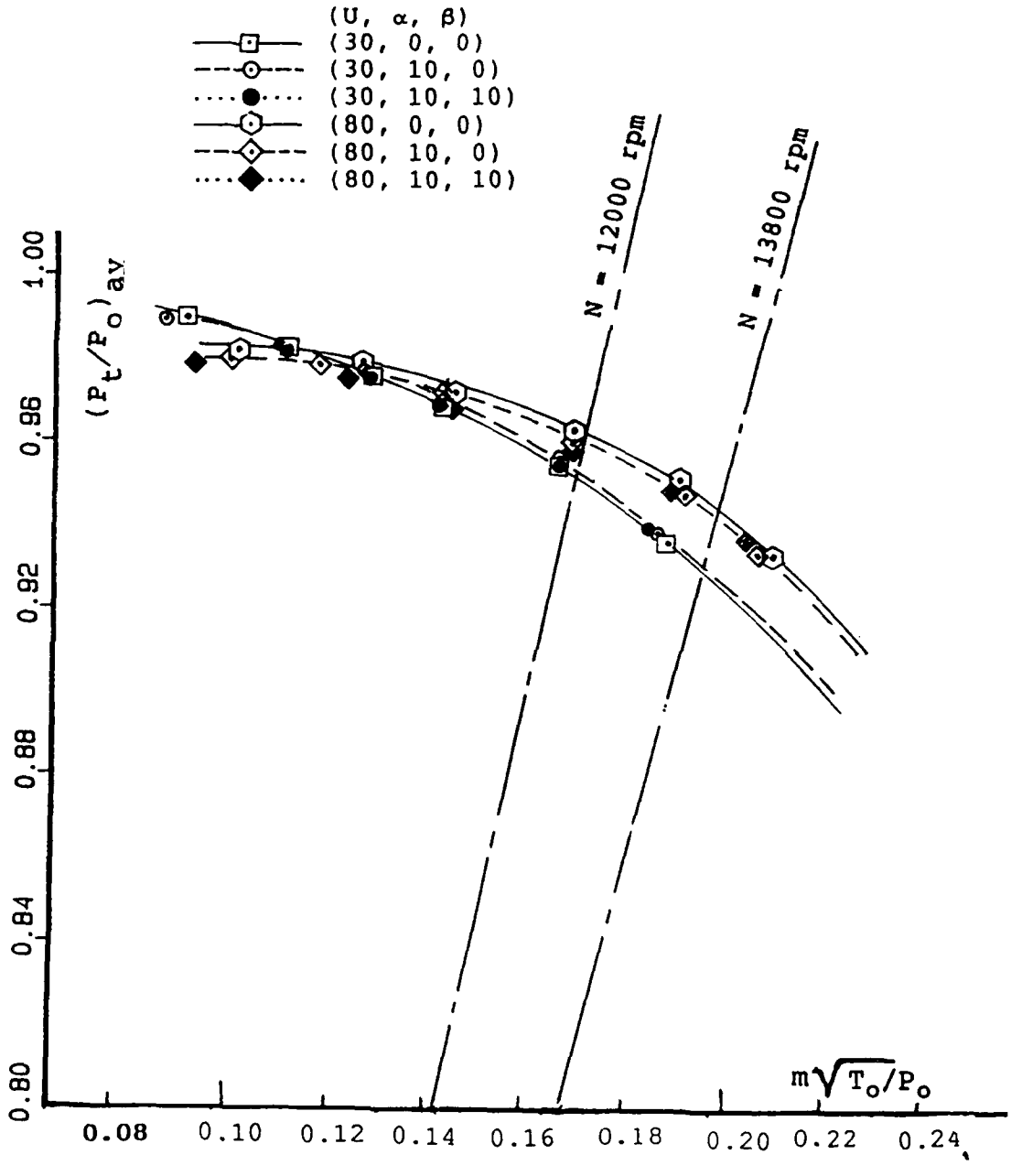

Figure 25: Engine face pressure recoveries for the louvered aperture auxiliary intake configuration at various forward speeds and α & β combinations.

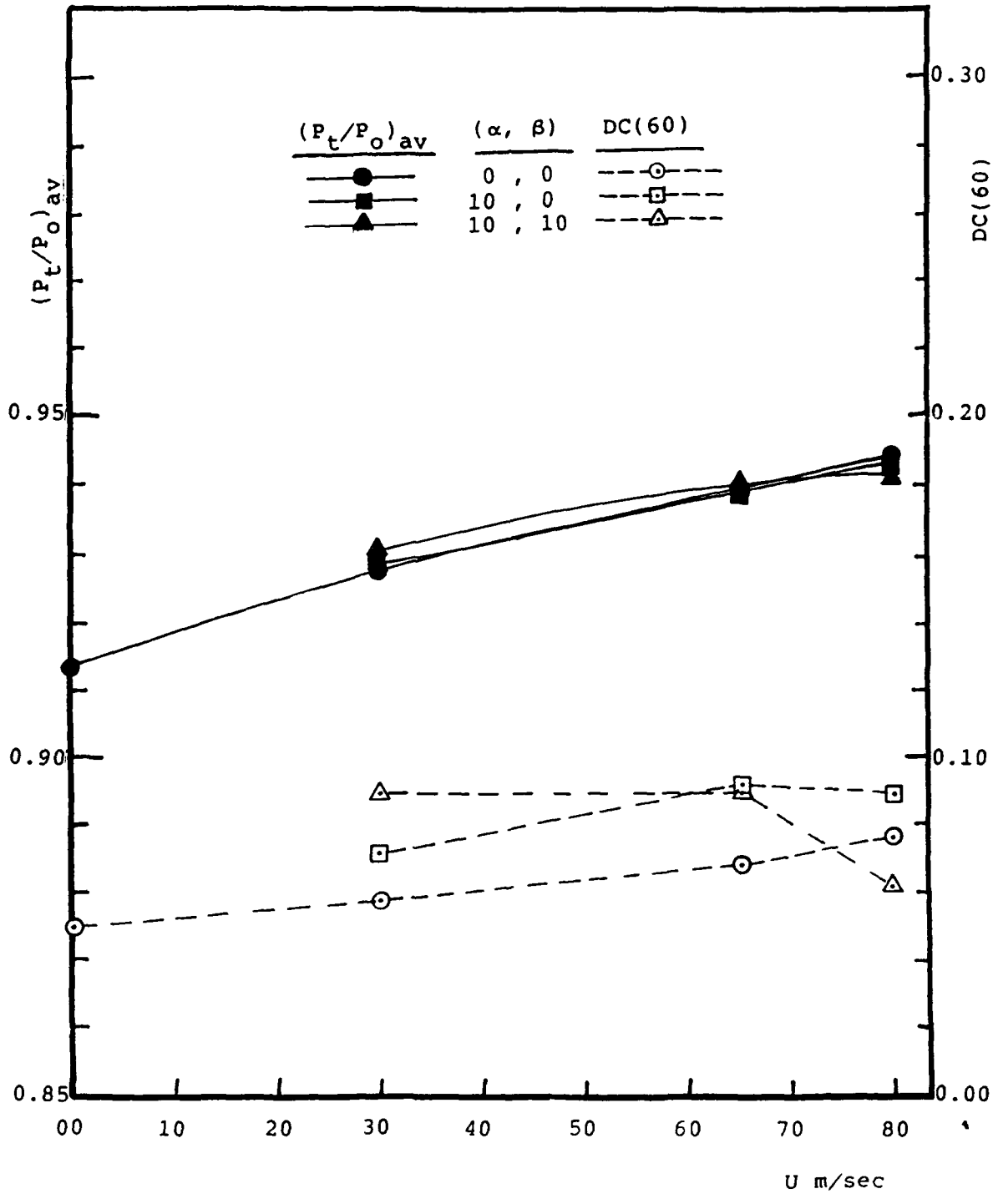

Figure 26: Effect of forward speed with the louvered aperture auxiliary intake for various α & β combinations, at N = 13800 RPM.

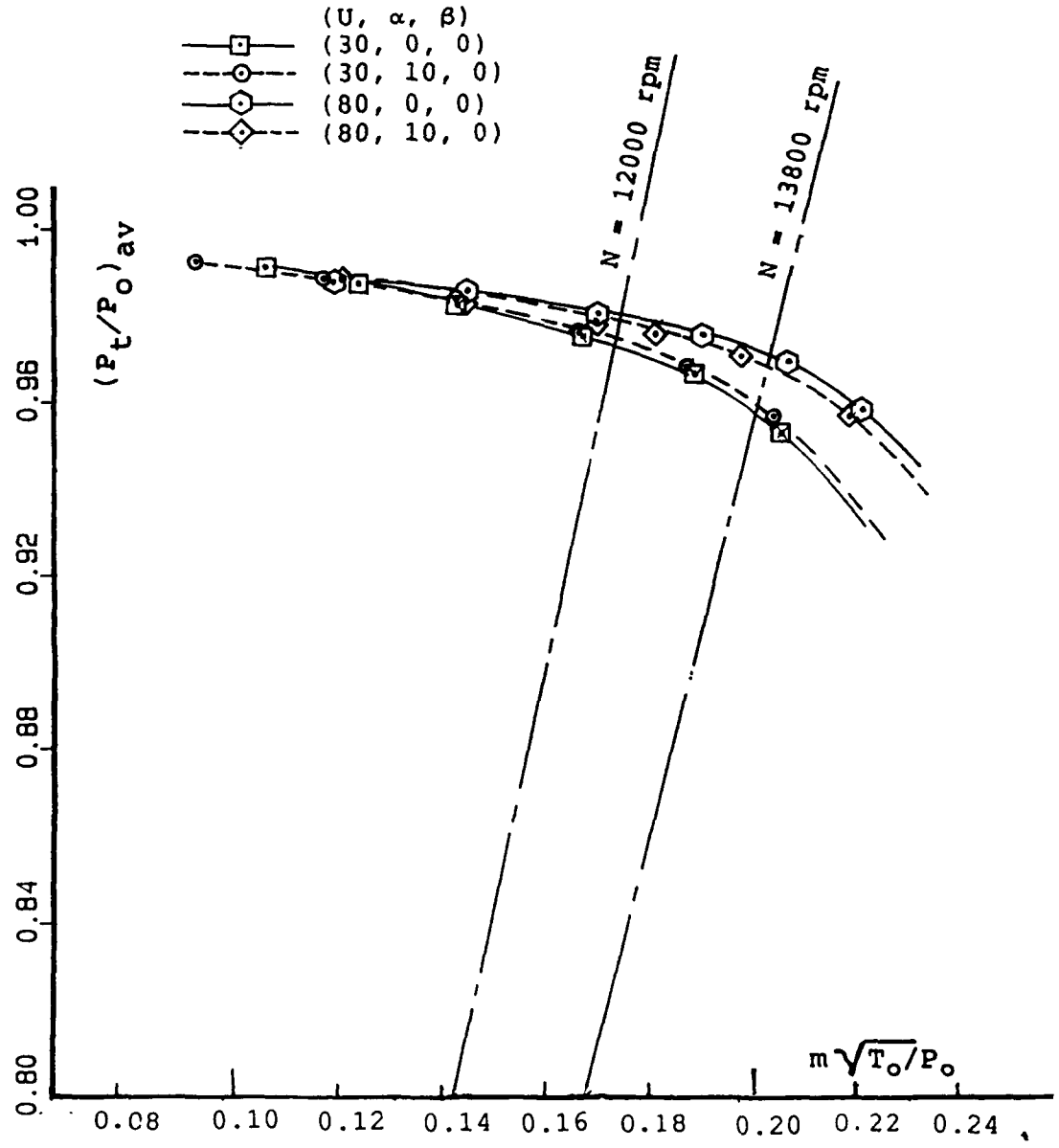

Figure 27: Engine face pressure recoveries for the profiled lipped auxiliary intake configuration at various forward speeds and α & β combinations.

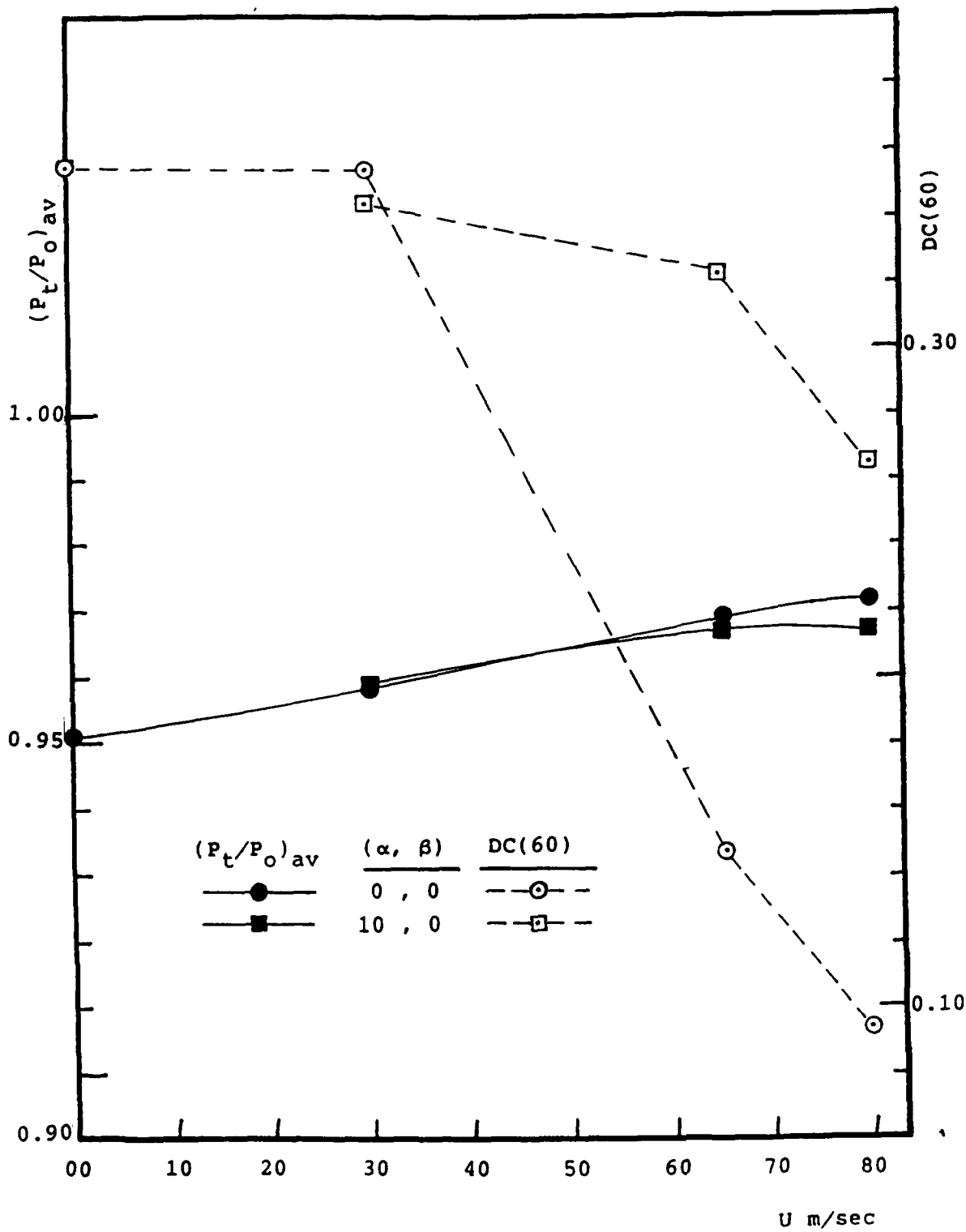

Figure 28: Effect of forward speed with the profiled lipped auxiliary intake for various α & β combinations, at N = 13800 RPM.

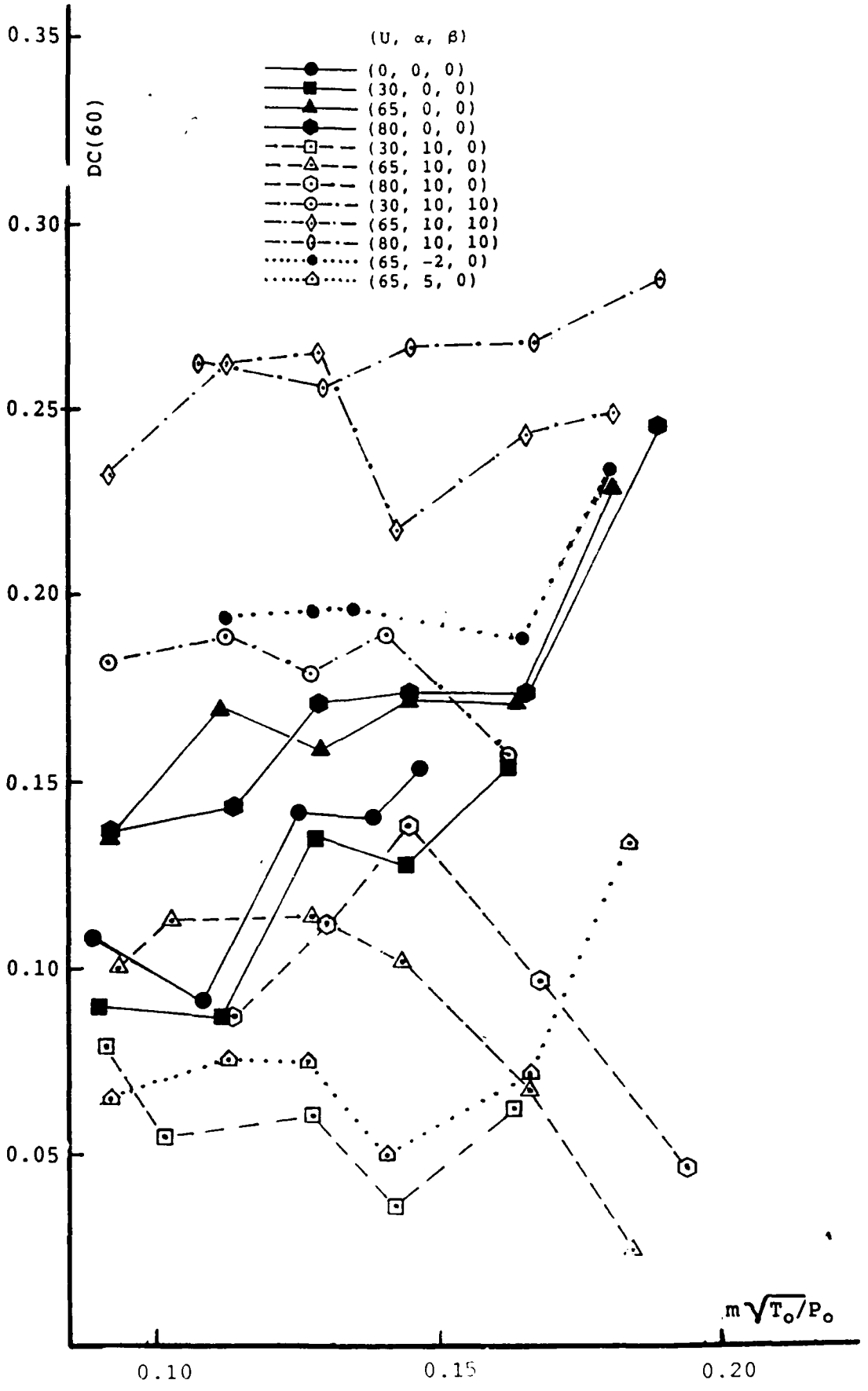

Figure 29: Distortion factors for the unmodified configuration for various U, α and β combinations.

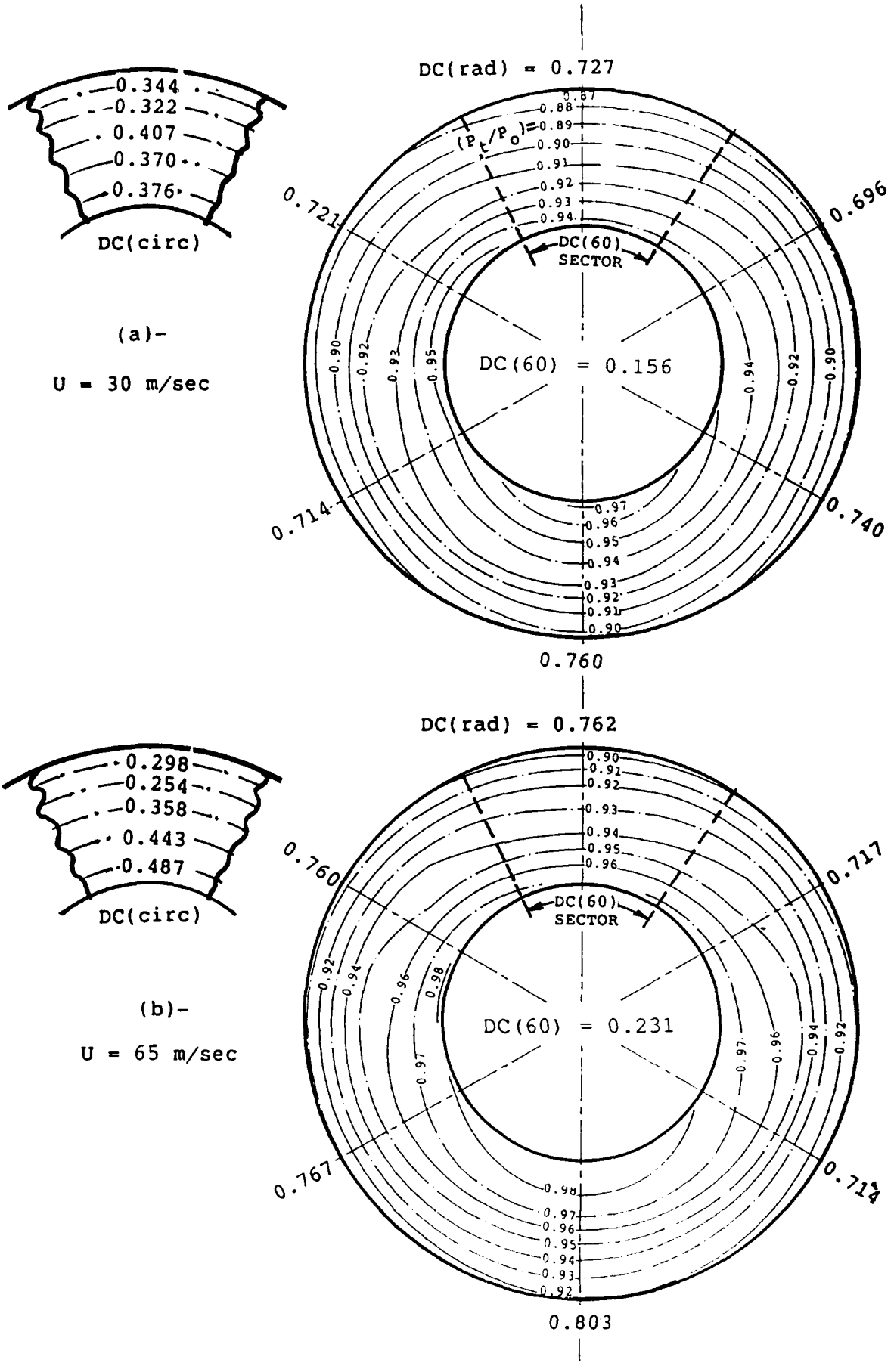

Figure 30- (a) and (b)

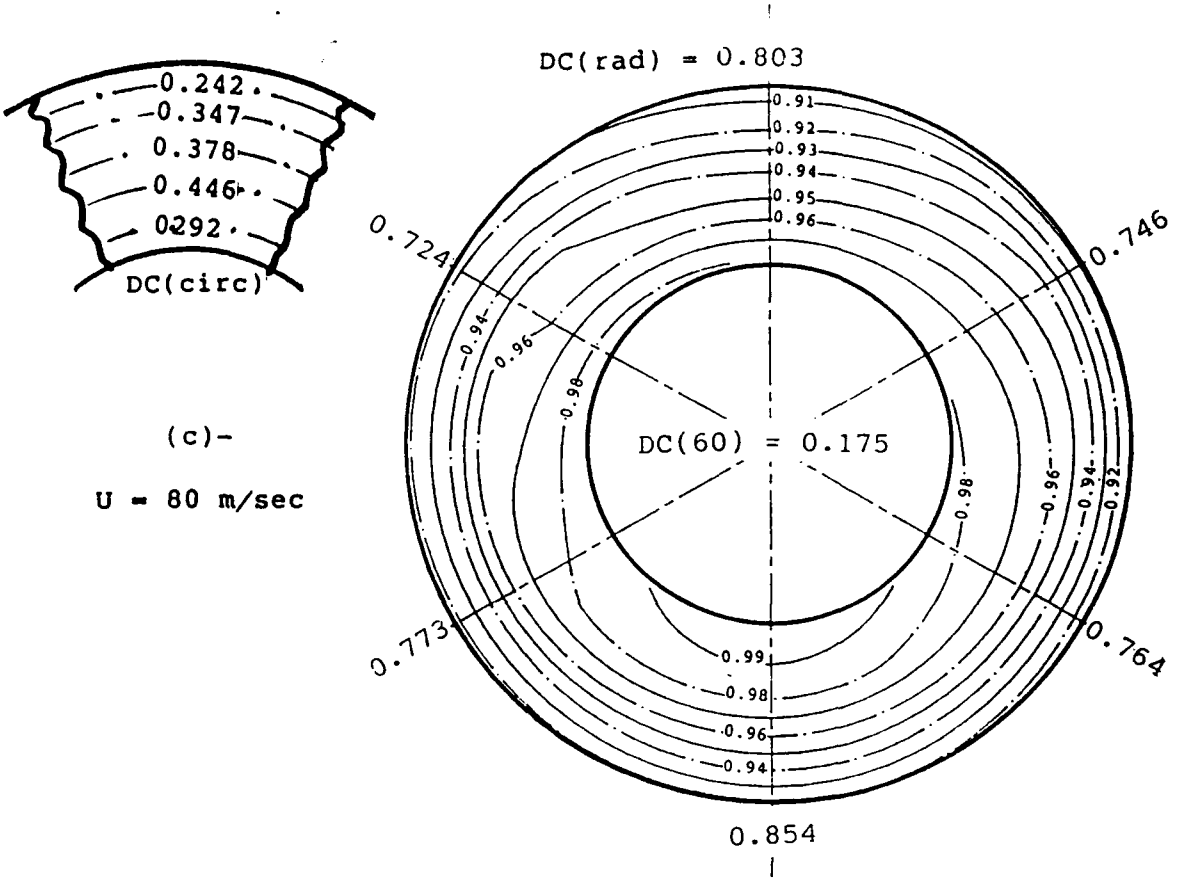

Figure 30: Effect of Forward speed on total pressure distribution at the engine face for the unmodified air intake duct at $\alpha = \beta = 0^{o}$ and N = 12000 RPM.

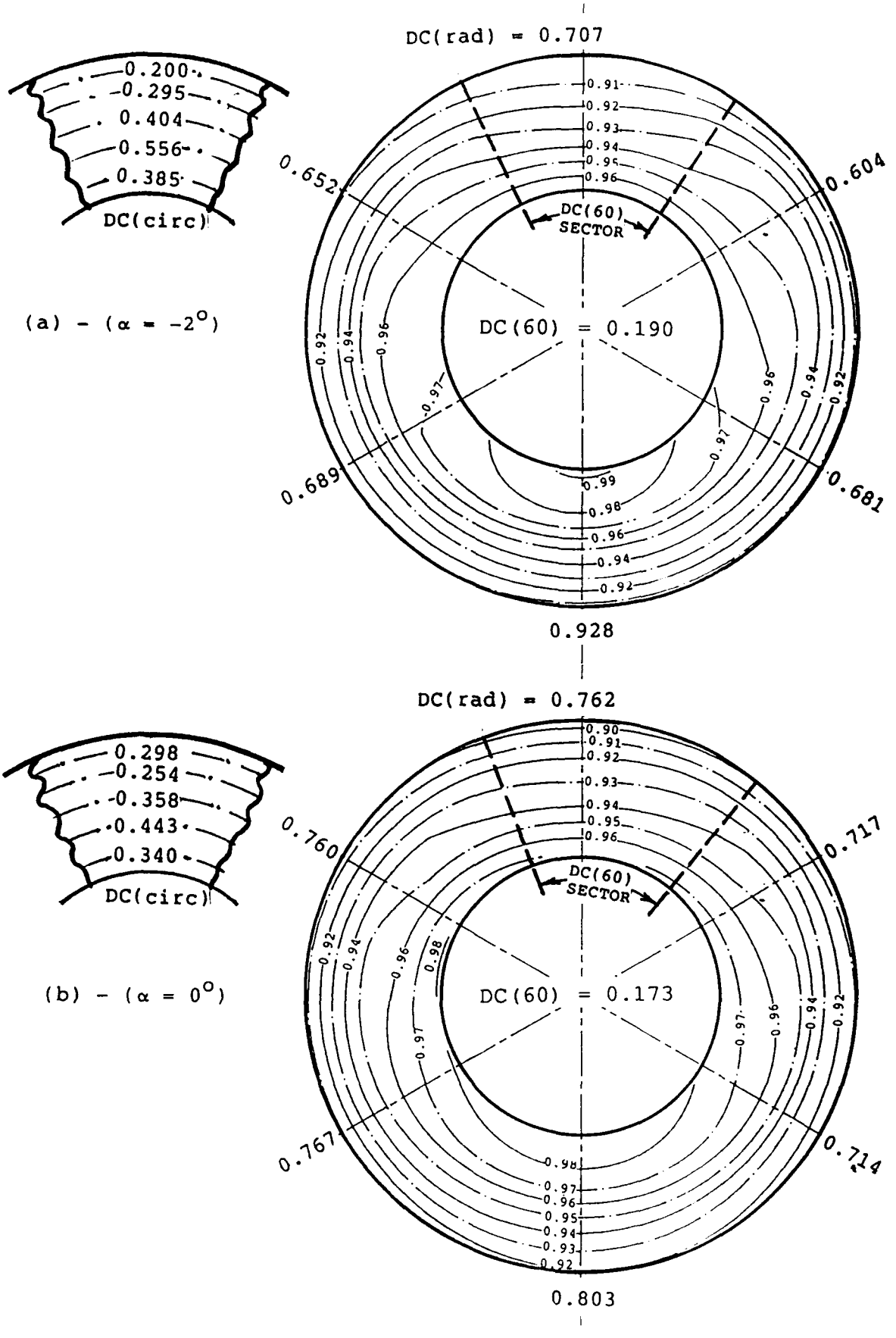

Figure 31- (a) and (b)

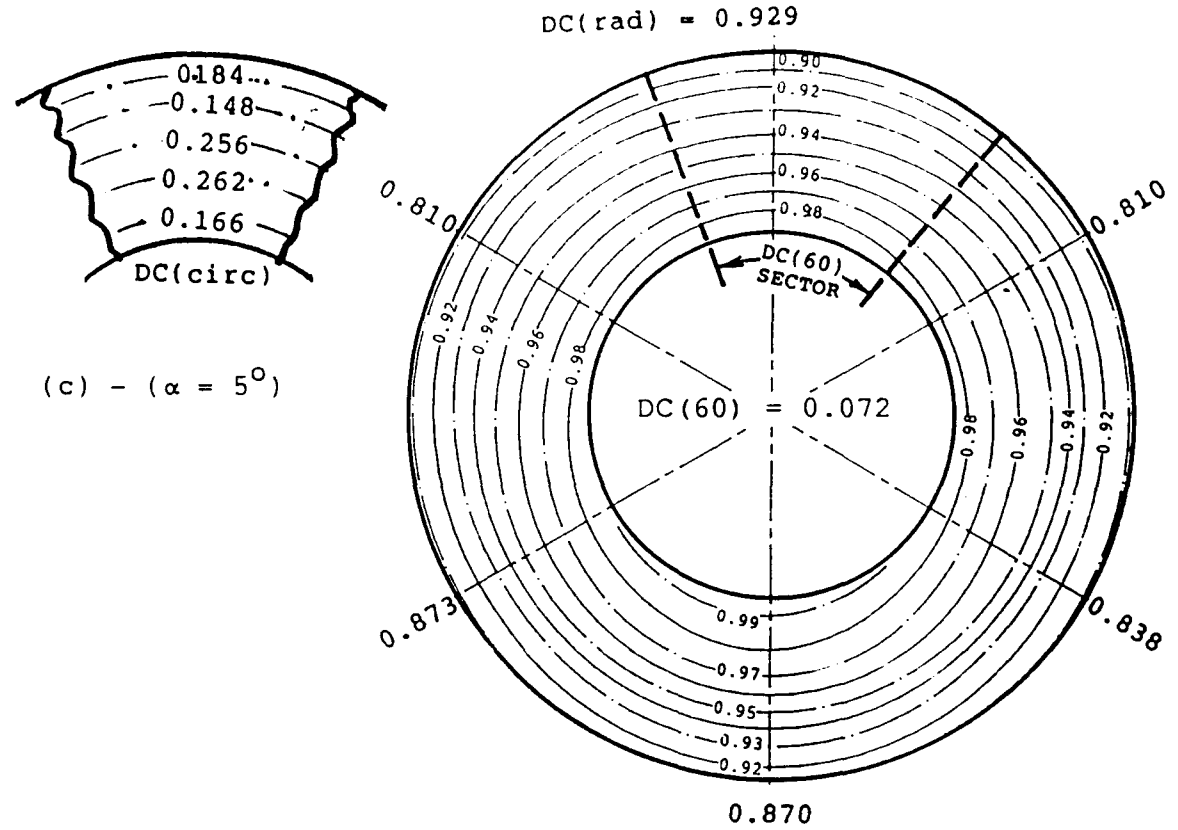

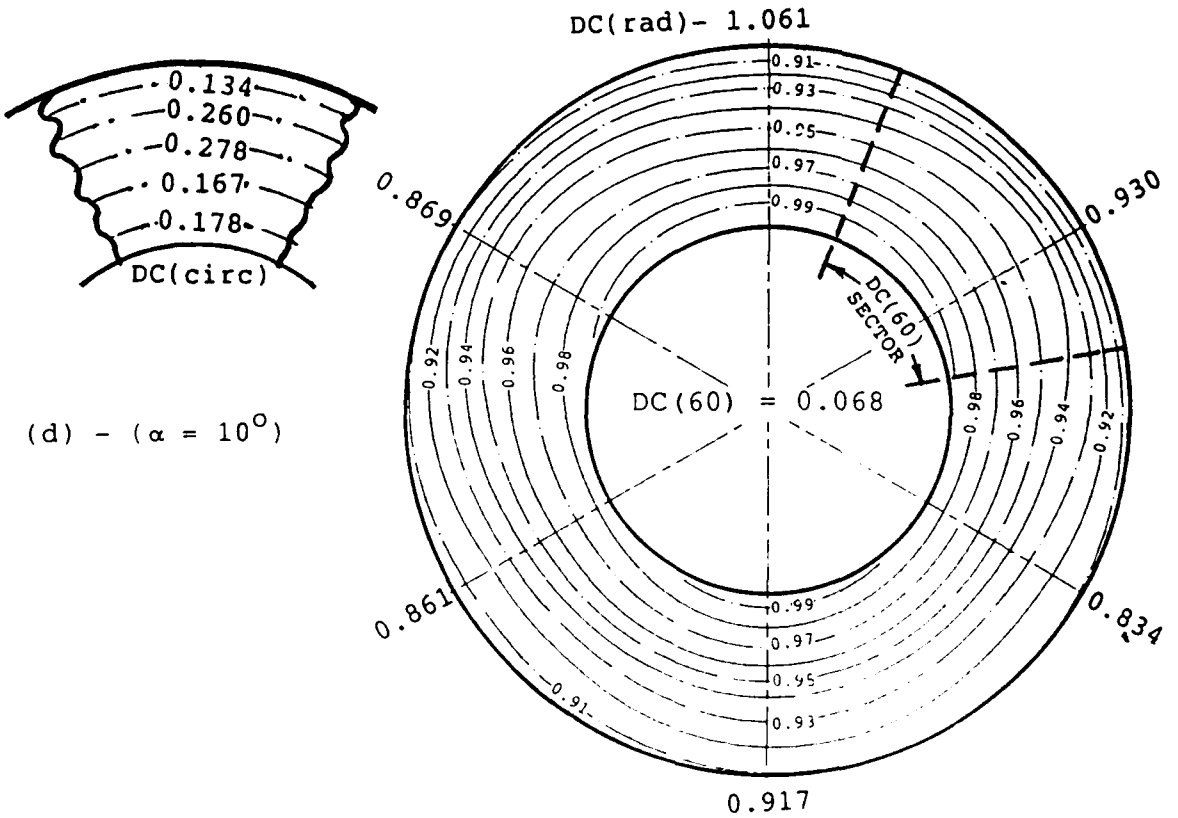

Figure 31: Effect of aircraft incidence on total pressure distribution at the engine face for the unmodified air intake duct at N = 12000 RPM, $\beta = 0^{o}$ and U = 65 m/sec.

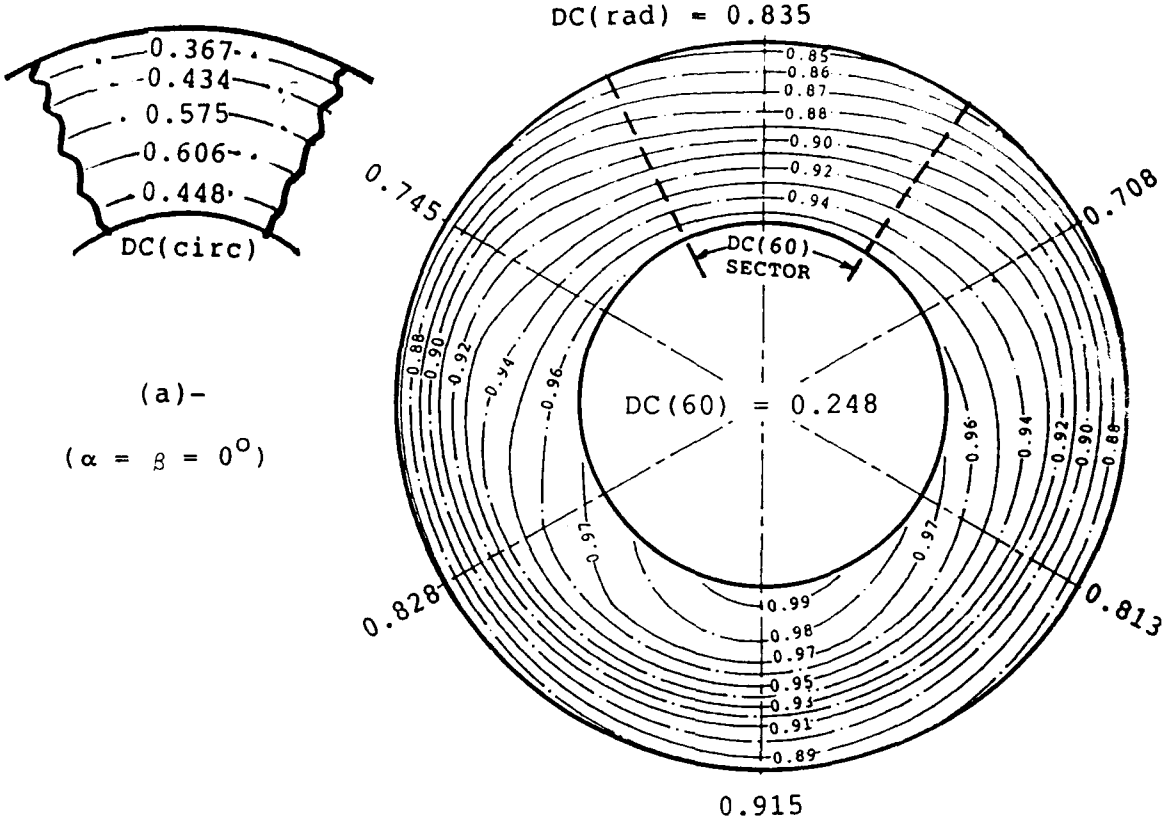

(a)-

($\alpha = \beta = 0^{o}$)

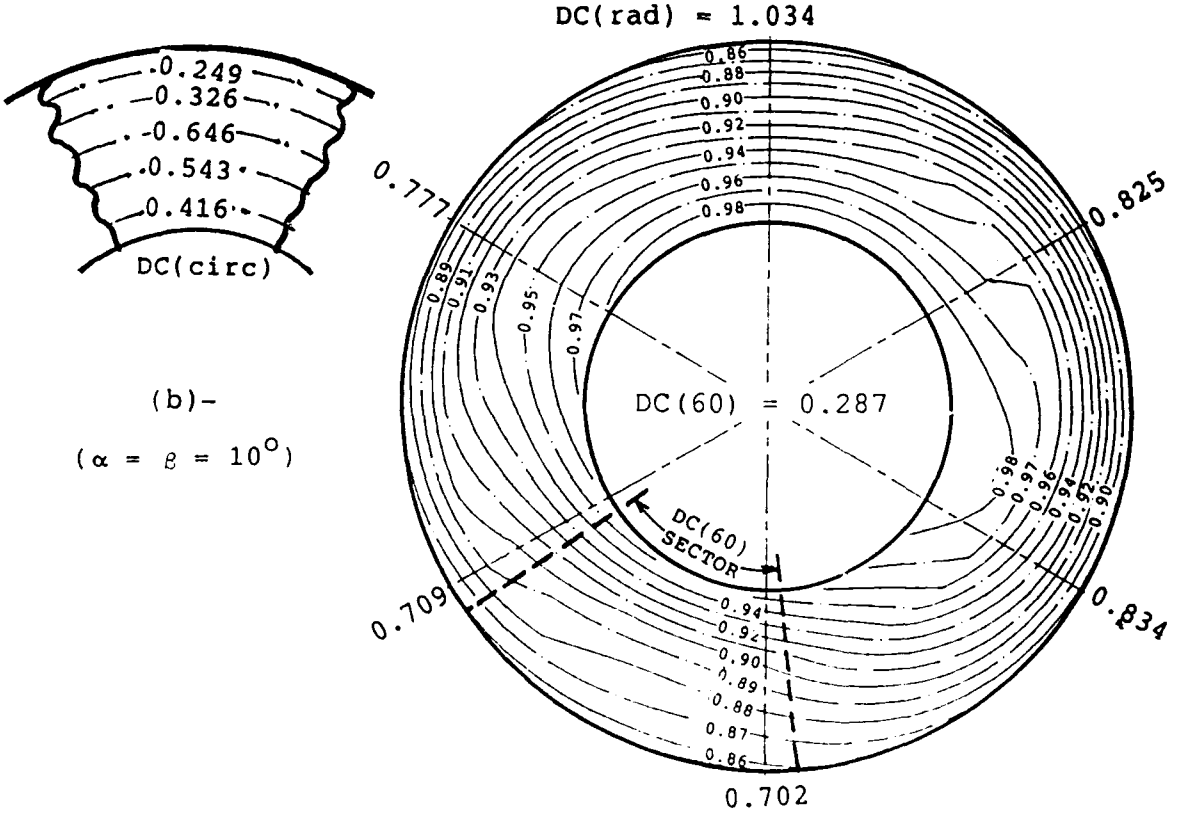

(b)-

($\alpha = \beta = 10^{o}$)

Figure 32: Comparison between zero incidence ($\alpha = \beta = 0^{o}$) and the extreme $\alpha = \beta = 10^{o}$ attitudes in terms of total pressure distribution at the engine face for the unmodified configuration at N = 13800 RPM and U = 80 m/sec.

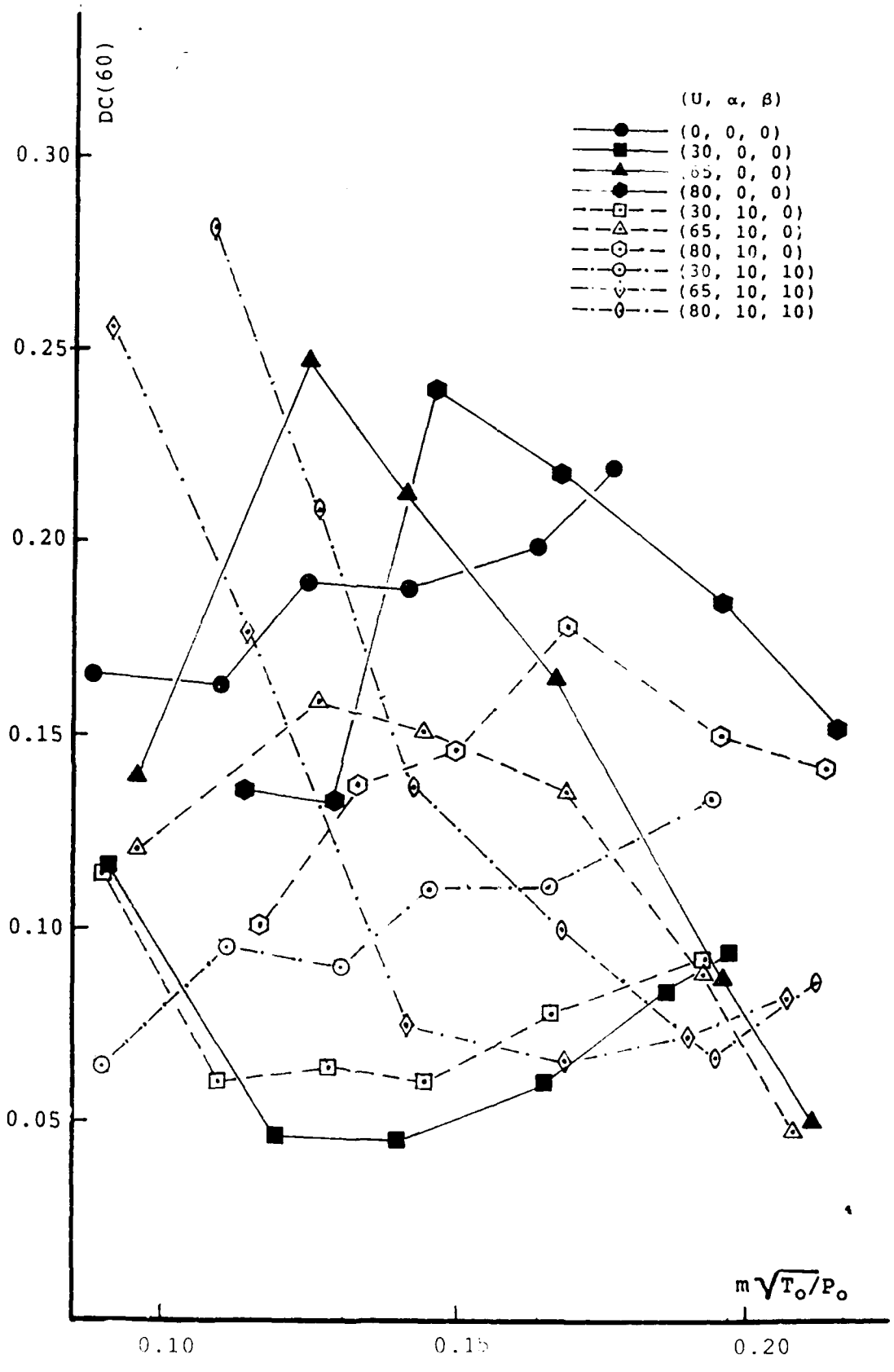

Figure 33: Distortion factors for the FOSD auxiliary intake configuration for various U, α and β combinations.

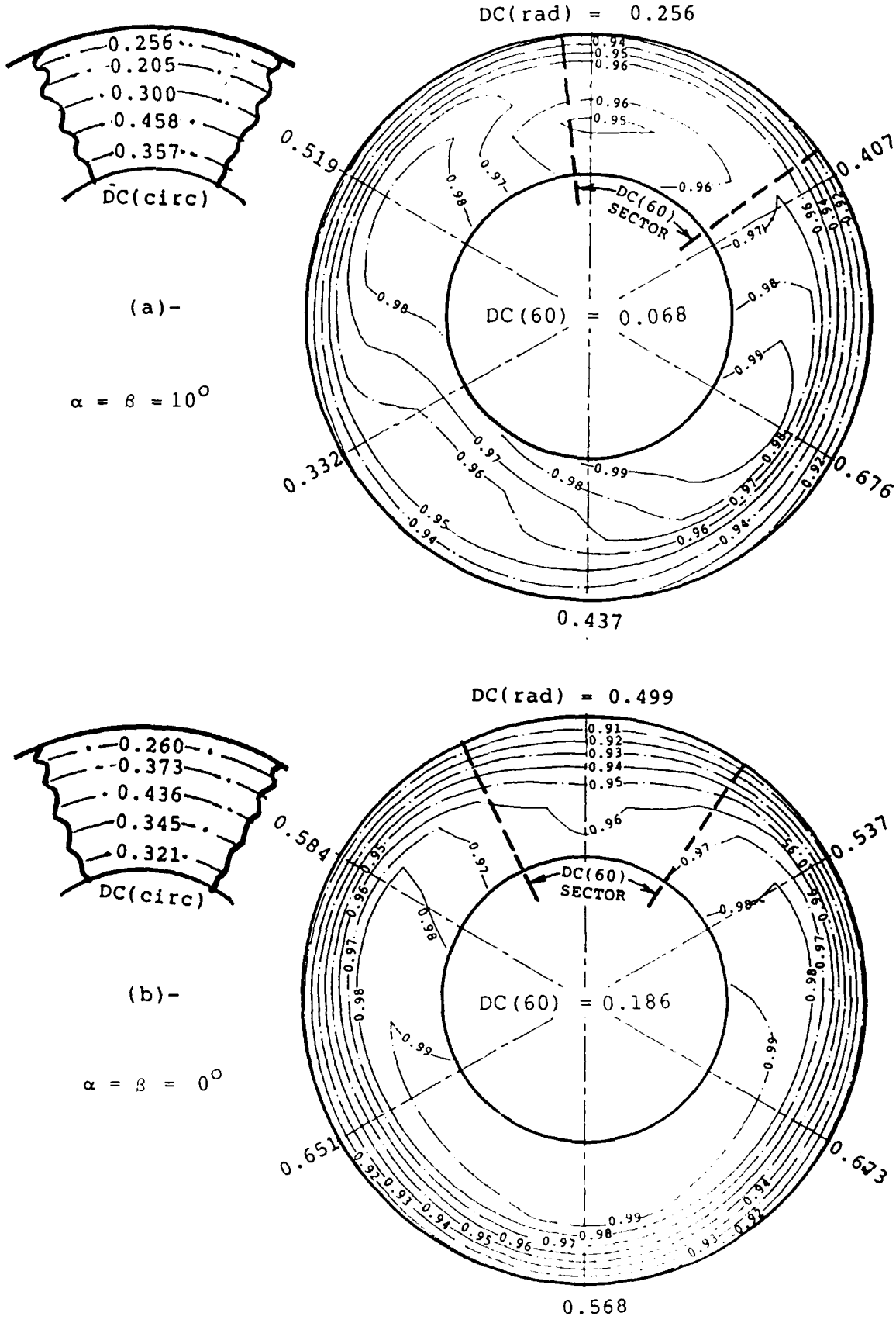

Figure 34: Comparison between the $\alpha = \beta = 0^{\circ}$ and $\alpha = \beta = 10^{\circ}$ attitudes in terms of total pressure distribution at the engine face for the FOSD configuration at N = 13800 RPM and U = 80 m/sec.

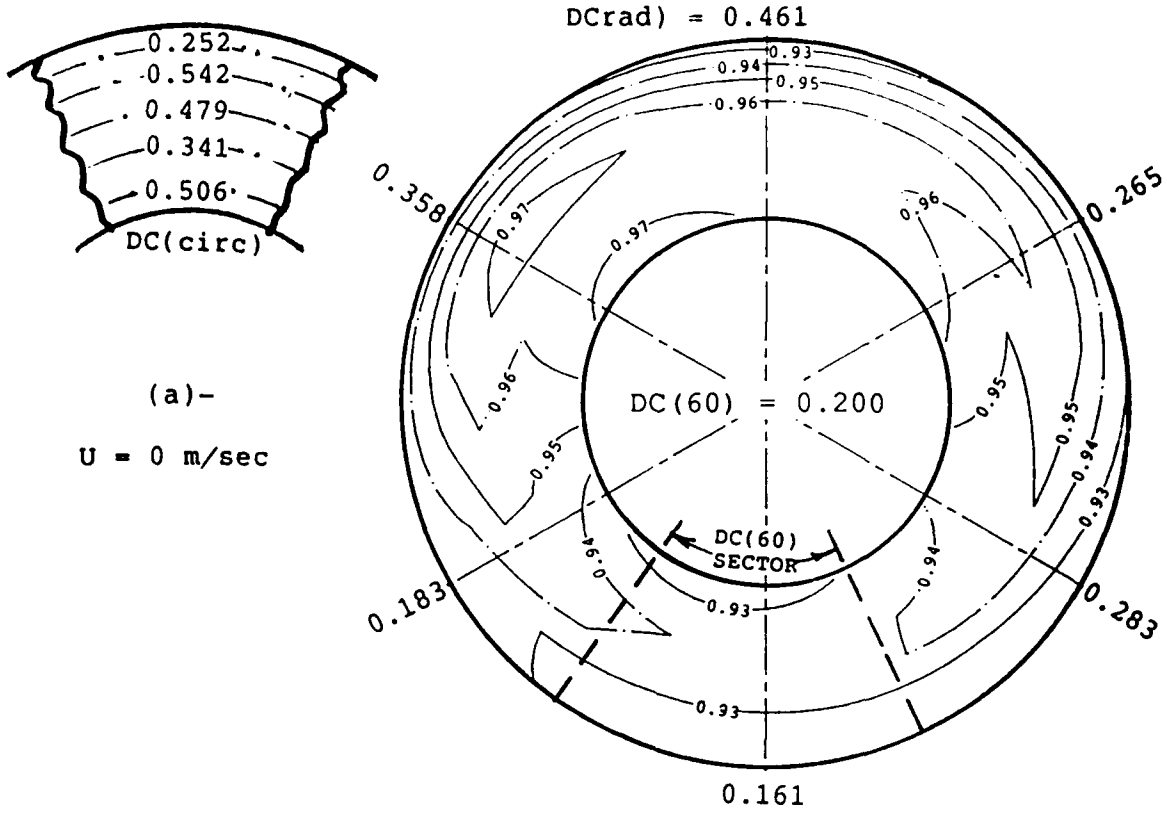

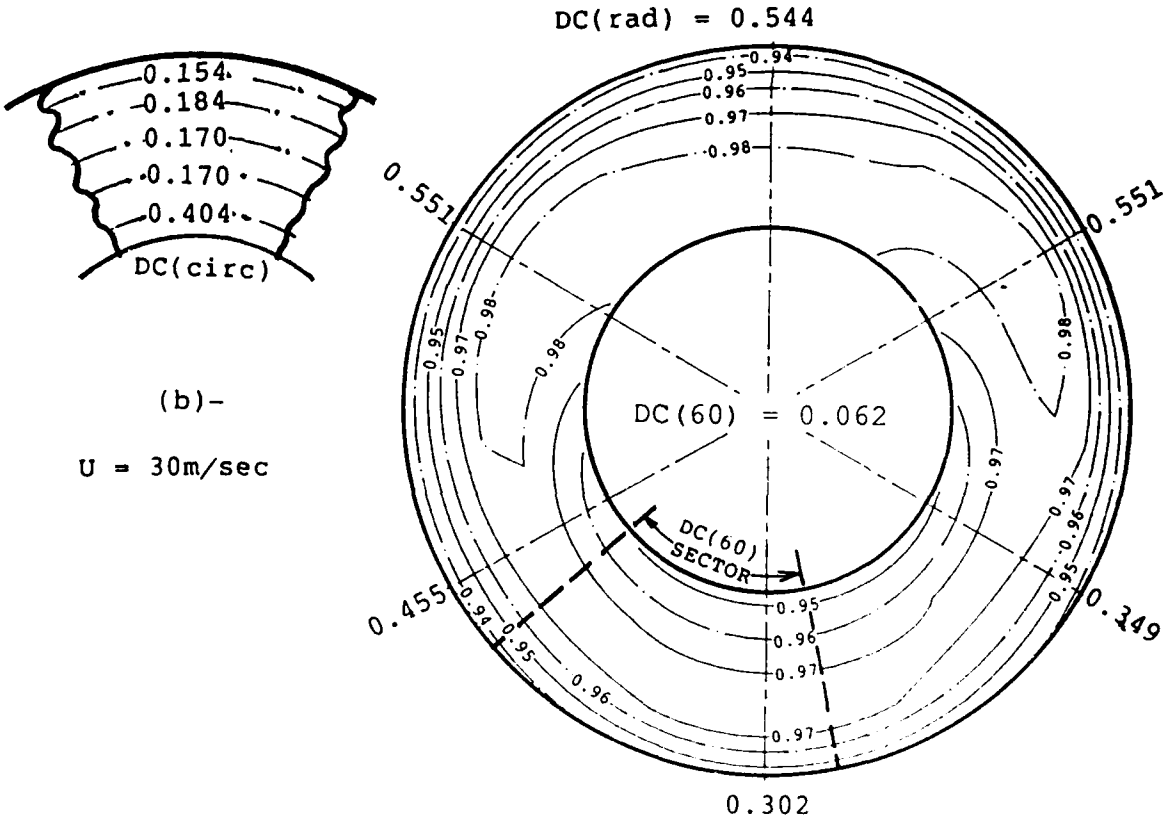

Figure 35- (a) and (b)

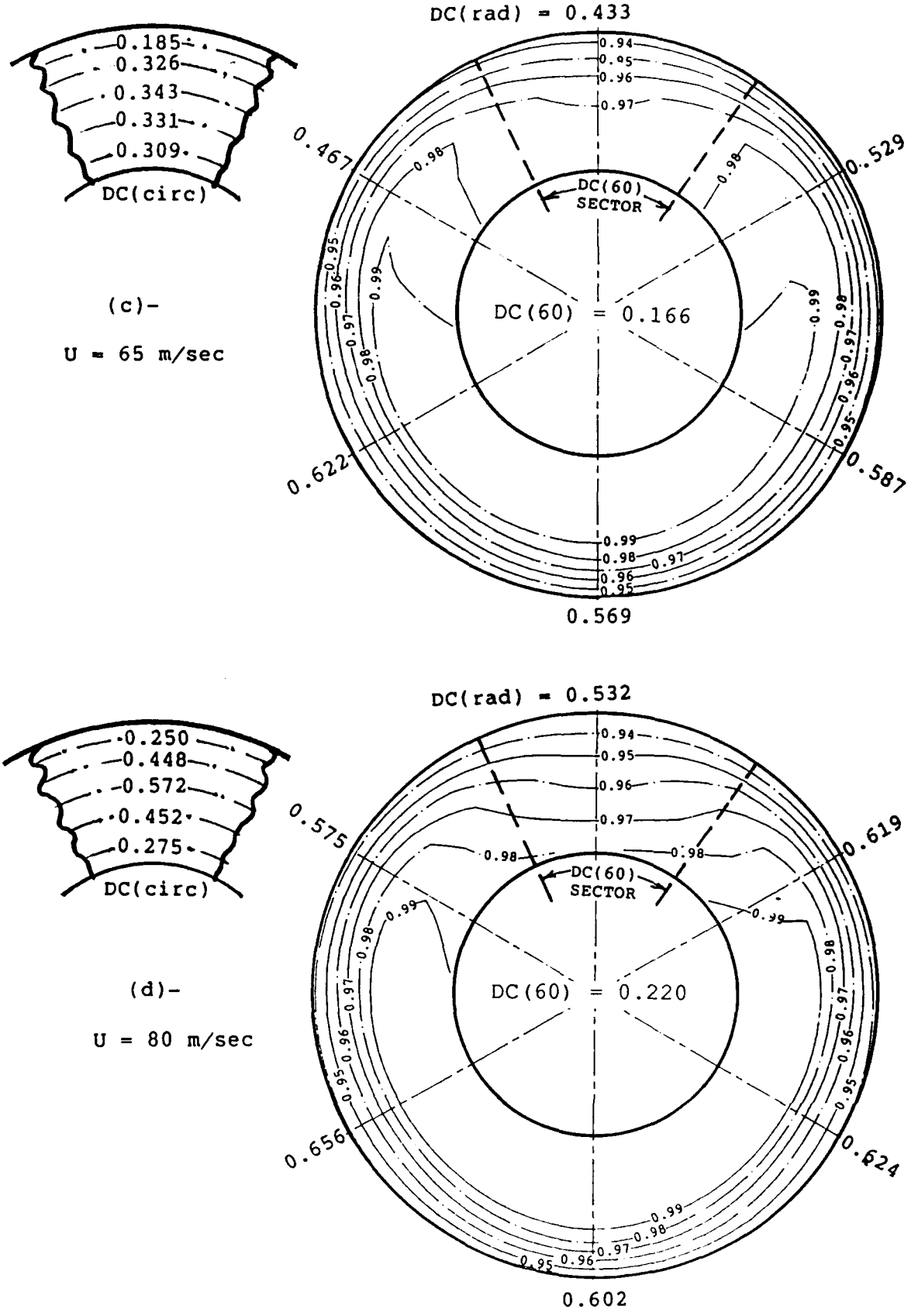

Figure 35: Effect of Forward speed on total pressure distribution at the engine face for the duct modified with the FOSD auxiliary intake at $\alpha = \beta = 0^{o}$ and N = 12000 RPM.

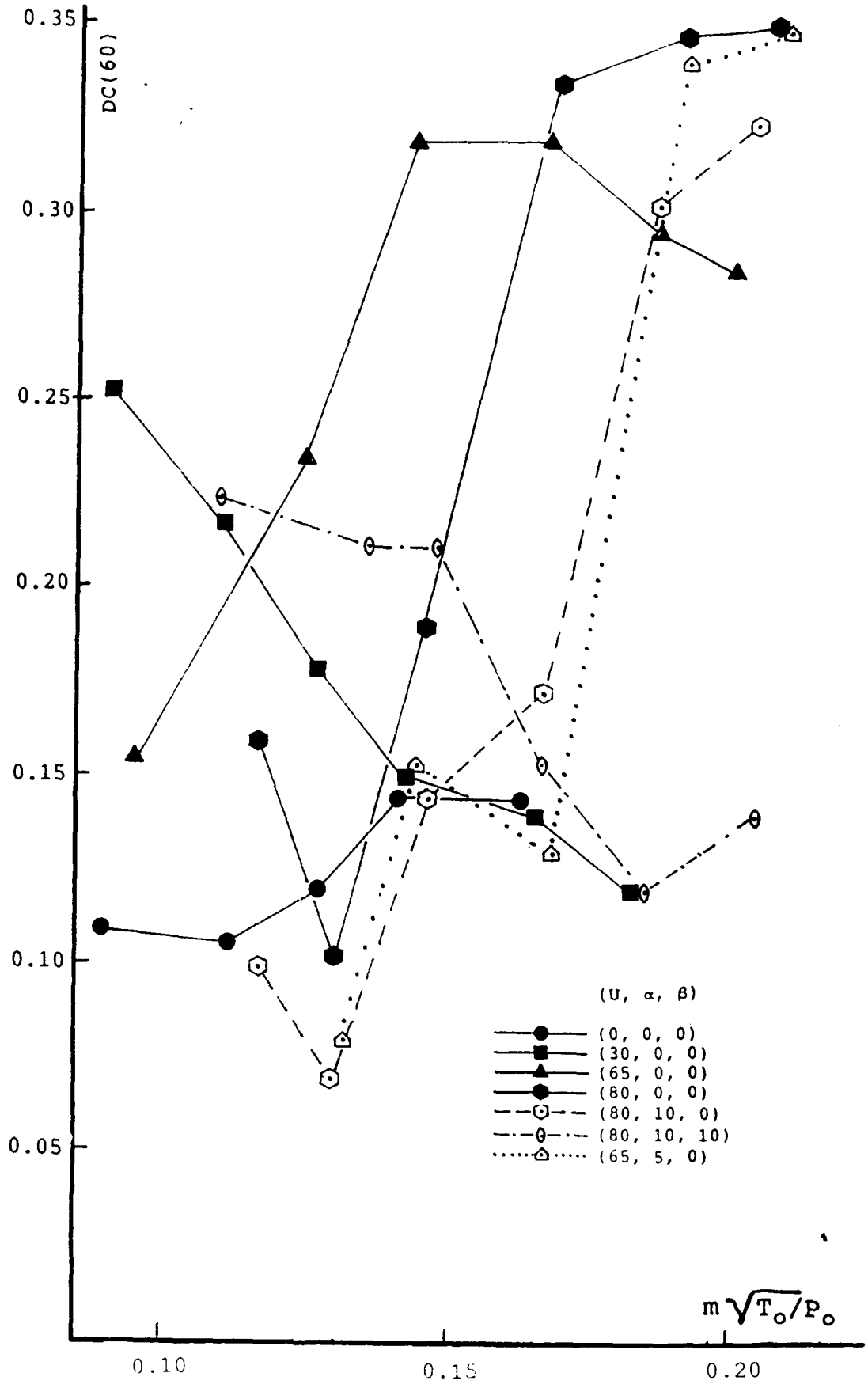

Figure 36: Distortion factors for the HOSD auxiliary intake configuration for various U, α and β combinations.

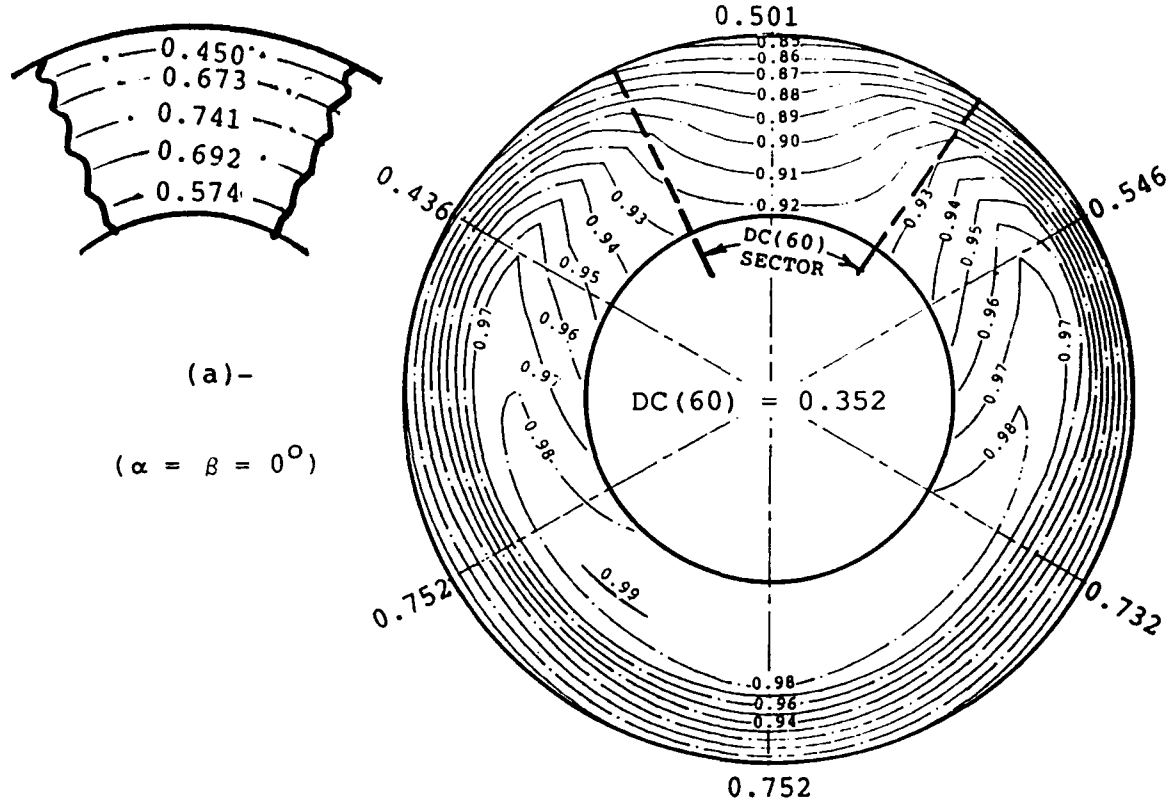

Figure 37- (a) and (b)

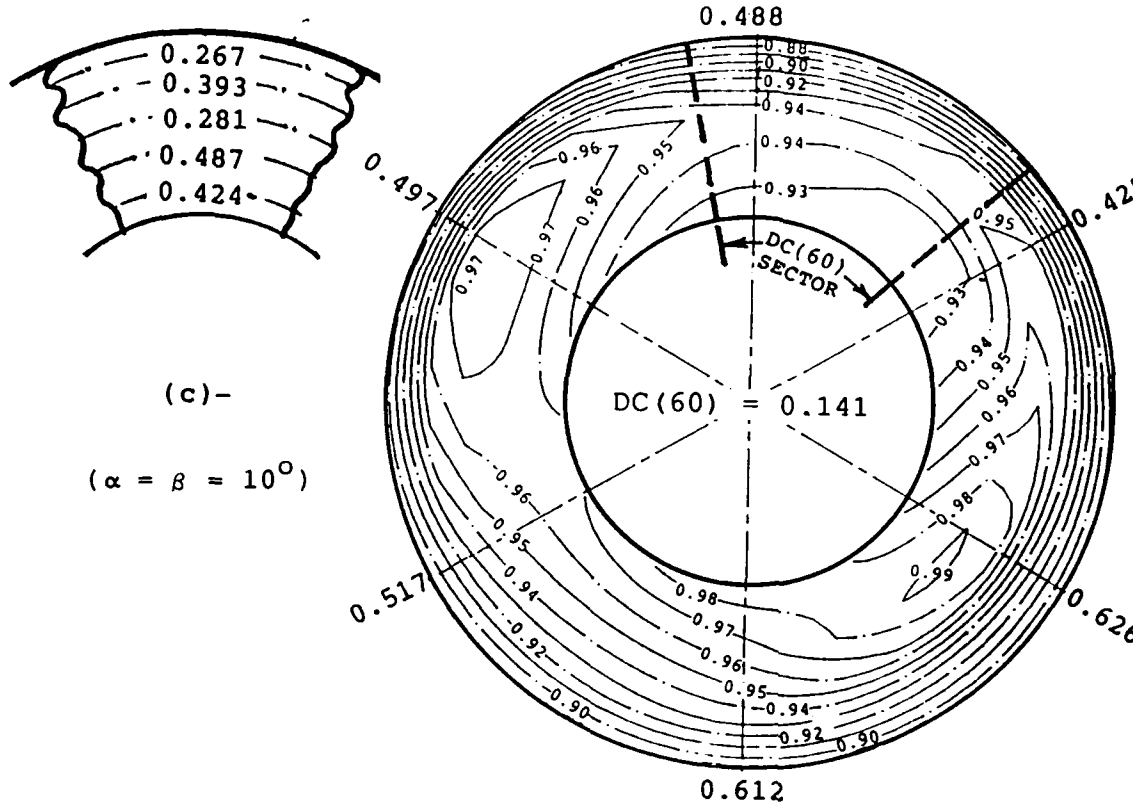

Figure 37: The total pressure distribution at the engine face obtained for the half open sliding door geometry at various α & β combinations for U = 80 m/sec and N = 12000 RPM.

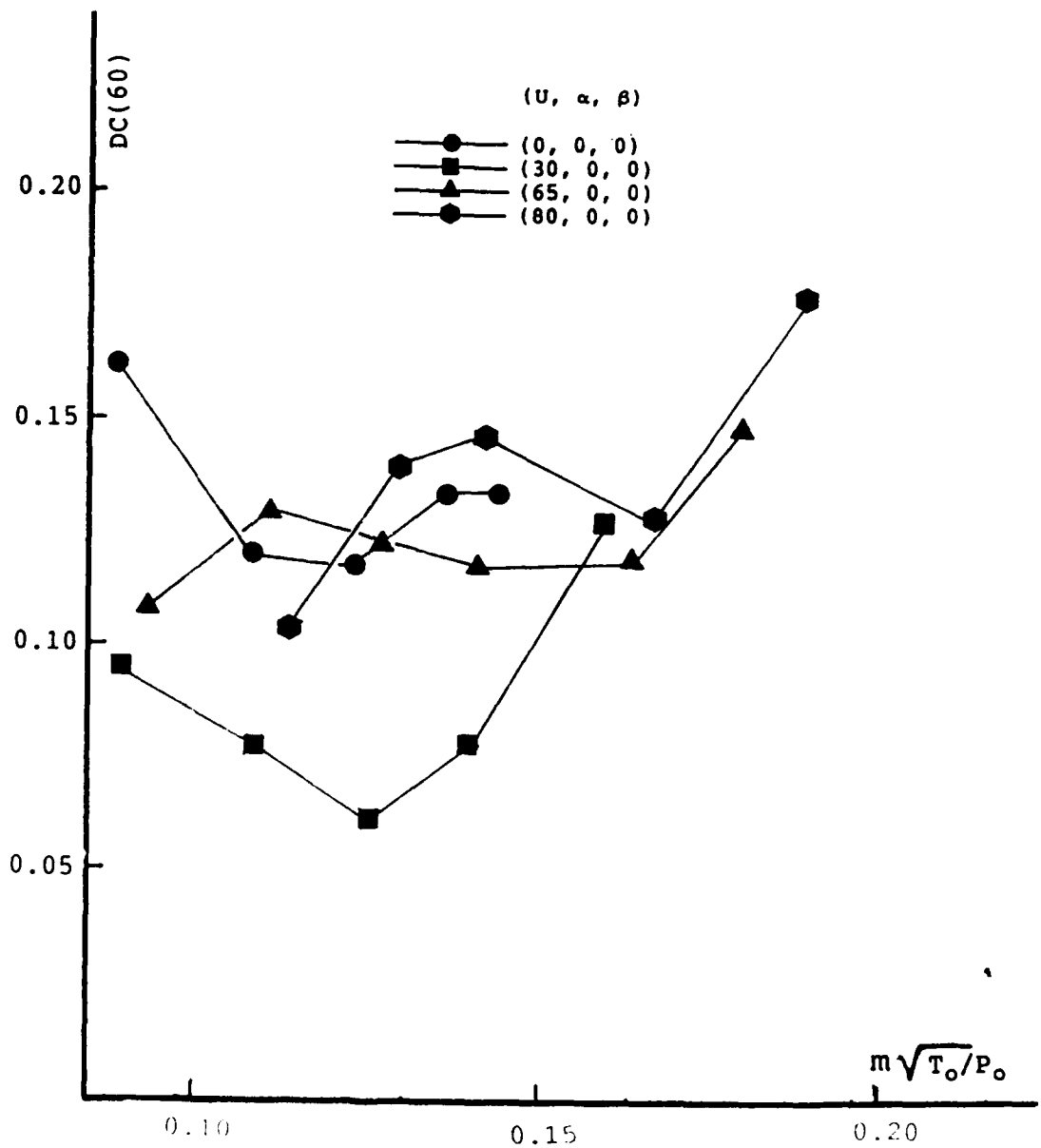

Figure 38: Distortion factors for the FCSD auxiliary intake configuration for various U, α and β combinations.

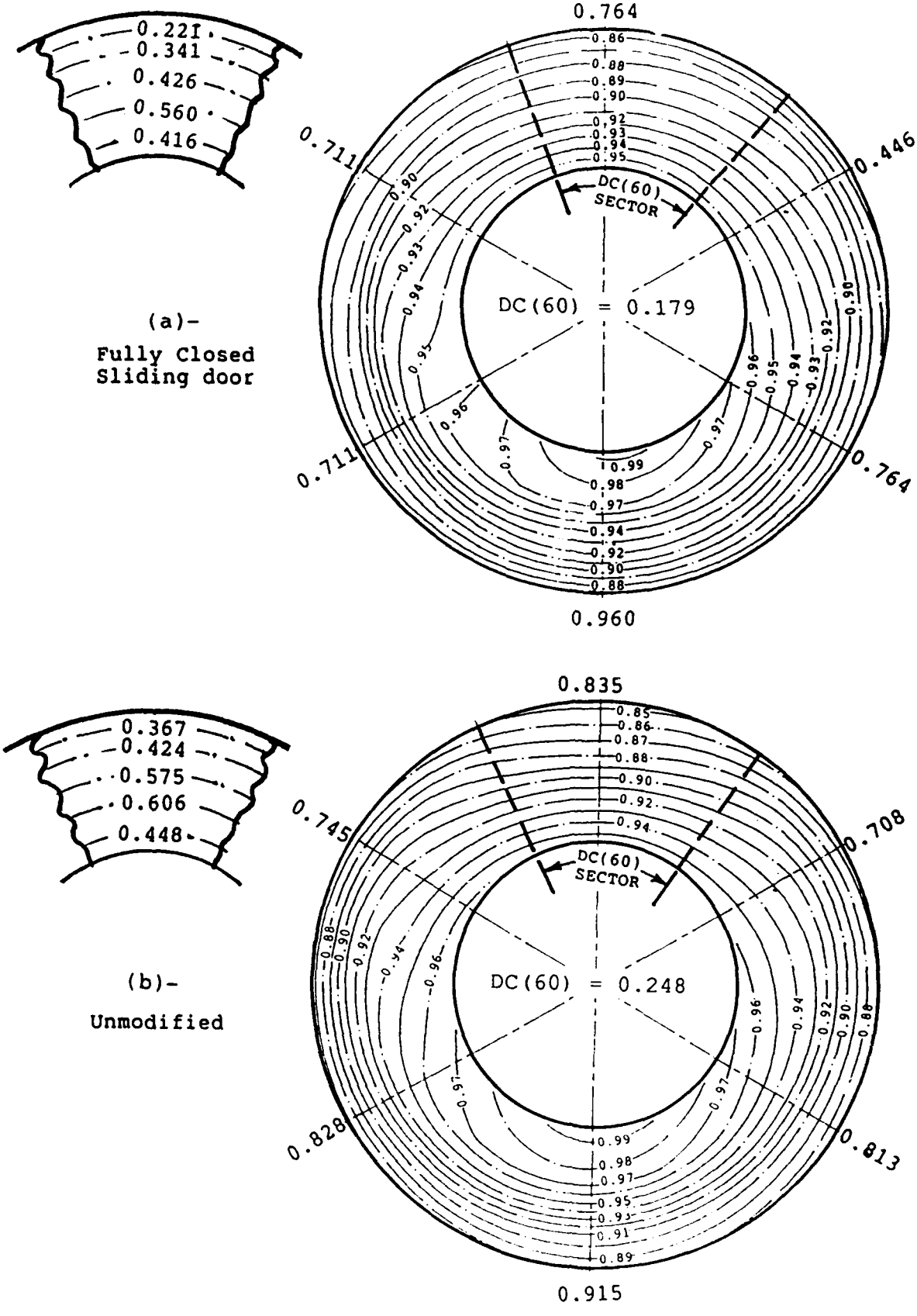

Figure 39: Comparison between the unmodified air intake duct and the fully closed sliding door geometry in terms of total pressure distribution at the engine face for $\alpha = \beta = 0^{\circ}$, U = 80 m/sec and N = 13800 RPM.

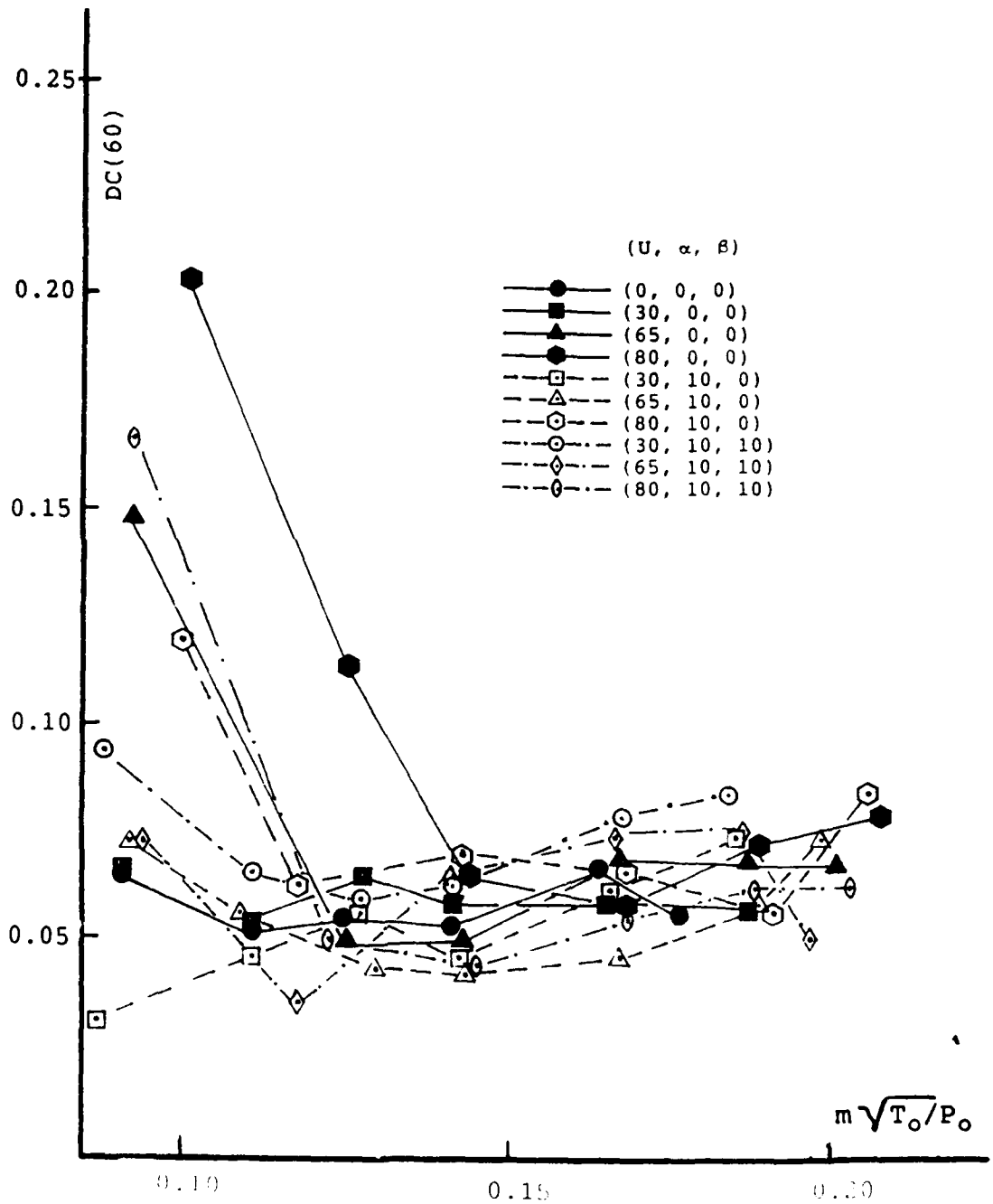

Figure 40: Distortion factors for the louvered aperture auxiliary intake configuration for various U, α and β combinations.

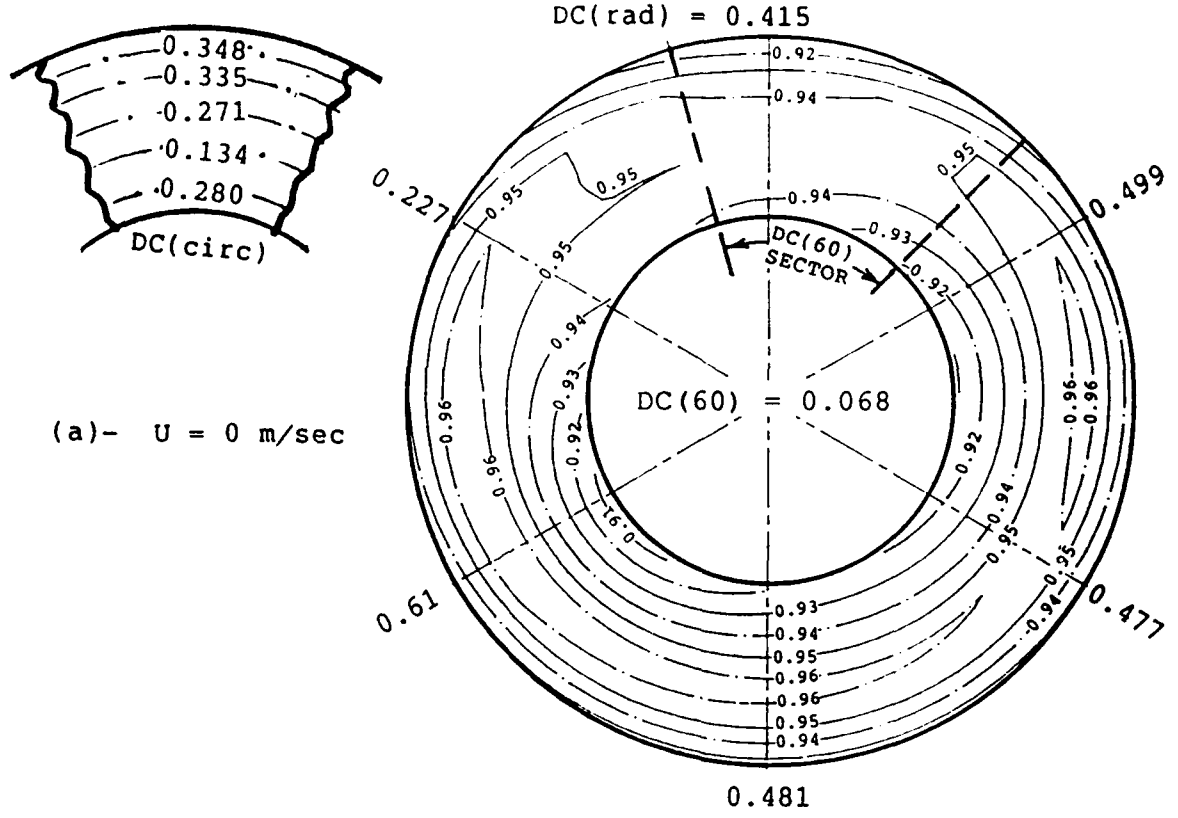

(a)- U = 0 m/sec

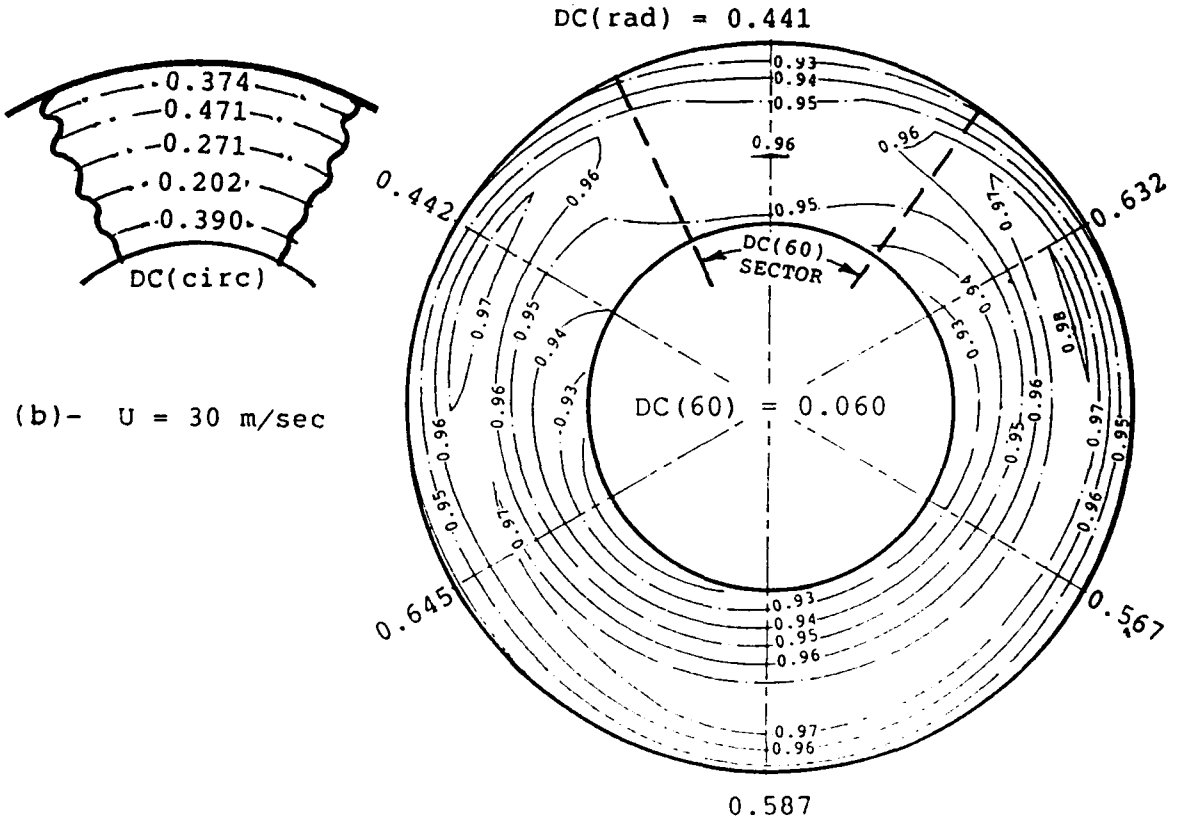

(b)- U = 30 m/sec

Figure 41- (a) and (b)

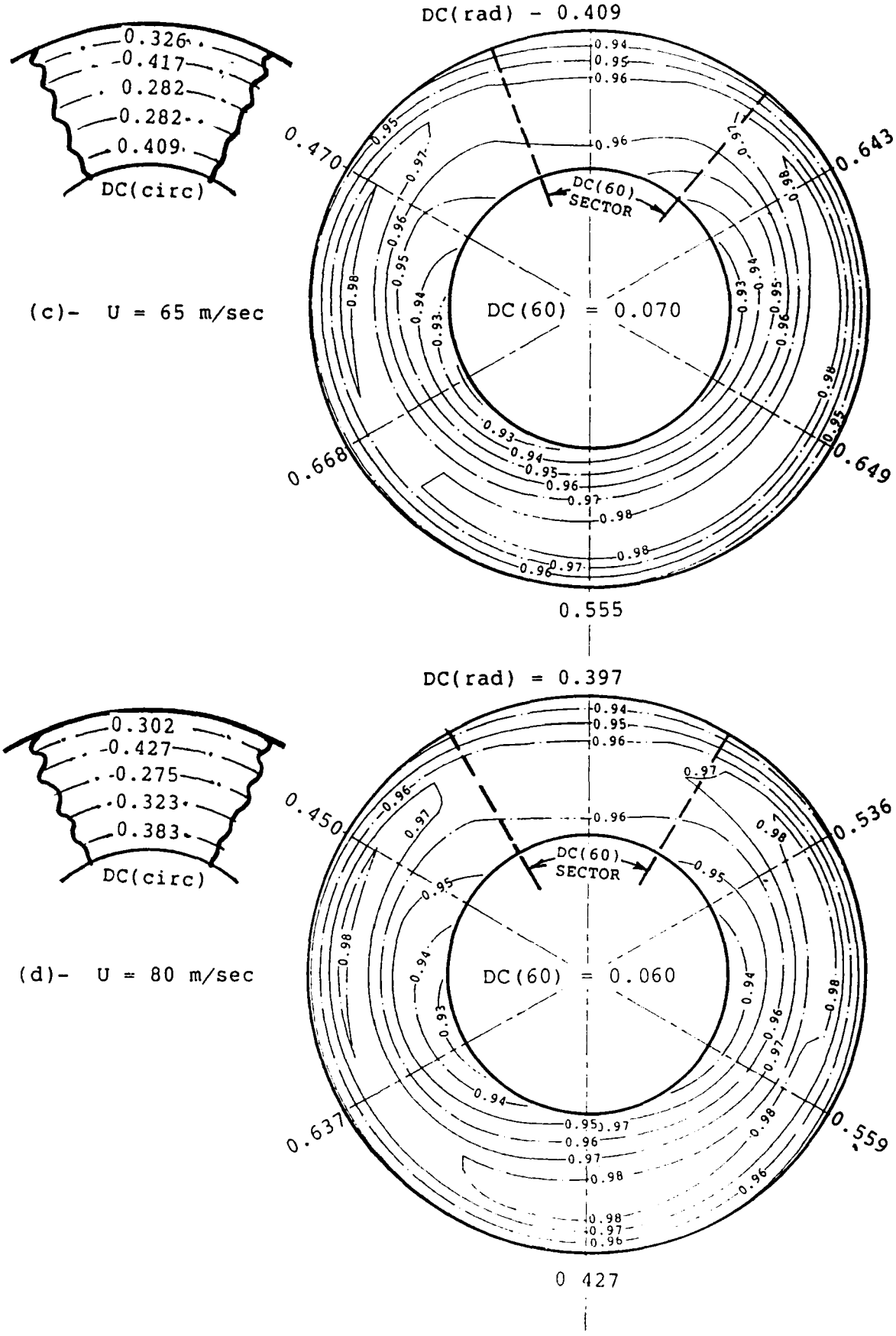

Figure 41: Effect of Forward speed on total pressure distribution at the engine face for the duct modified with the louvered auxiliary intake geometry at $\alpha = \beta = 0^{o}$ and N = 12000 RPM.

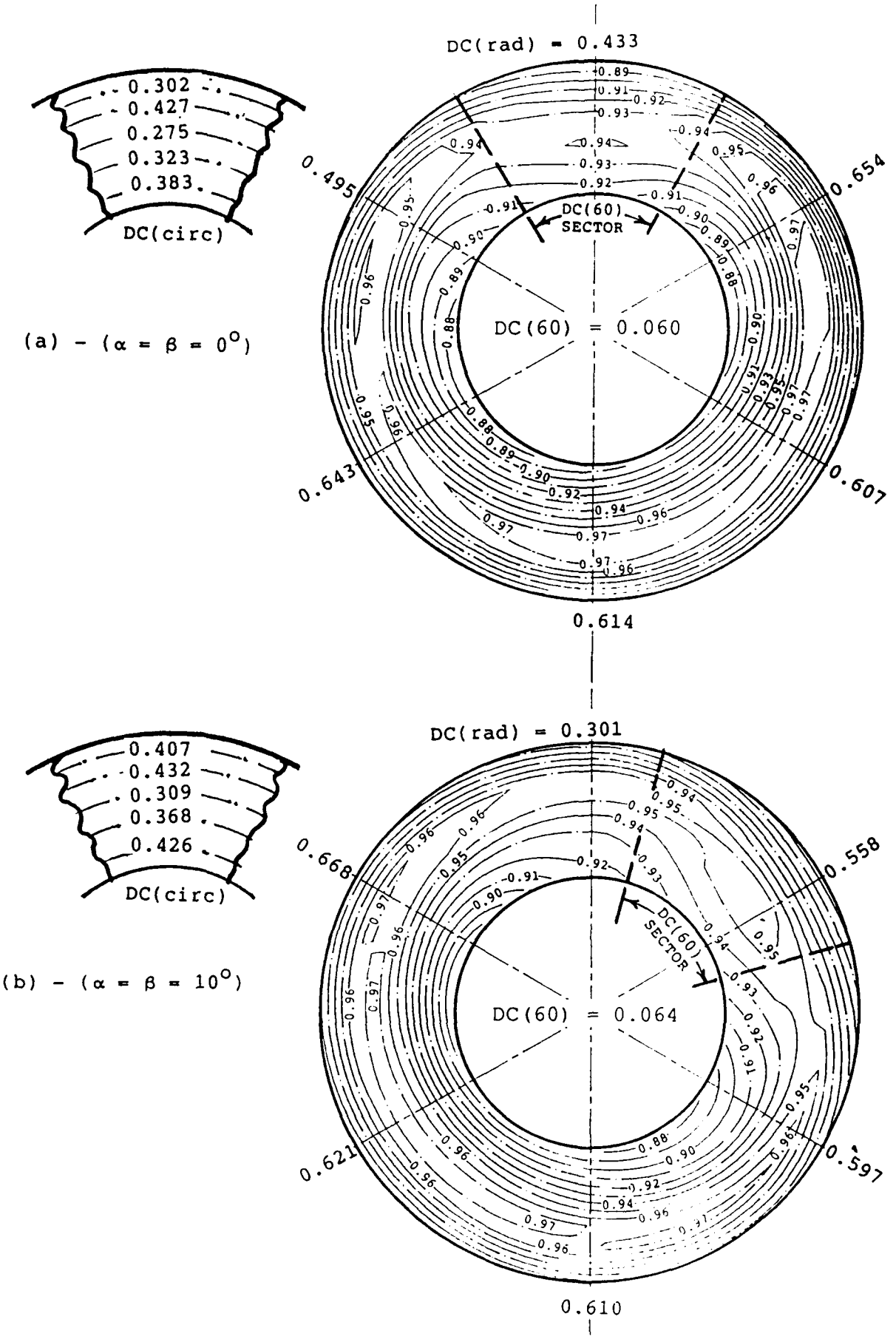

Figure 42: Comparison between the zero incidence and the extreme $\alpha = \beta = 10^{\circ}$ attitudes in terms of total pressure distribution at the engine face for N = 13800 RPM and U = 80 m/sec.

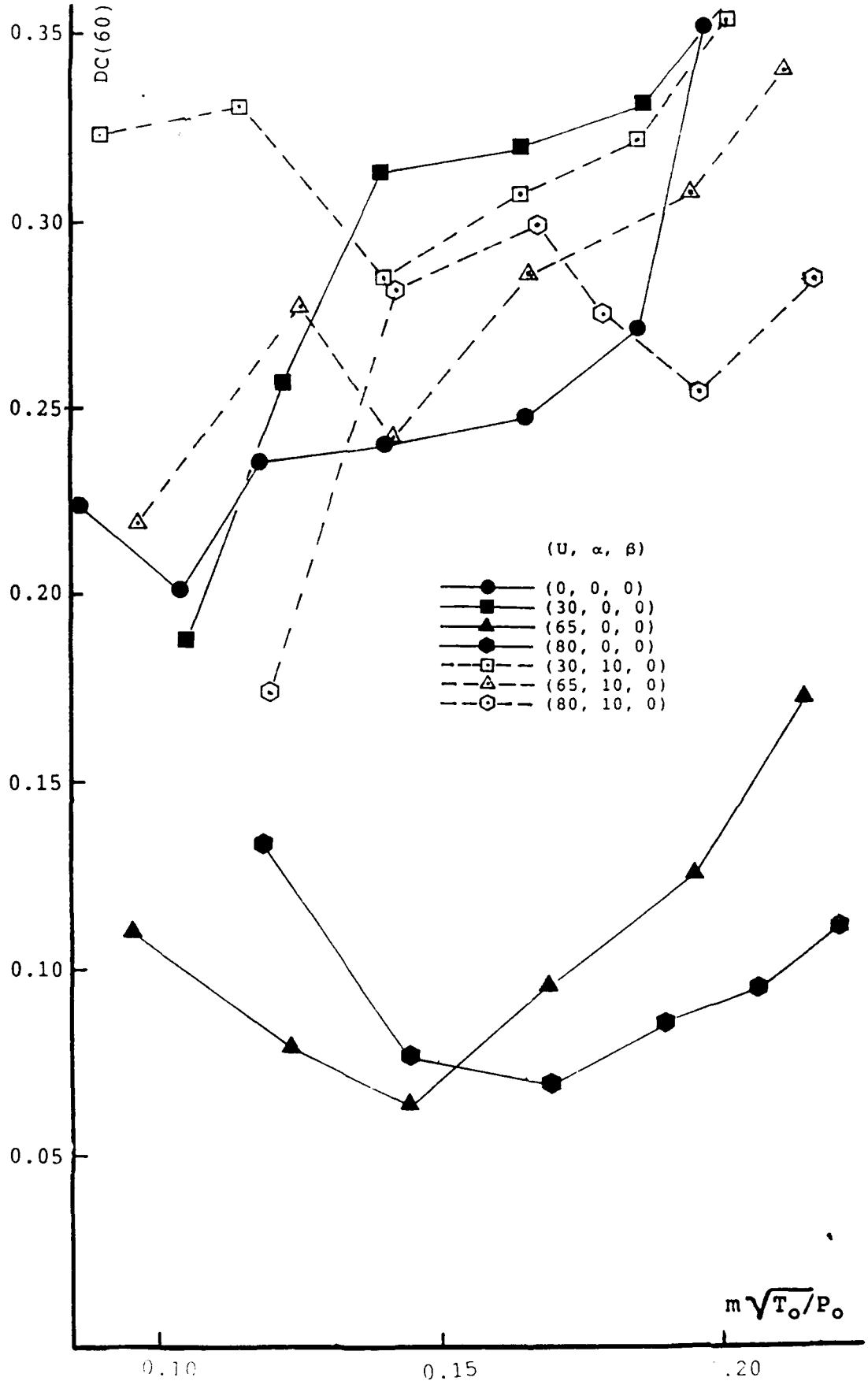

Figure 43: Distortion factors for the profiled lipped auxiliary intake geometry for various U, α and β combinations.

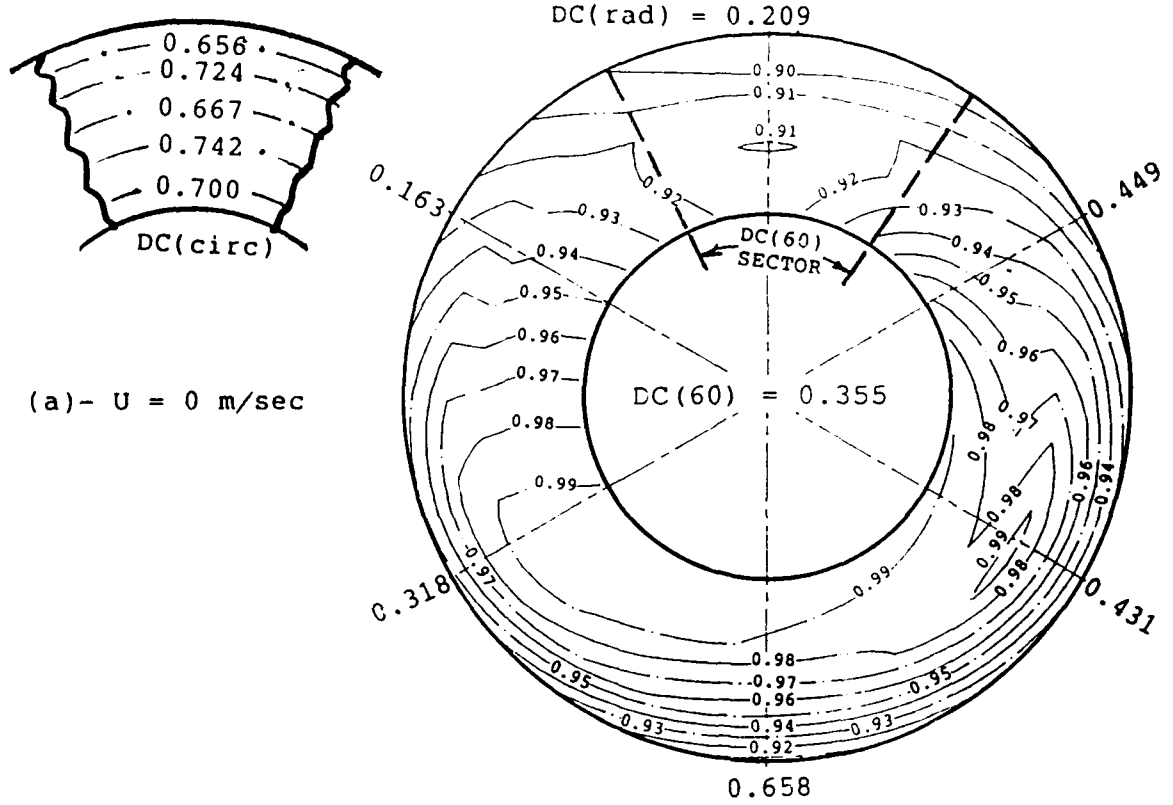

(a)- U = 0 m/sec

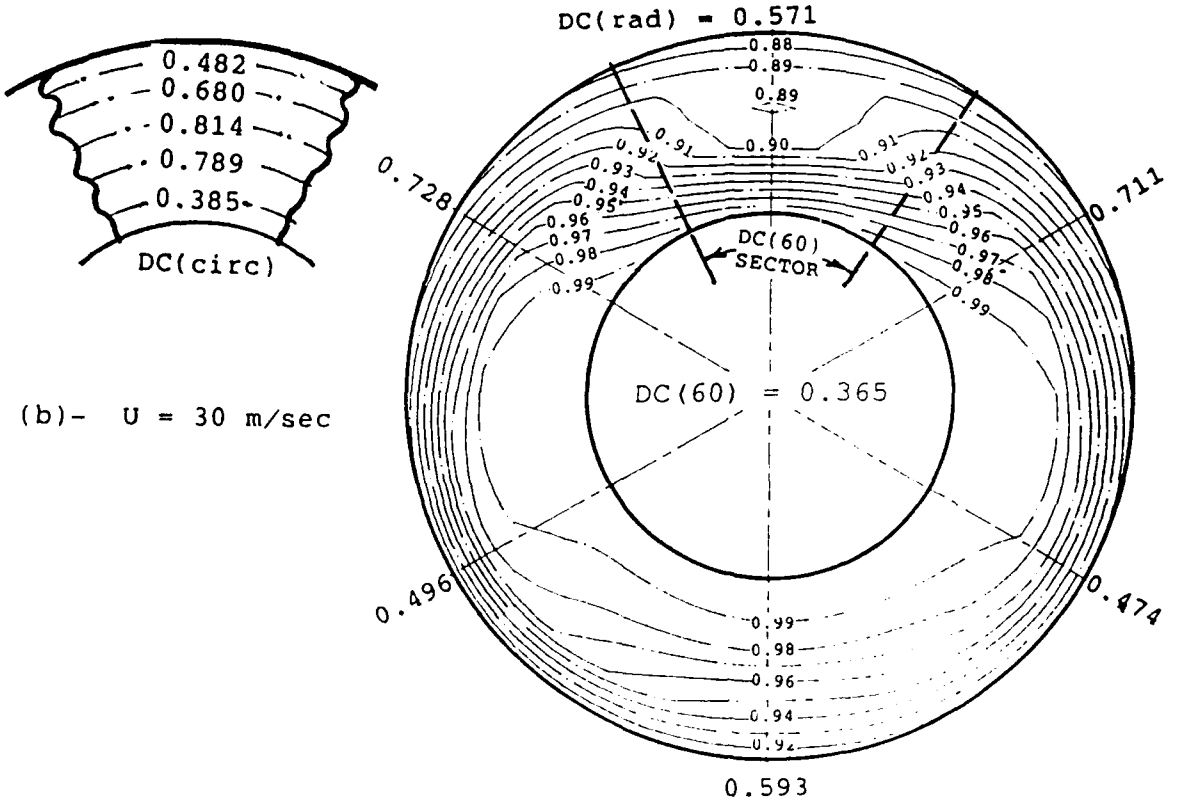

(b)- U = 30 m/sec

Figure 44- (a) and (b)

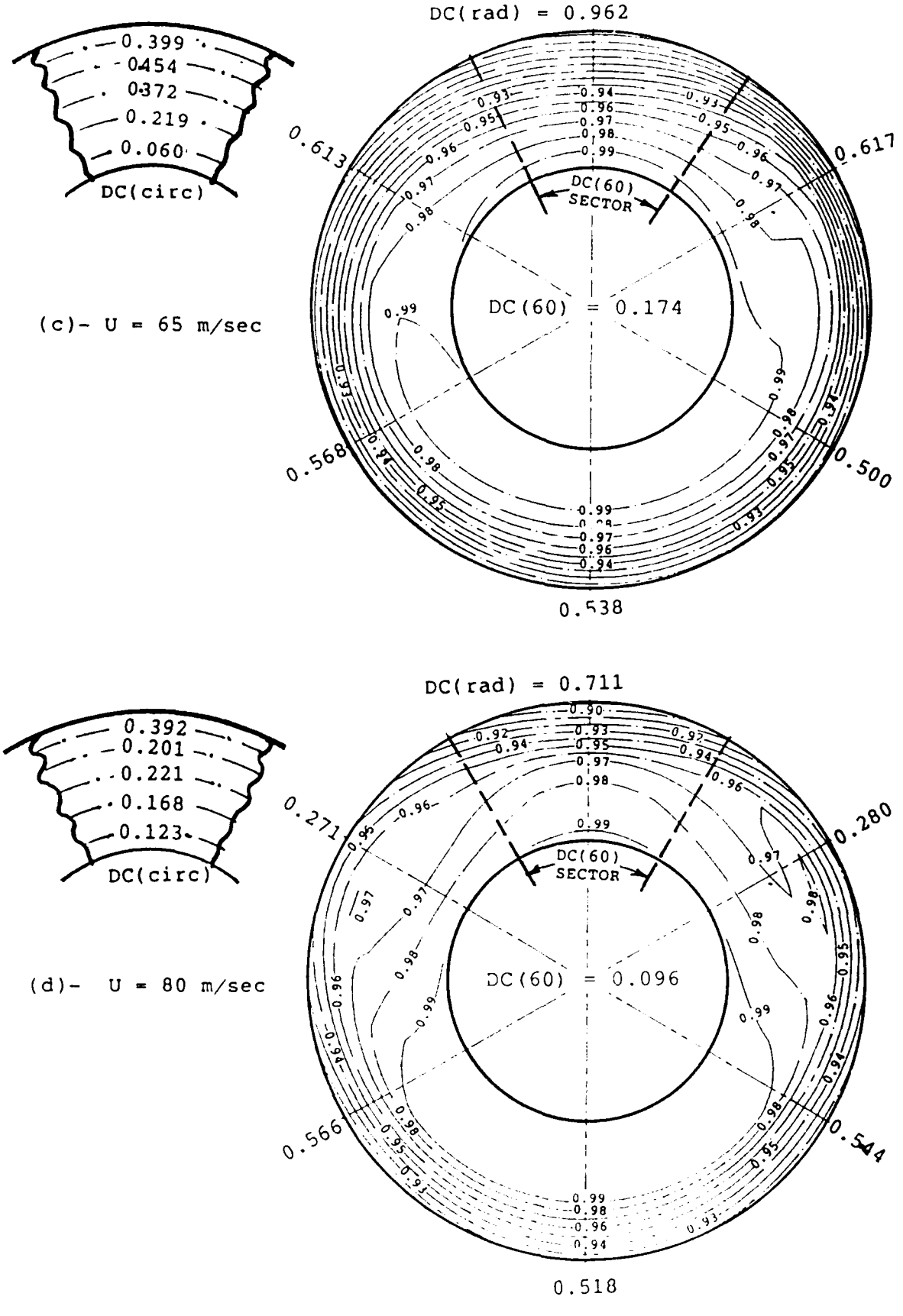

Figure 44: Effect of Forward speed on total pressure distribution at the engine face for the duct modified with the best profiled lip auxiliary intake geometry at $\alpha = \beta = 0^{o}$ and N = 4900 RPM.

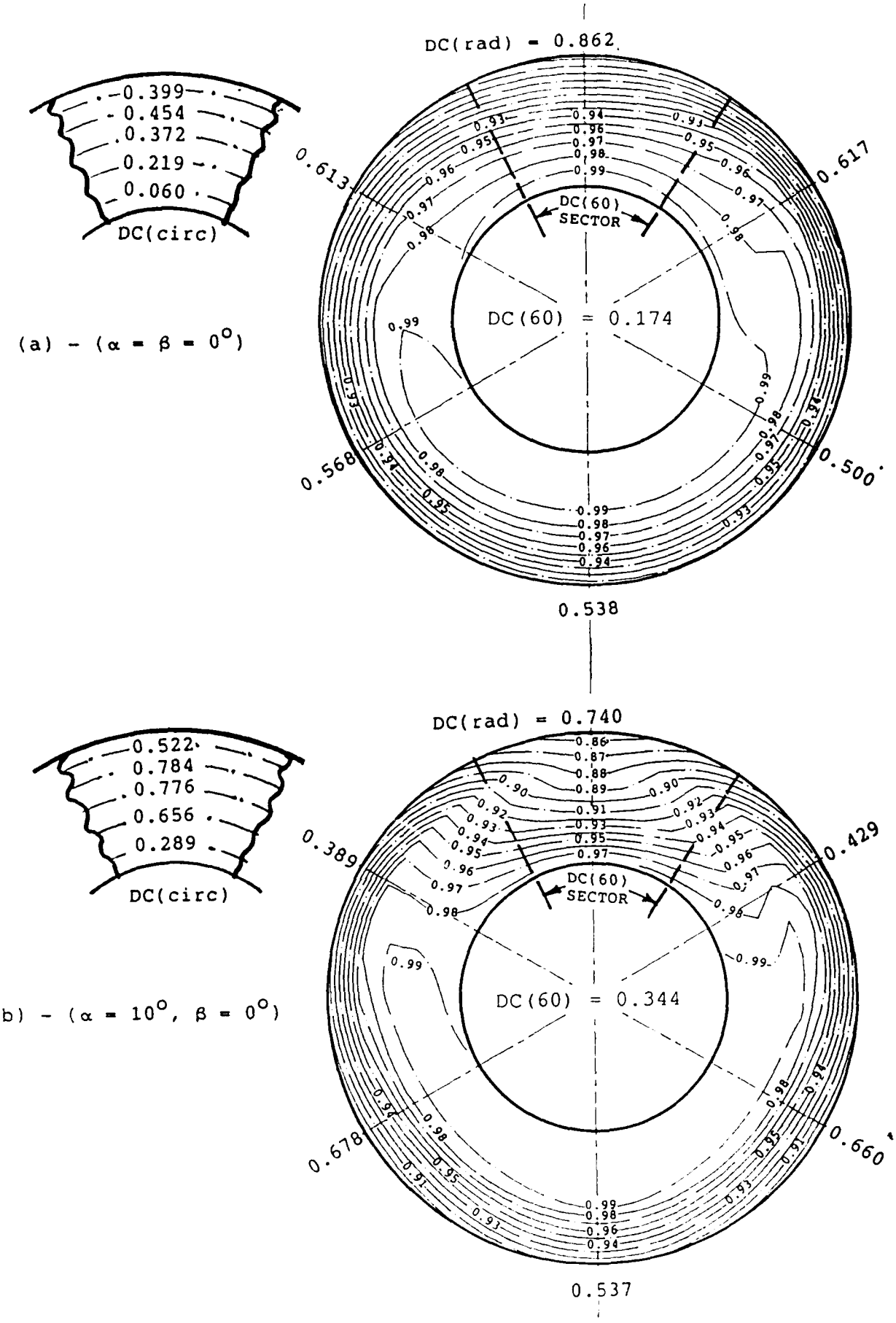

Figure 45: Effect of attitude on total pressure distribution at the engine face for the best profiled lip auxiliary intake geometry at N = 13800 RPM and U = 65 m/sec.

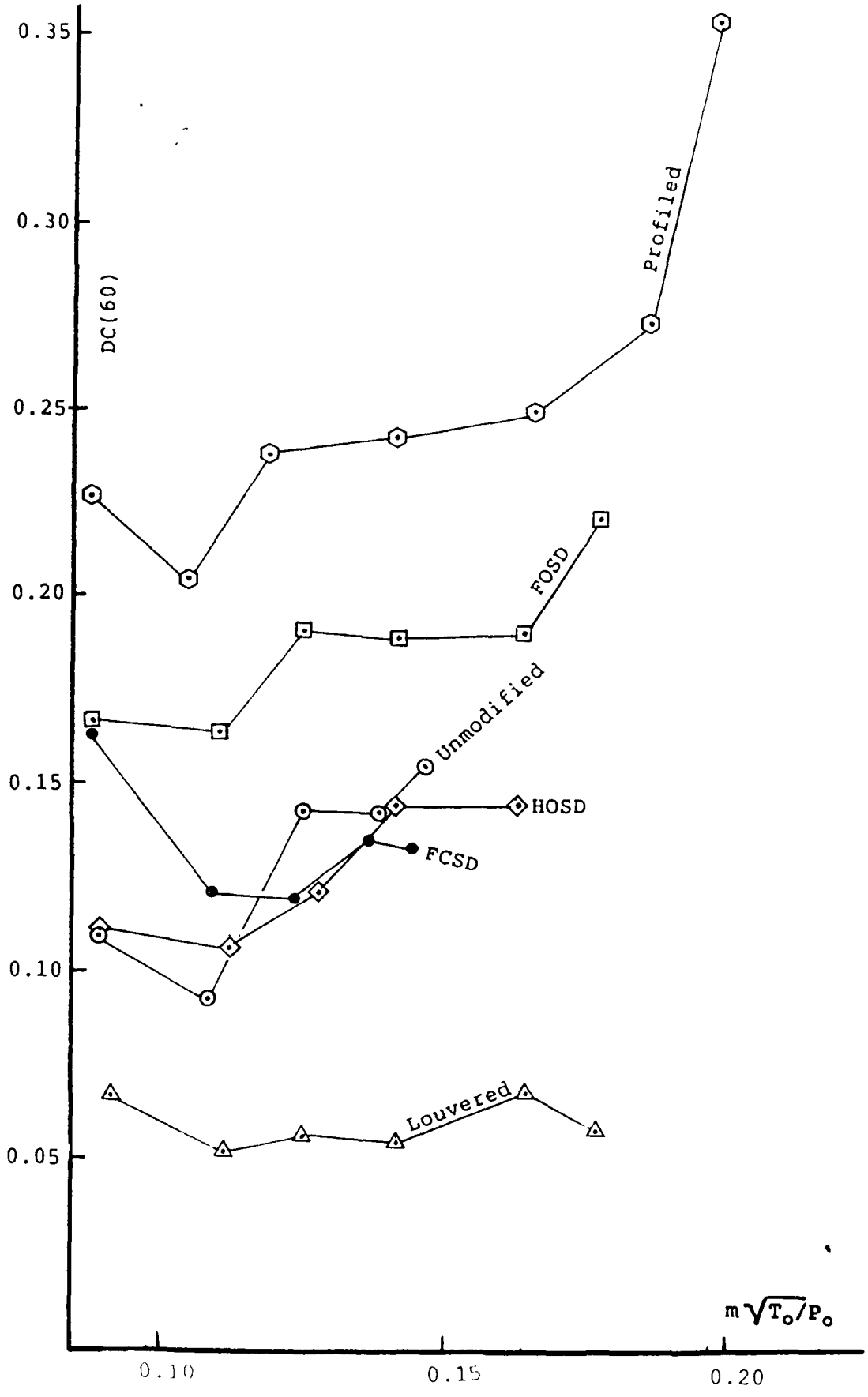

Figure 46: Comparison of distortion characteristics at $\alpha = \beta = 0^{o}$ and U = 0 m/sec.

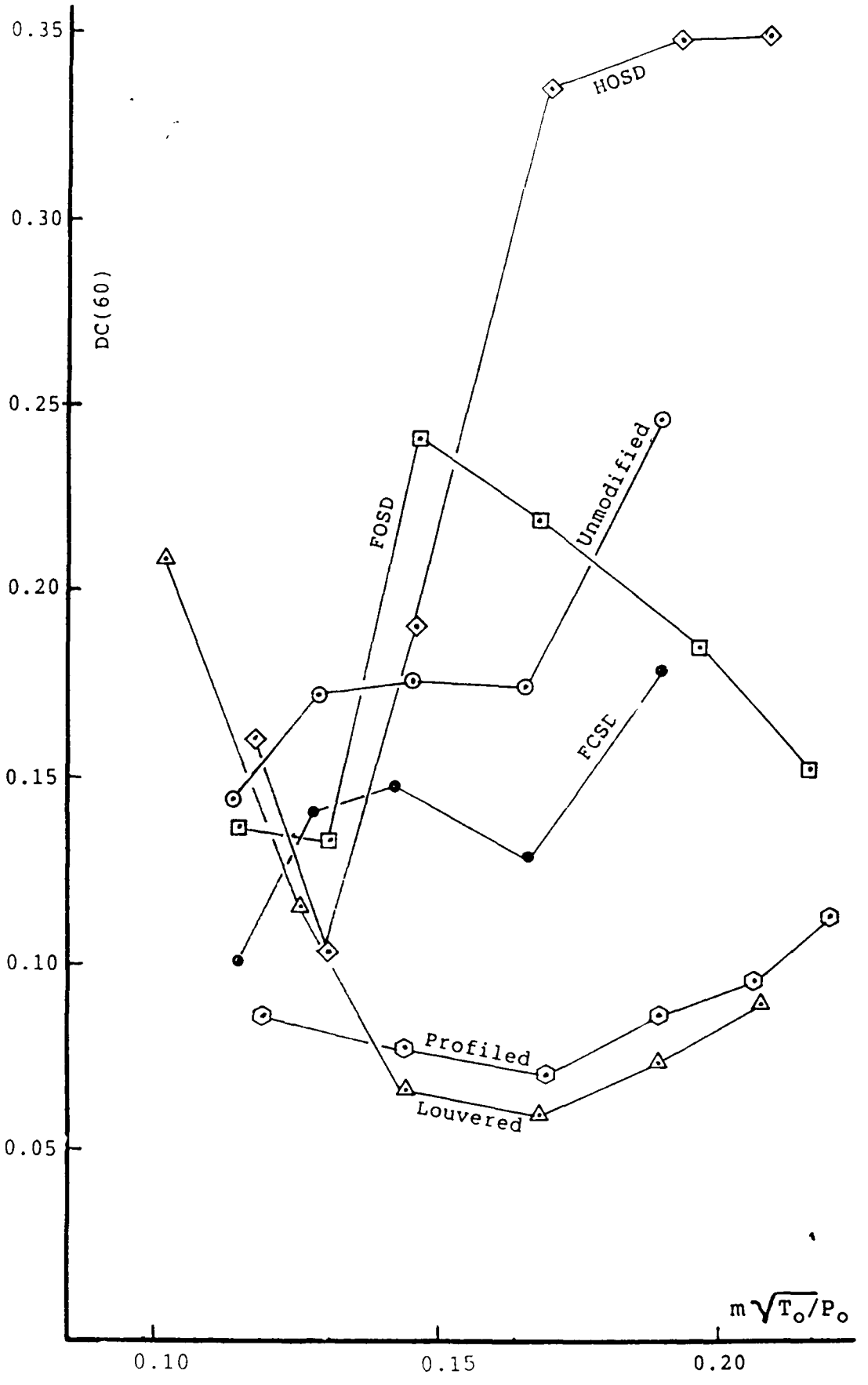

Figure 47: Comparison of distortion characteristics at $\alpha = \beta = 0^{o}$ and U = 80 m/sec.

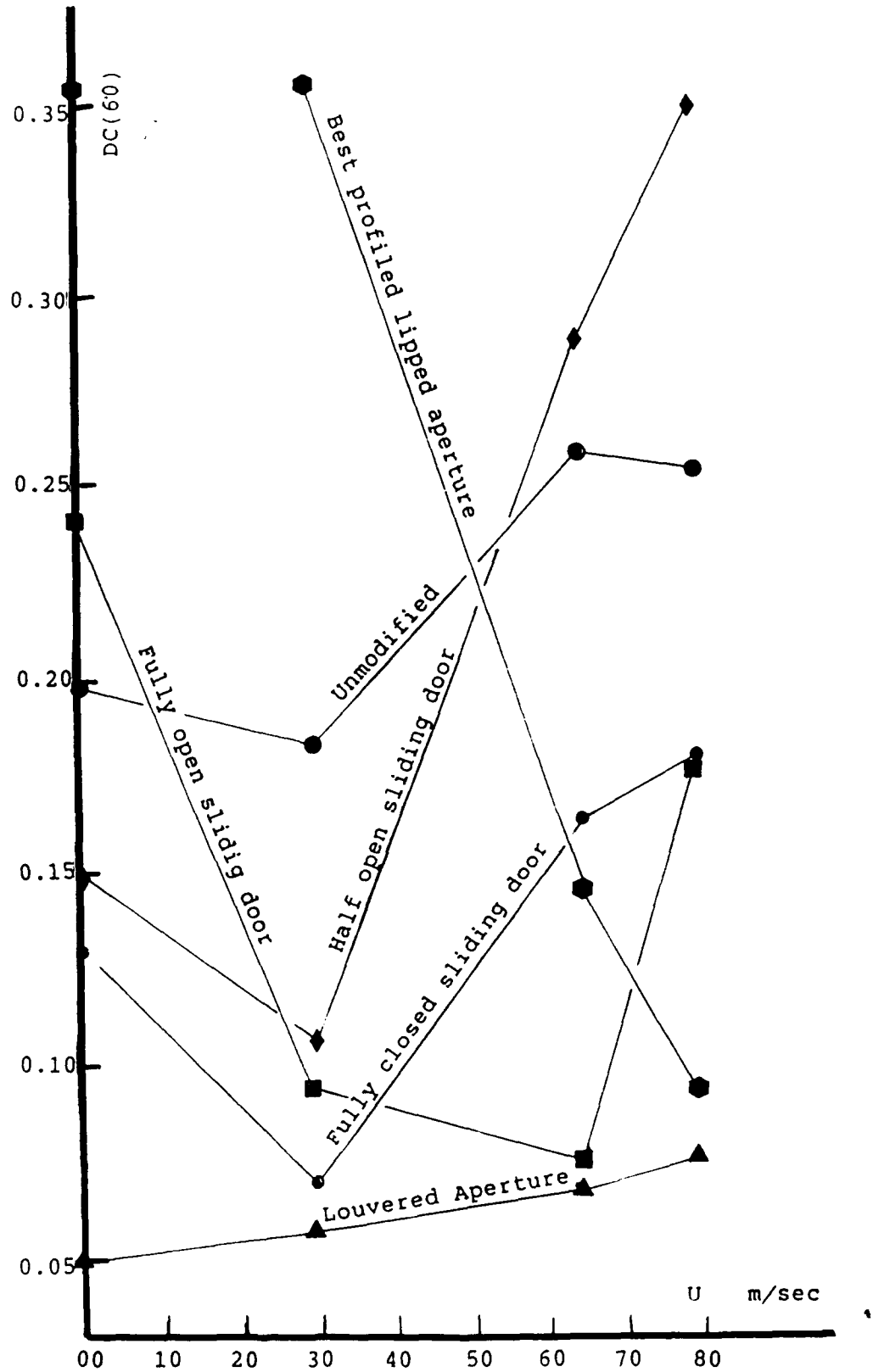

Figure 48: Comparison of distortion characteristics at $\alpha = \beta = 0^{o}$ and N = 13800 RPM.

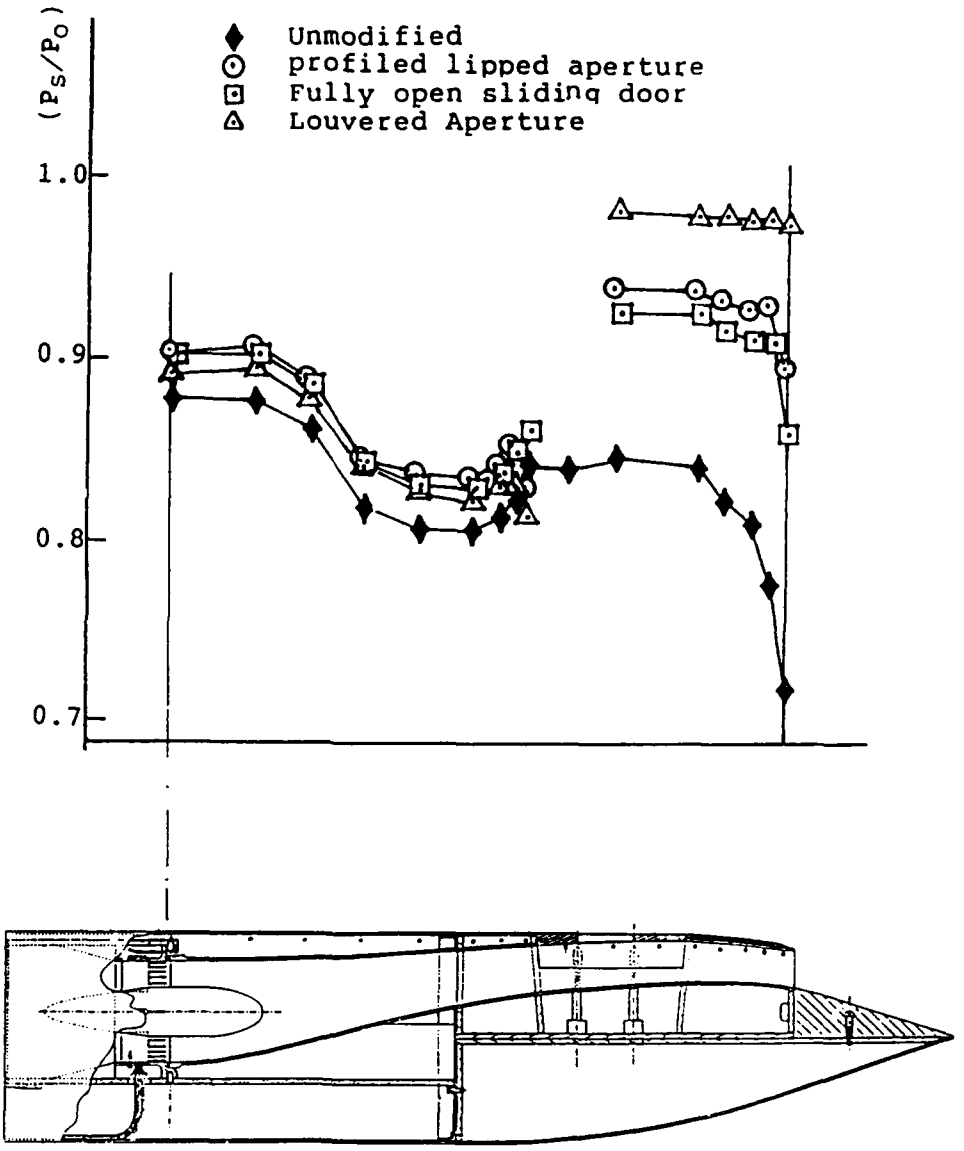

Figure 49: Internal static pressure distribution for various intake configurations at U = 80 m/sec, N = 12000 RPM and $\alpha = \beta = 0^{o}$.

DISTRIBUTION

AUSTRALIA

Department of Defence

Defence Central

Chief Defence Scientist)
AS, Science Corporate Management)shared copy
FAS Science Policy)
Director, Departmental Publications
Counsellor, Defence Science, London (Doc Data sheet only)
Counsellor, Defence Science, Washington (Doc Data sheet only)
Scientific Adviser, Defence Central
OIC TRS, Defence Central Library
Document Exchange Centre, DSTIC (8 copies)
Defence Intelligence Organisation
Librarian H Block, Victoria Barracks, Melb (Doc Data sheet only)

Aeronautical Research Laboratory

Director
Library
Chief Flight Mechanics & Propulsion Division
Head Propulsion Branch
Head Flight Mechanics Branch
Branch File Propulsion Branch
Authors: A.M. Abdel-Fattah (3 copies)
Y.Y. Link
D.E. Glenny
G.L. Merrington
N. Matheson

Defence Science & Technology Organisation - Salisbury

Library

Navy Office

Navy Scientific Adviser
DAIRENG - N
J. Washbrooke

Army Office

Scientific Adviser - Army (Doc Data sheet only)

Air Force Office

Air Force Scientific Adviser (Doc Data sheet only)
Engineering Branch Library

Statutory and State Authorities and Industry

Aero-Space Technologies Australia, Systems Division Librarian
ASTA Engineering, Document Control Office
Hawker de Havilland Aust Pty Ltd, Victoria, Library
Hawker de Havilland Aust Pty Ltd, Bankstown, Library

Universities and Colleges

Adelaide
Barr Smith Library
Professor Mechanical Engineering

Melbourne
Engineering Library

Monash
Hargrave Library

Newcastle
Library
Professor R. Telfer, Institute of Aviation

NSW
Physical Sciences Library
Library, Australian Defence Force Academy

Queensland
Library

Tasmania
Engineering Library

Western Australia
Library

RMIT
Library
Mr M.L. Scott, Aerospace Engineering

SPARES (6 COPIES)

TOTAL (53 COPIES)

AL 149 DEPARTMENT OF DEFENCE

DOCUMENT CONTROL DATA

PAGE CLASSIFICATION
UNCLASSIFIED

PRIVACY MARKING

1a. AR NUMBER	1b. ESTABLISHMENT NUMBER	2. DOCUMENT DATE	3. TASK NUMBER
AR-006-601	ARL-PROP-TM-472	MARCH 92	NAV 90/213

4. TITLE
WIND TUNNEL TESTS ON JINDIVIK AIR INTAKE DUCT WITH AND WITHOUT AN AUXILIARY INTAKE

5. SECURITY CLASSIFICATION (PLACE APPROPRIATE CLASSIFICATION IN BOX(S) IE. SECRET (S), CONF. (C) RESTRICTED (R), LIMITED (L) UNCLASSIFIED (U)).

DOCUMENT	TITLE	ABSTRACT
U	U	U

6. NO. PAGES
72

7. NO. REFS.
6

8. AUTHOR(S)
A.M. ABDEL-FATTAH
Y.Y. LINK

9. DOWNGRADING/DELIMITING INSTRUCTIONS
Not applicable

10. CORPORATE AUTHOR AND ADDRESS
AERONAUTICAL RESEARCH LABORATORY
506 LORIMER STREET
FISHERMENS BEND VIC 3207

11. OFFICE/POSITION RESPONSIBLE FOR:
SPONSOR NAVY
SECURITY -
DOWNGRADING -
APPROVAL CFPD

12. SECONDARY DISTRIBUTION (OF THIS DOCUMENT)

Approved for public release.

OVERSEAS ENQUIRIES OUTSIDE STATED LIMITATIONS SHOULD BE REFERRED THROUGH DSTIC, ADMINISTRATIVE SERVICES BRANCH, DEPARTMENT OF DEFENCE, ANZAC PARK WEST OFFICES, ACT 2601

13a. THIS DOCUMENT MAY BE ANNOUNCED IN CATALOGUES AND AWARENESS SERVICES AVAILABLE TO . . . .

No limitations.

13b. CITATION FOR OTHER PURPOSES (IE. CASUAL ANNOUNCEMENT) MAY BE [X] UNRESTRICTED OR [ ] AS FOR 13a.

14. DESCRIPTORS
Wind tunnel tests
Jindivik aircraft
Aerodynamic performance
Aircraft engine ducts
Intake systems

15. DISCAT SUBJECT CATEGORIES
0101
010301

16. ABSTRACT
Results are presented for a wind tunnel program to investigate the effect of forward speed, incidence and yaw angle on the aerodynamic performance of an auxiliary air intake system fitted to the Jindivik target aircraft. Tests were carried out on a 1/4 scale model of an unmodified air intake duct, and one modified with several designs of auxiliary intake developed during static tests. The wind tunnel tests showed that worthwhile improvements in pressure recovery can be achieved at take-off speeds with simple intake modifications without excessive flow distortion at the engine face. In terms of pressure recovery at the engine face, performance improved with forward speed for all intake geometries tested. In the range of test parameters, the effects of both aircraft incidence and yaw were found to be negligible. Coefficients for distortion in total pressure distribution at the engine face were found to be within the acceptable range specified by the engine manufacturer.

PAGE CLASSIFICATION
UNCLASSIFIED
PRIVACY MARKING

THIS PAGE IS TO BE USED TO RECORD INFORMATION WHICH IS REQUIRED BY THE ESTABLISHMENT FOR ITS OWN USE BUT WHICH WILL NOT BE ADDED TO THE DISTIS DATA UNLESS SPECIFICALLY REQUESTED.

16. ABSTRACT (CONT).

17. IMPRINT

AERONAUTICAL RESEARCH LABORATORY, MELBOURNE

18. DOCUMENT SERIES AND NUMBER	19. COST CODE	20. TYPE OF REPORT AND PERIOD COVERED
Propulsion Technical Memorandum 472	47 416F	

21. COMPUTER PROGRAMS USED

22 ESTABLISHMENT FILE REF.(S)

23 ADDITIONAL INFORMATION (AS REQUIRED)